Application of machine learning for the generalization of the response of levees to high-water events

Rossi, Nicola

University of Zagreb

Faculty of Civil Engineering

Nicola Rossi

APPLICATION OF MACHINE LEARNING FOR THE GENERALIZATION OF THE RESPONSE OF LEVEES TO HIGH-WATER EVENTS

DOCTORAL DISSERTATION

Zagreb, 2023

University of Zagreb

Faculty of Civil Engineering

Nicola Rossi

APPLICATION OF MACHINE LEARNING FOR THE GENERALIZATION OF THE RESPONSE OF LEVEES TO HIGH-WATER EVENTS

DOCTORAL DISSERTATION

Supervisor:
prof.dr.sc. Meho Saša Kovačević

Zagreb, 2023

Sveučilište u Zagrebu

Građevinski Fakultet

Nicola Rossi

PRIMJENA STROJNOG UČENJA ZA GENERALIZACIJU PONAŠANJA NASIPA ZA OBRANU OD POPLAVA TIJEKOM VISOKIH VODA

DOKTORSKI RAD

Mentor:
prof.dr.sc. Meho Saša Kovačević

Zagreb, 2023

IZJAVA O IZVORNOSTI

Izjavljujem da je moj doktorski rad izvorni rezultat mojeg rada te da se u izradi istoga nisam koristio/la drugim izvorima osim onih koji su u njemu navedeni.

Potpis

DECLARATION OF ORIGINALITY

I declare that my doctoral thesis is the original result of my work and that I did not use any sources other than those listed in it.

Signature

Abstract

Levees are earthen structures which, along with other hydraulic and geotechnical structures, are part of larger networks designed primarily for flood protection. Extreme floods are rare events which may pass unnoticed if all goes well, or may cause disastrous consequences if any part of the flood protection system fails. Considering the high variability of geotechnical materials, it is advised that usage of full probabilistic analyses is employed, which imply being able to define a probabilistic distribution of the materials' parameters of interest and calculating the failure in terms of probabilities. Often, geotechnical engineers have to work with a very limited scope of investigation works, which makes it hard to define the parameters probabilistically. This thesis investigates several methodologies which are applicable for the assessment of the stability of river levees with regards to the various failure mechanisms which may occur during high-water events, with the purpose of creating fragility curves and generalizing the levees behaviour in response to such events. The tools used for the analyses presented here are complex numerical analyses, coupled with statistical, probabilistic and machine learning techniques for creating predictive models and fragility curves, as well as to understand the behaviour of levees exposed to various loading situations. This thesis is presented as a compilation of this thesis' author's research papers published in scientific journals. The cumulative results of the thesis aim to improve levee management with regards to predicting failure and early warnings to potential failure. This is achieved through the generalization of the levees composed of highly different cross sections found throughout a whole area of interest, and predicting their behaviour based on the most important input parameters. It is found that out of over a hundred parameters required to uniquely define any complex levee section as realistically as possible with numerical models, only about a third are the ones governing their behaviour regarding several failure mechanisms. These are the parameters which would need to be collected into a database for the considered levees in the specified area, such that the predictive models can be readily employed for prediction and early warning. The models focus on unreinforced levees. However, levees reinforced with geogrids have also been considered separately and the relative contributions of various soil and reinforcement factors are identified, which is a step towards their efficient inclusion in new predictive models.

Keywords: machine learning, flood protection, fragility curves, levees

Prošireni sažetak

Brane, nasipi, akumulacije i prirodne retencije, zidovi i mnoge ostale građevine dio su kompleksnih sustava za upravljanje poplavnim događajima. Statistički podaci pokazuju da je velik dio svjetske populacije pod utjecajem razornih poplava, i/ili su zaštićeni dijelom sustava obrane od poplava. Iz tog razloga ulaže se velik trud na svjetskoj razini za poboljšanjem postojećih i gradnjom novih pouzdanih komponenata sustava, ocjenom stanja i sigurnosti postojećih građevina te unaprjeđenjem strategija upravljanja sustavima obrane od poplava. Fokus ovog rada nalazi se u zemljanim građevinama sustava, a najviše u nasipima za obranu od poplava za koje postoje procjene ukupnih duljina u Europi i SAD-u od nekoliko stotina tisuća kilometara, iako sistematizirane baze podataka ne postoje te su podaci često manjkavi ili nepostojeći. Nasipi su od davnina građeni na naplavnim ravnima velikih rijeka s primarnom funkcijom obrane od poplava, no druge strateške funkcije su također bile od značaja. Danas nasipi zadržavaju primarnu funkciju obrane od poplava, uz dodatak raznih drugih sporednih funkcija u skladu s našim vremenom. S obzirom na svoju starost, često nasipi imaju kompleksnu povijest izgradnje, odnosno nadogradnje, često uz dodatna ojačanja prirodnim i sintetičkim materijalima, zbog učestalih povećanja intenziteta poplavnih događaja, kao i strožih kriterija sigurnosti. Nasipi novijeg doba sagrađeni su od nekoliko komponenti koje imaju svoje uloge u zadovoljenju jednog ili više kriterija otpornosti nasipa na visoke vode, u smislu vanjske otpornosti, stabilnosti, nepropusnosti, drenaže i filtracije. Ekstremne poplave su rijetki događaji koji mogu praktički neprimjetno proći, ili ostaviti katastrofalne posljedice u slučaju da bilo koji dio sustava obrane od poplava popusti/otkaže. Zbog velike inherentne varijabilnosti tala, kako temeljnih tala tako i onih od kojih su izgrađeni nasipi, često se preporuča upotreba probabilističkih metoda za provođenje odgovarajućih analiza. Iako se ukupna nesigurnost najčešće pridružuje inherentnoj varijabilnost, ona može potječi i od drugih uzroka kao što su gradnja, životinjske nastambe, degradacija materijala, itd. Probabilističke analize impliciraju mogućnost definiranja svih relevantnih parametara pomoću distribucija (raspodjela) vjerojatnosti, a rezultate proračuna otpornosti u obliku vjerojatnosti otkazivanja. Uz navedene izvore nesigurnosti, često se u praksi geotehničari susreću s vrlo malim opsegom istražnih radova, više ili manje kvalitetnih, što otežava pouzdano definiranje distribucija vjerojatnosti. Osim toga, za pouzdano upravljanje nasipima potrebno je provoditi mjerenja (monitoring) nad njima. Dobar sustav monitoringa ima funkciju detektiranja neželjenog ponašanja nasipa dovoljno rano kako bi se spriječile moguće katastrofalne posljedice brzim reakcijama. Ideja instrumentacije nasipa koji daljinski, automatski i u realnom

vremenu dostavljaju mjerene podatke često se naziva “pametnim nasipima”, koji trebaju biti dio većeg “pametnog” sustava obrane od poplava.

U ovoj disertaciji istražno je nekoliko metodologija primjenjivih za ocjenu stabilnosti riječnih nasipa, s obzirom na različite mehanizme sloma do kojih može doći tijekom visokih voda, s ciljem izrade krivulja vjerojatnosti oštećenja (ili otkazivanja) i generalizaciju ponašanja nasipa kao odgovora na takve događaje. Korišteni alati su kompleksne numeričke metode, zajedno sa statističkim i probabilističkim metodama, i metodama strojnog učenja, za izradu prediktivnih modela i krivulja vjerojatnosti oštećenja, kao i unaprjeđenja našeg razumijevanja ponašanja nasipa izloženih raznim uvjetima opterećenja. Krivulje vjerojatnosti oštećenja/otkazivanja prikazuju ovisnost uvjetne vjerojatnosti da će promatrani sustav ili građevina doseći neko granično stanje nosivosti ili uporabivosti u odnosu na intenzitet promatranog događaja (u ovom slučaju poplava). Ovakve krivulje u primjeni su od 80-ih godina prošlog stoljeća za različite vrste građevina i razne događaje. S druge strane, metode strojnog učenja za izradu ovih krivulja, i konkretno u primjeni nasipa za obranu od poplava, nešto su noviji pristup koji se danas u sve većoj primjeni u odnosu na ostale analitičke i numeričke metode koje se za isto mogu primijeniti.

Ovaj rad prezentiran je kao kompilacija autorovih članaka objavljenih u znanstvenim časopisima. Kumulativni rezultati ove disertacije imaju u cilju unaprjeđenje upravljanja nasipima za obranu od poplava, u smislu predviđanja vjerojatnosti otkazivanja i ranog upozorenja potencijalnog otkazivanja, kako bi se mogle donositi pravovremene odluke i reakcije. To je ostvareno kroz generalizaciju nasipa značajno različitih poprečnih presjeka koji se nalaze unutar područja od interesa, i predviđanja njihovog ponašanja na temelju ključnih parametara. S obzirom na različitost presjeka s kojima se možemo susresti unutar promatranog područja, potaje neefikasna izrada krivulja za svaki pojedini presjek, stoga je generalizacija ovdje od velikog značaja. Osim toga, s obzirom na kratki vremenski rok unutar kojega dolazi do sloma (vremenski rok u naj dužem slučaju odgovara trajanju visokih voda), prikupljanje podataka i provedba analiza nekog kritičnog presjeka u kritičnom trenutnu također nije održiva. Iz toga razloga, uz bolje razumijevanje ponašanja nasipa i veći opseg pripremnih analiza, mogu se izraditi modeli strojnog učenja čija se primjena može u kritičnim trenutcima brzo implementirati na različitim presjecima. Za izradu takvih modela s fokusom na generalizaciju ponašanja, od izuzetnog je značaja identificirati ključne parametre koji najviše utječu na ponašanje nasipa. Od preko 100 parametara potrebnih za jednoznačno definiranje svakog pojedinog presjeka na što realniji mogući način numeričkim modelima, otprilike jedna trećina njih su oni koji većim dijelom upravljaju ponašanjem nasipa prilikom relevantnih mehanizama sloma. Mehanizmi sloma odnose ne na stabilnost nasipa, prelijevanje, vanjsku i unutarnju eroziju, pri čemu se unutarnja erozija može dodatno dijeliti na nekoliko vrsta. Ovim radom obuhvaćena je primarno stabilnost, a obrađene su i unutarnja erozija i prelijevanje. Kada bi se tako identificirani parametri skupili u baze podataka relevantne za pojedino promatrano područje, ovakvi modeli bili bi primjenjivi za brza i efikasna predviđanja ponašanja kao i u sustavu ranog upozorenja o potencijalnih katastrofama.

Ovdje razvijeni modeli fokusirani na neojačane nasipe, no nasipi ojačani geomrežama su također zasebno promatrani i ustanovljeni su relativni doprinosi parametara tla i elemenata ojačanja na stabilnost nasipa, što je korak ka i njihovom uključivanju u spomenute modele.

Ključne riječi: strojno učenje, obrana od poplava, krivulje vjerojatnosti otkazivanja, nasipi

Contents

List of Figures

List of Tables

Chapter 1

Introduction

1.1 Background

Dams, levees, dikes, artificial accumulations and natural retentions, flood walls and many other hydraulic structures, are part of complex flood defence networks for the management of the risk of flooding. Statistics show that a large portion of the world's population are somehow affected by damaging floods which cause great damages and losses when compared to other natural disaster, and/or are protected by hydraulic and geotechnical structures [3–5]. Thus, a large effort is put into improving existing and constructing new reliable systems, safety assessment of existing structures, and improving the management strategies, which include visual inspections and surveying (monitoring) [6], decision making regarding resource allocation and required actions [7], and finally maintenance. Out of the mentioned structures, this study's focus in on the earthen components of the network, and more specifically on river levees. Estimates show that there may be well over several hundreds of thousands of kilometres of levees in Europe and USA alone [8], but a systematic database does not exist and informations are often very lacking and incomplete. However, some global databases focused on certain aspects of levee control are being developed [9, 10].

Levees have been constructed since ancient times, as early as 2500 B.C.E. in the Indus river valley in today's Pakistan for protecting the land from high waters, but have also been used in various other instances for other strategic purposes [11]. Soil reinforcement and improvement, and thus levee reinforcement, has also been known for almost as long as the construction of levees, with various methods being used to construct structures, from roads to large buildings [12]. Today's levees' primary function remains that of flood defence, but secondary functions can vary between environmental, amenity, health and safety, access, and others [8]. They often have complicated construction histories over several decades or centuries of exploitation due to the gradual increases of water-events intensities, as well as standards becoming more rigorous. This is most often done by cutting steps within the existing levee and leaving it as a core for the new body which is being built around it. With stricter design criteria, which as seen in [7,

Table 2-1] can greatly vary between different standards and protected areas, as well as other factors such as space limitations due to the cadastral parcels' width, available materials, etc., the new levees require some sort of additional reinforcement to be able to withstand the water, traffic and seismic loads imposed on them during their design life period. Most often these reinforcements are in the shape of geosynthetics, namely geotextiles and geogrids. Geotextiles and geogrids are synthetic materials in the form of sheets or grids characterized by their strength, deformability, and other product-specific characteristics for separation, filtration, drainage, etc. Geotextiles in levees are mostly used for separation and filtration, to reduce the risk of forming pipes during seepage by stopping the filtering of the fine-grained particles through the coarse-grained ones, but are also sometimes used as reinforcement. Geogrids on the other hand are mostly used for reinforcement, but also stabilization to reduce settlements. Levees are made of many different components, or elementary structures, which must be appropriate for the loads and applications to which they will be subjected to. These include protection against erosion on both sides of the levee and on the crown, resistance to internal erosion, and stability of the levee together with its foundation soil. There is often some overlap between the functions of the various components, such that the levee requirements can be fulfilled by a combination of components characteristics. The final product needs to fulfil the requirements for external protection, stability, impermeability, drainage and filtration [8]. If any one of the mentioned requirements is not satisfied, the appropriate failure mechanism may initiate and ultimately result in breaching during high-water events.

With this in mind, a good monitored-levee system has the purpose of detecting unwanted behaviour initiation early enough to prevent catastrophic consequences with a timely reaction. However, surveying/monitoring can be too expensive and inefficient to perform regularly and consistently, especially during the short period of time when high-water events are happening, which is the time when the most catastrophic failures occur. The idea of creating a remotely monitored levee which provides real-time data is often referred to as "smart levees", and are part of a larger "smart" management network [13]. Measurements by instruments can generally be divided in two types: local/in-situ where the instruments are placed in the soil or on the surface and the measurements are conducted in a single point or along a line, and remote sensing/ex-situ which take measurements from a remote location (from land or air) [14]. Measurements conducted on the surface or within the body of the levee can be categorised as any of the two types, depending on the type of measurement (deformation and cracking—in-situ, geophysical measurements—usually considered ex-situ) [14]. This classification, however, only regards the closeness of the measuring instrument to the medium whose physical properties being measured, but not the presence of the surveyor. Remote sensing can already be easily associated with automated measurements, but the same can be achieved with instruments installed in-situ [15], which is of extreme interest in "smart levees". Measurements can further be classified by either the frequency of conducted measurements, whether the resulting parameters are measured directly or indirectly, and/or by the spatial coverage of measurements which can

be done in a single point, along a line or over a surface. To evaluate local conditions on found weak spots, focus is often placed on monitoring of pore pressures inside a levee, even though recently other innovative physical measurements inside and on levees are being performed [16]. Such methods include optical fibers with thermal and strain sensors as a convenient method for monitoring long embankments, to identify new leakages and deformations [17]. Inaudi [6] also conclude that fiber optic sensors are a reliable way to measure strains and temperatures in long structures such as levees, at very dense intervals along the structure. However, many other in- and ex-situ measurements have been used in practice, from temperature probe measurements to detect seepage [17, 18], micro electro-mechanical systems (MEMS) such as piezometers, thermal sensors, inclinometers and accelerometers [18], seismic methods, particularly MASW, which have been shown have to a high potential for embankment investigation [19], GPR which has been shown to be useful in specific applications, such as detection of repair patches or animal burrows, but not so much to gain insight into on the embankment characteristics other than layering, and airborne LiDAR technology to investigate large stretches of levees for the assessment of levee damage and stability [20]. Several levees in the Netherlands and abroad have been instrumented this way in order to asses their stability in real time [21]. Given that loading of standard levees during high water events normally results with relatively small deformations, of the order of magnitude of a few centimetres, monitoring instruments used to perform measurement must have high enough accuracy or resolution, depending on the monitoring method used (e.g., inclinometers [22, 23]).

Levees, being structures that run parallel to rivers, built mostly on top of alluvial deposits of the flood plains, and often build from similar, locally available materials, are prone to more uncertainties than other earthen structures such as dams [8, 24]. The uncertainties are mostly associated with the high inherent variability of soils, but also construction methods, material (natural and synthetic) deterioration due to loading conditions, animal burrows, human actions, weathering, etc., as well as the sparsity and quality of geotechnical investigations. Each of these effects can be taken into account (some more, some less), usually in a semi-probabilistic approach by various partial factors [25–27]. However, in most design cases only the inherent variability is considered, either by partial factors [e.g. 28] or parameters' distributions through probabilistic analyses [see 29–31]. The results of such probabilistic analyses are measures of failure or unwanted behaviour expressed in terms of probabilities. Fragility curves are often formed from these probabilities, showing the dependence of the conditional probability of failure or unwanted behaviour to the event intensity (water level, or other) that may occur, and as such are constructed throughout this study. Their usage in civil engineering began in, at least, 1980 with the work of Kennedy et al. [32] related to the safety of a nuclear power plant. Later, their usage in flood protection started in 1991 with a USACE Policy Guidance Memorandum [33], followed by a further explanation in a 1993 USACE Engineer Technical Letter [34], as reported by Jasim and Vahedifard [35]. Today, their usage in slope stability is widespread [35–37], with regards to seismic events, rainfall, and rising water level. Probabilistic analyses can be

performed by a variety of methods, with the First Order Reliability Method (FORM), the First Order Second Moment (FOSM), the Point Estimate (PE) and Monte Carlo simulations being among the most common in geotechnical engineering. Their implementation for the construction of fragility curves can be achieved by using analytic models with a close-form solution [38, 39] or numerical models for more complex problems [39–42]. When a problem is complex enough to require numerical analyses, it becomes time consuming to create models and conduct analyses for each cross-section of interest. Their usage then becomes impractical and inconvenient in complex situations, and machine learning models are used instead, which are used to try and establish a functional relationship between the input and output parameters. They, however, require a much longer preparation time, but are much more efficient in their usage once created. Often used machine learning methods in practice are neural networks [41, 43, 44], and other supervised learning methods such as SVM, MARS, KNN, DT etc. [39, 42, 45–49]. With the help of the mentioned methods, non-linear relationships are found between the target and input features, which are used to get results almost instantly for a specified problem. Machine learning methods have been used in levees to predict internal erosion and deformations due to earthquake loading, partly considering the variable geometry of levees [50, 51], which makes the developed models partly adaptable to different cross sections. When creating such predictive models, it is necessary to first choose the most important features (parameters), such that no feature is left out which may have significant effect on the results. Mirosław-Świątek et al. [52] conducted qualitative analysis of some features on levee stability, based on experts' opinions, and categorized them by their importance and their two-factor interactions. Liao and Liao [47] quantitatively determined the relative importance of several parameters chosen beforehand and their two-factor interactions, based on results of deterministic slope stability analyses. To analyse an arbitrary number of parameters, classic methods become inefficient, so the usage of sequential methods becomes interesting. Contrary to the classic methods which require a previously established number of analyses/data points to perform the feature importance analyses, sequential methods collect data during the analyses, and all the collected data is used to make decisions about the further development of the analysis [53]. There are various methods which collect data and develop sequentially, among which is the Sequential Bifurcation (SB) method, developed by Bettonvil [54] in his doctoral thesis in 1990. If we consider the possible variations in subsoil stratigraphy, geometry, complex constitutive models, and all other relevant physical and mechanical characteristics, for the general case or reconstructed levees we could identify more than 100 possible features which would unambiguously define a single cross section. Sequential methods are used to quickly and efficiently identify the important features, while additional analyses, if required, can be performed to also identify their two- or three-factor interactions. Due to the fact that generally in machine learning the more features we have the more observations are required, such a reduction of features to only the most influential ones is of utmost importance, considering all the complexity of data acquisition via both numerical analyses and monitoring. When doing machine learning models, the focus can

either be on prediction or interpretation. Prediction models focus on predicting the correct output value from the input values, while interpretative models focus on gaining insight into the system's behaviour. To achieve generalization, first a good understanding is required which is achieved with interpretative models, often conducted on very specific systems where conclusions can be extrapolated to more general cases, and then predictive models are created with the knowledge of the analysed systems' behaviour to predict the behaviour of many different systems, i.e. achieve generalization.

1.2 Scope of the Research

This thesis looks at the safety of levees in term of their probability of failure or unwanted behaviour and the methods which may be used to improve levee management in that regard. Its intention is to improve the understanding of the behaviour of reinforced and unreinforced levees under various water loads which arise from flood events, and predict the probabilities of unwanted behaviour associated with them and with regard to the various failure mechanism which may occur. Wolff [24] identifies several such mechanism, namely overtopping, slope stability, external erosion, underseepage and through-seepage, with the latter two being considered as internal erosion mechanisms. Extensive studies have been performed for each of those mechanisms, while the focus of this study is mostly on slope stability, and less on overtopping and internal erosion. Andreev and Zhivkov Zhelyazkov [55] have observed the overtopping and slope stability of earth dams in a probabilistic framework and constructed fragility curves for both mechanisms based on numerical analyses. Ko and Kang [56] constructed a smaller-scale physical model coated and mixed with an innovative reinforcing substance to investigate its effect on breaching reductions caused by overtopping. Experiments have also been performed on full scale levees investigating overtopping with the associated external and internal erosion [57, 58]. Small-scale, laboratory, and numerical investigations have also been performed to investigate the process of internal erosion [see 59–62]. Slope stability analyses for probability of failure assessment have been performed by both limit-equilibrium methods (LEM) [63, 64] and numerical methods [65, 66]. It would be fruitless to discuss which failure mechanism is the most frequent and/or damaging. Özer, van Damme, and Jonkman [9] found that different failure mechanisms are predominant when looking at different time periods, and each mechanism produces various types of failure—partial, total, and total with scour. Vergouwe [67] found that in the Netherlands the internal erosion mechanism is much more significant than previously thought, especially on big rivers. Rarer mechanism may lead to larger breaches, and vice versa, so attention should be given to them all. All of these mechanism can be initiated by flood events, but also other high-intensity events such as earthquakes, heavy rainfall, and actions from accidental situations. Various studies have considered slope stability of levee with regard to rainfall [36, 68, 69], as well as peak ground acceleration [37, 70]. The probability of the joint occurrence of the various events is also something to be considered, such as in [68], as

shown for earthquakes and flood events in [71], and for the combined effects of surge and wave overtopping [72–74].
Failure of levees usually occurs within a short time frame, which means that it is mandatory to have ways to quickly evaluate the measured deformations if they are to be used in flood prevention frameworks. Since levees are structures with variable cross section geometry, different materials with high inherent variability, and variable subsoil stratigraphy, creating models for each characteristic cross section which may be found in a specific area is not convenient, and neither is the calculation time. Because of this, machine learning models are interesting, whose goal is to find a function relationship between the input and output parameters.
The objective of this research is to establish functional relationships between the key levee parameters (geometrical, physical, and mechanical) with parameters that indicate the stability of levees (deformations, factors of safety against sliding, exit hydraulic gradients), with the help of machine learning methods, which would be valid for levees of different geometry and physical and mechanical characteristics, on subsoils with different stratigraphy. The implementation of the developed model for improved management of flood protection levees is discussed. The hypothesis for this research is that there are functional relationships between the key parameters of the levees and subsoils that control the levee behaviour, and the parameters which indicate the stability of levees, such as levees' deformations, potential slip surfaces with the associated factors of safety, and hydraulic gradients which develop during high-water events. It is thought possible to generalize the behaviour of levees through the creation of models which relate the input parameters with the parameters that indicate stability, which can be applied to levees of different geometry within the area of interest.
The determination of the key parameters of the subsoils and levees (geometrical, physical, and mechanical), which have the most effect on the levees' behaviour, and at the same time allow for the generalization of the functional relationships between the parameters of different levees and the outputs concerning different limit states (deformations, slope stability, hydraulic stability), present a scientific contribution to the understanding of the levees' behaviour. The developed predictive models will be applicable on a whole range of possible levees' cross sections and subsoil profiles, with eventual corrections for the specific case, for safety assessment. This makes them applicable for decision making and timely reactions within a continuously monitored flood protection system.

1.3 Outline of the Thesis

This thesis is presented in the format of a thesis by publications. As such, it is a compilation of a number of separate publications, presented here as chapters. Chapters 2 to 5 represent published, submitted or draft journal papers. The status of each journal paper as of time of submission of this thesis is outlined at the start of each chapter. The author was the main contributor in all articles but has received guidance from other researchers. These researchers are

listed at the beginning of each chapter. As the thesis consists of a number of journal papers on the same overall theme there is regrettably some repetition between chapters, mostly confined to introductory sections. Appropriate efforts have been made to avoid all unnecessary repetition. However for ease of readability, some repetition is necessary. In the following paragraphs an overview of the content of each chapter in this thesis is given. The first two chapters are focused on the interpretative models where some specific behaviours of the levee systems are investigated, while the next two chapters try to generalize that behaviour to a variety of different levees.

1.3.1 Development of Fragility Curves for Piping and Slope Stability of River Levees

This chapter gives an overview of a methodology based on Monte Carlo simulations used to assess the vulnerability of levees to two failure mechanisms—piping and slope stability. The assessment is done through the construction of fragility curves which show the conditional probability of failure with water level increase. Overflow is also somehow considered through its effect on slope stability, which is done by increasing the water pressures on the river-side of the levee, and applying appropriate load boundary conditions on the land-side slope and soil surface. To define "failure" for the fragility curves, for slope stability the simple criteria of $FS < 1$ is used, while for piping the critical head difference (ΔH_{crit}) from the Sellmeijer's analytical 2-force rule is used. The uncertainty which generates a probability comes almost exclusively from inherent soil parameters' variability gathered from literature. The methodology is performed and is applicable to single cross sections with fixed geometry. It investigates the effect that parameters' variations have on the probability of failure, and as a result gives multiple curves which can represent the boundaries for any specific section. In a way, this enables the applications of such fragility curves on whole reaches defined by similar geometry and material types, but with different material parameters' variabilities.

1.3.2 Fragility Curves for Slope Stability of Geogrid-Reinforced River Levees

This chapter, similarly to the first chapter, investigates a the vulnerability of levees to slope stability, but reinforced with multiple layers of geogrids. The methodology is based on the Response Surface Method (RSM) to first find the relationship between four random variables and the factor of safety, and then the First Order Reliability Method (FORM) to calculate the reliability index (β) and the design point, and from that the probability of unwanted behaviour by assuming a normal joint distribution of the random variables. The reliability index and the design point are searched for by updating the observations with the new design point values from

the previous step, until convergence is achieved. The unwanted behaviour is defined by two factors of safety, one representing failure (1), and another an arbitrary value (1.5), for both of which fragility curves are constructed. For any factor of safety between these two values which defines some unwanted behaviour, the fragility curve will be found between the two boundary curves. The uncertainty in this study comes from inherent parameter variability, as well as the degradation of the synthetic materials. The methodology is again restricted to one specific levee section.

1.3.3 Methodology for Identification of the Key Levee Parameters for Limit-State Analyses Based on Sequential Bifurcation

The behaviour of levees is dependent upon many parameters which uniquely define each section, and cannot thus be reliably predicted by only a handful of the most commonly used parameters, especially with generalization in mind. This chapter presents a novel methodology for the identification of the key levee parameters, including their geometrical characteristics and the parameters of the foundation soils, which affect the behaviour of levees under high-water load conditions. The analysed behaviours regard deformations, slope stability and internal erosion failure mechanisms. The methodology is based on the Sequential Bifurcation (SB) method, and its intended purpose is to perform preliminary analyses for the detection of the important parameters of levees found within a specific area of interest. Due to the differences in construction and design practices in different locations, different parameters are expected to control the levee behaviour in each analysed area. The variability of each considered parameter is assessed from the documentation of each levee in the area of interest, and unlike the previous studies, it does not come from the inherent soil variability but from the ranges of the parameters' values which can be observed in the selected area. The resulting list of important parameters and their effect's value is representative for all the levees whose parameters are found within the ranges used for the analyses.

1.3.4 Machine Learning Tools for the Generalized Assessment of the Levees' Behaviour

The final chapter is a continuation of the previous chapter, as it uses the factors identified by the proposed methodology to create predictive models for the behaviour of levees found in the specified area of interest. Predictive models are created using Support Vector Machines (SVM) to first predict the deformations of the crown, and then the factors of safety using the predicted deformations. Predictions are also made regarding the hydraulic gradients, but with less success than the first two targets. The models, not being perfect representations of reality, contain a

certain amount of errors which can be added to the predicted mean to account for them. In the same way, a distribution of the mean predicted factors of safety can be obtained, from which the reliability index can be calculated with regards to failure ($FS < 1$). Repeating the prediction process using both models for an increasing water level and a levee with specific characteristics, fragility curves can be efficiently constructed for any cross-section of interest. Here, the failure probability was not calculated based on inherent parameter variability (not considered), but based on prediction errors alone (model uncertainty). However, the same procedure can be used by considering the parameters' inherent variability, which will result with larger confidence intervals for the predictions and the constructed fragility curves. Again, the models are valid for any cross-section defined by parameters which can be sampled from the defined distributions.

Chapter 2

Development of Fragility Curves for Piping and Slope Stability of River Levees

Authors:
Nicola Rossi, Mario Bačić, Meho Saša Kovačević, Lovorka Librić
Paper status:
Published, https://doi.org/10.3390/w13050738

2.1 Introduction

As earthen structures constructed for the purpose of flood defence, the levees should be verified for several potential failure modes. According to Wolff [24], these include overtopping, slope stability, external erosion, underseepage and through-seepage, with the latter two being considered as internal erosion mechanisms. These failure modes are conditioned by the levee's geometrical configuration, its material properties, and overall hydraulic conditions of the site. Based on the examined breach characteristics of hundreds of failures, Özer, van Damme, and Jonkman [9] identified the external erosion as the most frequent for levees, while failures due to internal erosion and instability are less frequent but lead to larger breaches, and as such are emphasized within this study. Of all the internal erosion mechanisms, backward erosion piping is considered to be the primary failure mechanism for levees [75], and even accounts for one-third of all piping failures that occurred in the last century [62]. Various design situations such as rainfall, high water level, seismic peak ground acceleration, etc., can be triggering factors for one or more failure mechanisms, directly or indirectly. Extensive studies have been conducted with various approaches regarding slope stability, Figure 2.1a, with respect to rainfall [36, 69], high water levels [48, 76], and peak ground accelerations [37, 70], as well as combinations of various events [68]. Regarding the piping failure, Figure 2.1b, and depending on the mechanism of soil particle removal (e.g., removal of particles by water forces, chemical dispersion of clays, migration of fine material through coarse matrix, etc.), various modes are identified,

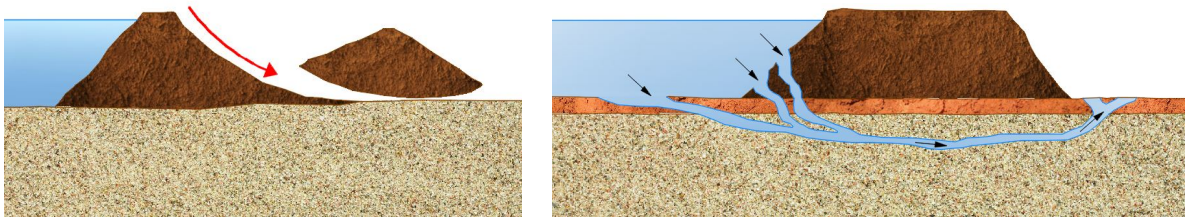

(a) (b)

Figure 2.1. Levee failure mechanisms analysed in the study: slope instability (a) and internal erosion (b).

all pertaining to internal erosion under or through the levee [77–80]. The analysis of different levee failure mechanisms within the Eurocode 7 design code [28] is based on the use of recommended, singular values of partial safety factors (PSFs), with a defined combination of PSFs for action and resistivity (material), depending on the adopted calculation approach for a specific design situation. The code, however, prescribes constant values of PSFs for limit states, with no variation depending on the nature or the duration of the design situation and no recommendation regarding the target reliability values. Thinh [81] notes that, during the design process, an engineer must select a set of characteristic values and the corresponding PSFs, hoping to obtain in the end a design that satisfies a prescribed reliability level. On the other hand, the design code Eurocode 0 [82] provides minimum values for the reliability index for three consequence classes, but these are only defined for buildings, not for geotechnical structures. Some other design codes, such as those in [83], acknowledge the uncertain nature of soils, by defining target values of p_f and equivalent reliability indices for three consequence levels, based on random finite-element analyses.

Concerning the soil related uncertainties, Phoon and Kulhawy [84] identified three main sources of geotechnical uncertainties: (1) inherent soil variability, which describes the variation of properties from one spatial location to another, (2) measurement error, which implies the scatter of measurements on presumably homogeneous soil volumes, and (3) transformation uncertainty, where, in the process of model characterization, which includes linking the on-site and laboratory test results to the design parameters, some degree of uncertainty is introduced. By implementing a Eurocode 7 semi-probabilistic approach, which utilizes statistical methods to select characteristic values of geotechnical parameters, both spatial correlations between the same parameter sat different sampling points and cross-correlations between different parameters at the same sampling point are neglected [85]. Further, depending on the associated failure mechanisms of levees, different material parameters will control the limit states and different models are necessary to predict the resistance, and thus no uniform reliability level can be obtained with the load and resistance factor design method [27]. The degree of uncertainty involved in calculation of levees is especially high for slope stability [86] and piping mechanisms [87]. Even though the geotechnical community has been more progressive in the implementation of different probability-based methods in analyses of levees, understanding of levee failure mechanisms

is still limited [88], while their behaviour during critical conditions mostly remains uncertain. This paper contributes to the efforts of levee vulnerability evaluations, through the demonstration of a methodology for calculation of fragility curves for relevant failure mechanisms of slope stability and piping. Among the many available probabilistic methods [29], this study adopts the Monte Carlo simulation to determine the levee probability of failure when the hydraulic head rises on the riverside up to the levee crown and over, to simulate overflowing. Even though this method takes the most time to run due to its slow convergence, which is its largest disadvantage, it gives the most accurate results when a sufficient number of runs is chosen. For relatively simple calculations such as the limit equilibrium formulation, the number of runs and computation time to solve the problem are acceptable. Additionally, given that it is applicable to both linear and particularly to non-linear problems [29, 89], with many random variables which may be differently distributed [29], this method is used in this study. The method does not identify the relative contribution of each random variable to the safety factor, as some other methods do (e.g., FOSM), but for this purpose sensitivity analyses were conducted. The demonstrated methodology, applied to the river levee in Croatia, results in sets of fragility curves, which can then be used in risk assessment and categorization of levees [90, 91], based on calculated probabilities of failures. This provides a support for the decision making process regarding the optimization of resources for levee reconstructions or maintenance [92]. Furthermore, future design protocols and monitoring activities of levees can be enhanced [93].

2.2 Methodology for the Development of Fragility Curves

To assess the vulnerability of the levee exposed to raising water levels up to and over the levee crown, with respect to identified failure mechanisms of landside slope stability and piping in the foundation soil, a series of numerical simulations were conducted. Within these simulations, the water level on the riverside is raised until the levee is sure to fail ($p_f \approx 1$). Overtopping (i.e., overflow) is usually a result of a high-water event (surge) or it can occur due to wave overtopping. The combined effect of surge and wave overflow is discussed by many authors [73, 74, 94]. However, if a river levee is considered, only a surge type of overflow is relevant. The results of numerical simulations feed into the proposed methodology of fragility curve development, giving insight into the probability of failure relative to the design event intensity. Sensitivity analyses indicate the influence of certain parameters on the fragility curves' shapes, i.e. on the variation of the failure probability.

2.2.1 Slope Stability Evaluation

Slope stability analyses can generally be conducted by limit equilibrium (LEM) and numerical methods incorporated in many commercially available programs, where each method has its own pros and cons [95]. As one of the oldest methods for slope stability calculations, the LEM has been significantly modified, from the introduction of the circular sliding surface [96] to its enhanced versions [97, 98], and is still one of the most used methods for slope stability analyses.

Opposite to the deterministic approach which searches and pinpoints a critical slip surface with the lowest factor of safety, many probabilistic studies, such as multivariate adaptive regression splines analysis (Wang et al. [48]), utilize slope stability methods to identify a slip surface with the highest probability of failure. To give an overview of different possibilities and the results they yield, Akbas and Huvaj [63] compared results of probabilistic slope stability analyses by using LEM with integrated Latin Hypercube and Monte Carlo simulation, and by a numerical finite element method (FEM) with integrated Rosenblueth's point estimate method, as well as random finite element method analyses. They found that FEM analyses resulted in higher probabilities of failure.

This study utilizes LEM and Monte Carlo simulations to conduct series of probabilistic slope stability analyses. The initial total stress state and the pore pressure distribution from steady and transient seepage analyses are modelled separately for each water level increment using FEM, with triangle mesh element sizes of 0.2 m in the body, and 0.5 m elsewhere. The results of both analysis types are tested with different element shapes and sizes, and the resulting distributions are unchanged. Both steady state and transient two-dimensional seepage analyses are governed by a partial differential equation (Eq. (2.1)), where the term on the right-hand side is equal to zero for the steady state.

$$\frac{\partial}{\partial x}\left(k_x \frac{\partial H}{\partial x}\right) + \frac{\partial}{\partial y}\left(k_y \frac{\partial H}{\partial y}\right) + Q = \frac{\partial \Theta}{\partial t} \tag{2.1}$$

where H [m] is the total head, k_i [m⁄s] is the hydraulic conductivity in the i direction, Q $[(m^3/s)/m^2]$ is the applied boundary flux, and Θ [-] is the volumetric water content.

The stress states as well as the water pressures feed into the LEM for slope stability calculation, as shown on the diagram in Figure 2.2. A reason for generating a stress state separately is to yield more realistic results by defining a stress state with stress concentrations closer to the levee toe, instead of calculating it as the product of unit weight and depth. The advantages of defining the stress state in this way do not come to fore with a low angle of levee slope where a low stress concentration can be expected; however, a significant difference is evident in the case of levee overflow where shear stress can be applied on the surface of the slope and the stress state adjusted accordingly. Thus, for consistency reasons, all the analyses are conducted using this procedure. Another benefit of separate generation of the stress state is a drastic reduction in calculation time, since the LEM utilizes an iterative procedure to find the interslice forces and

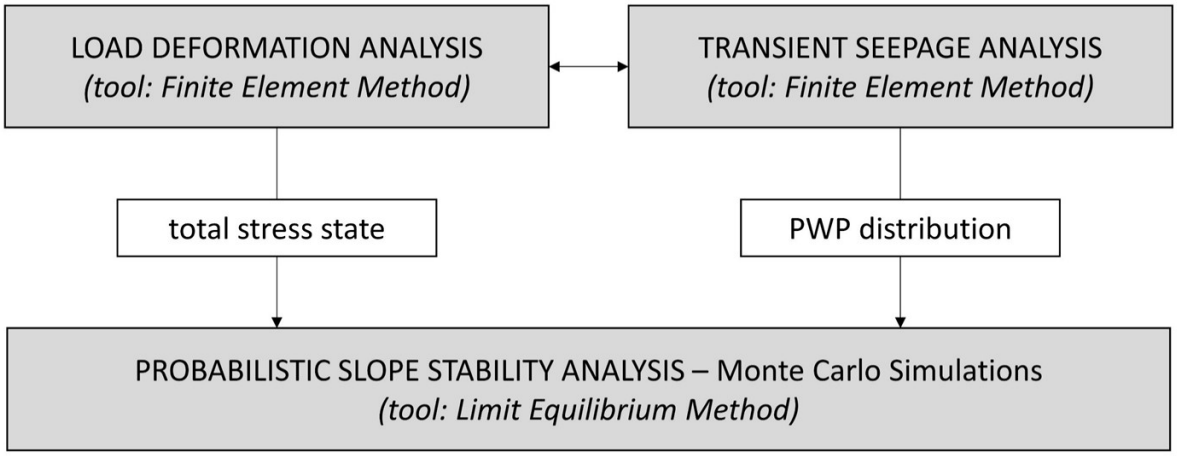

Figure 2.2. Workflow of probabilistic analysis of levee slope stability.

thus requires multiple calculations to find the safety factor for just one slip surface. With the imported stress state, the stresses are already defined so the safety factor can be immediately calculated for a trial slip, which is significant considering the number of runs required to conduct a Monte Carlo simulation.

Since the intention of this study is to inspect the probability of failure of the levee due to the water rising, the fragility curves were constructed by incrementally increasing the water level from the levee toe to the levee crown, and over for the case of surge overflow, by calculating the pore pressure distribution from seepage analyses. The overflow was simulated by applying the equivalent shear stress, caused by water flow, along the crown and landside slope, while keeping the water level at the crown height for the free water surface generation through the levee body. When the complete fragility curve was obtained, based on the input of parameters with probabilistic distribution, a sensitivity analysis followed. This included varying the values of parameters, while keeping the other parameters at their means, to assess their influence on the shape of the curve and stability of the levee. The investigated parameters are the statistics of the strength parameters, the permeability, and the duration of the flood. For the latter, additional transient flow analyses were con-ducted with various water level durations, and the results were then once incorporated into the LEM calculations. The results of these variations are shown as new fragility curves, shifted to the left or right of the ones from the mean analyses.

2.2.2 Internal Erosion (Piping) Evaluation

The most prominent trigger for internal erosion is the high-water event, and as such this has been subject of many studies. To investigate the erosional behaviour of soil at the microscale (granular) and macroscale (levee), various methods have been used from physical models [61, 99]—numerical simulations such as FEM, FDM, DEM [78–80, 100, 101], the material point method [102] and random lattice models [62]. Other tools such as neural networks were also

used to help predict soil behaviour under seepage forces based on laboratory and field tests [51, 77, 103]. Despite many advantages of these advanced tools, the geotechnical community in many cases still relies on the simple empirical or semiempirical rules [104].
Within this study the closed-form analytical Sellmeijer 2-force rule [51], which resulted from a neural network based on field and laboratory tests and numerical analyses, was used for piping analyses. This approach is used in many state-of-the-art levee risk assessment methodologies, such as the VNK2 approach [104, 105]. The closed-form solution predicts that for a given head difference a pipe of specific length will form. Once the critical head difference value is reached (ΔH_{crit}), the pipe will start to progress continuously until failure:

$$\frac{\Delta H_{crit}}{L} = F_R \cdot F_G \cdot F_S \tag{2.2}$$

In Eq. (2.2), L [m] is a seepage path, equal to the width of the levee, and the factors F are the resistance, geometry, and scale term, respectively, and are functions of unit weight, drag force factor, angle of repose, relative density, effective grain size (d_{70}), kinematic viscosity, coefficient of uniformity and particle angularity. The critical head difference needs to be higher than the actual head difference reduced by the value of $0.3 \cdot D_{blanket}$ (thickness of the top clay layer that covers the aquifer), assuming the levee lays on a clay cover over the underlaying sandy aquifer. The parameter which was used as the random variable is the hydraulic conductivity of the aquifer, while all the other values were kept constant at their measured mean values or suggested mean values for the parameters for which measurements or correlations were not available. To assess the validity of the results obtained by the Sellmeijer's equation, the levee and the subsoil geometry and parameters should fall within certain limitations for which the rule was developed. The levee should lay on top of a homogeneous sandy aquifer of finite thickness, with horizontal ground surface in the cross-section direction [104]. Some guidelines [93] suggest applying the Sellmeijer method only if the thickness of the aquifer is less than the seepage length. Regarding the range of the parameters, Sellmeijer and Koenders [59] note that the routine is stable over the entire range of practically feasible parameters, while Sellmeijer et al. [51] give ranges for some new parameters introduced in the formula. The ratio of seepage length to hydraulic head difference for which the formula should be applied is $L/\Delta H > 10$.

2.3 Case Study Example: River Drava Levee

River Drava, with the overall length of 710 km, flows from Italy to eastern Croatia where it merges with Danube, and is historically known for major flood events [106], where prominent events have occurred in the last several years. The case study levee stretches across 6.8 km of the Drava old riverbed, from county Selnica to accumulation lake Dubrava. The levee is fragmented into three segments because of the presence of two smaller rivers, Bednja and Plitvica, flowing

perpendicularly to the Drava (Figure 2.3).

The reach of interest for this study is defined by height and is the starting section of second

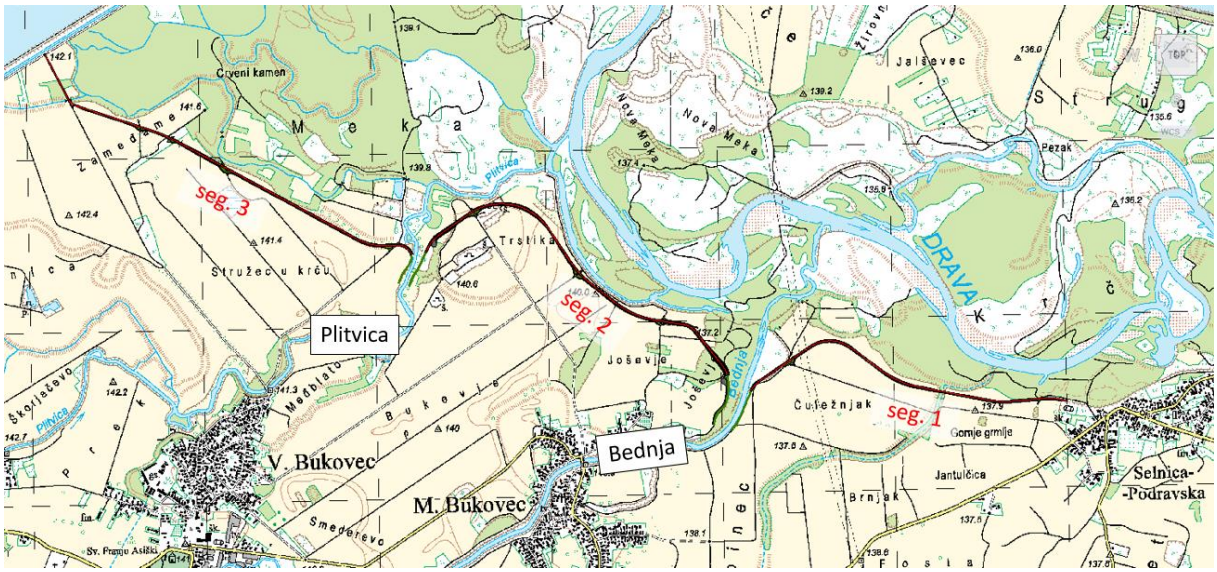

Figure 2.3. An overall layout of the Selnica–Dubovica levee with its distinctive segments.

segment, just after the Bednja river, where the levee's highest cross-section is present (Figure 2.4). By the request of the stakeholders, the designed crown level is 0.5 m above the 100-year high water, while the crown is 4.0 m wide. The levee slopes are at 1:3 and the service road is located on the levee's landside toe.

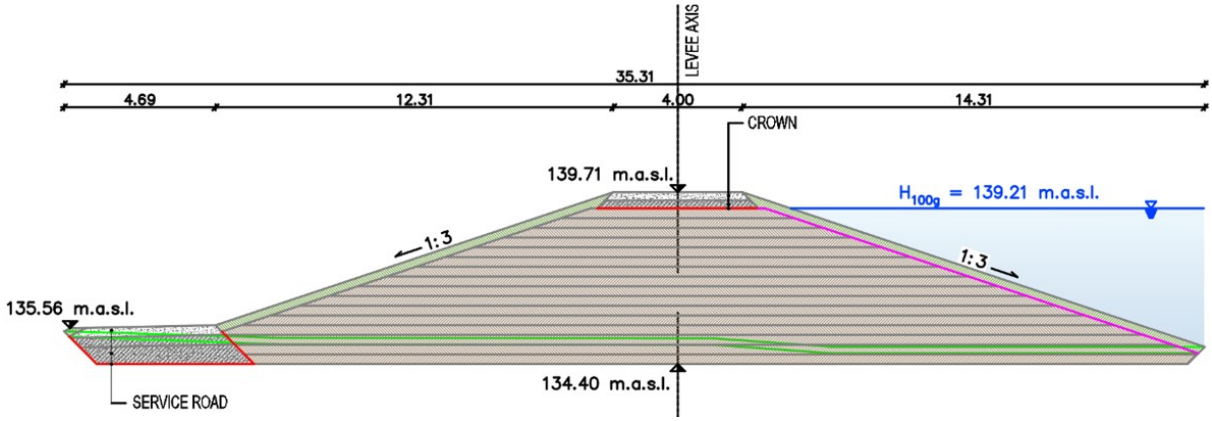

Figure 2.4. A cross-section of the case study levee.

2.3.1 Conducted Investigation Works

To obtain insight into the layering and physical-mechanical characteristics of the subsoil, an extensive geotechnical investigation campaign was conducted, consisting of 12 boreholes at equal spacings along with conduction of Standard Penetration Tests (SPTs), 12 Cone Penetration

Tests with pore water measurements (CPTus) and 12 seismic refraction geophysical profiles. Both undisturbed and disturbed samples were taken during the geotechnical drilling, which were tested in a laboratory to determine their physical and mechanical characteristics. In addition to the in situ and laboratory direct test results, transformation models were implemented to relate the on-site and laboratory test results with the design parameters to infer geotechnical properties from indirect measurements. Based on these field and laboratory investigation works, a reliable geotechnical model of the subsoil was formed for the reach of interest regarding stratification and soil parameters to conduct calculations.
The subsoil was divided into a top layer of lower permeability underlined by the thick coarse-grained layer. At the location of the analysed cross-section, the upper low permeability layer was not detected ($D_{blanket} = 0$) and only coarse-grained soil was identified. Considering the investigation data scattering because of the mentioned inherent soil variability, measurement error and transformation uncertainty, to develop fragility curves by the means of probabilistic analyses some variation in the soil parameters, need to be considered.

2.3.2 Probabilistic Characterization of Soil Parameters

Since the soil parameter distributions can vary significantly, they should be limited to keep the values in the realm of possibility for a specific soil, thus avoiding illogical values. Phoon and Kulhawy [84] give a detailed literature review showing the ranges and number of samples for certain obtained statistics. These values for the internal friction angle are taken as guidelines for specifying the limits of their distributions. Since the slope stability of the levee is governed dominantly by the body and berm materials, these materials were probabilistically evaluated. Effective cohesion has seldom been reported in the literature on soil parameters variability, where it is considered as either normally or log-normally distributed, with CoV values similar to those for undrained shear strength reported in the literature [55, 107, 108]. This study assumes log-normal distribution and the commonly accepted CoVs, thus only the upper limit would be needed. However, as the mean values are already very low, the range for the distribution of $\pm 5\sigma$ is acceptable. Various authors reported that neglecting the correlation coefficient between cohesion and internal friction angle yields conservative results in slope stability calculations if their correlation is actually negative [109, 110]. Results from tests conducted by Lumb [109] show a strong negative correlation for the compacted samples, and since the levee in the case study is compacted during construction, a negative correlation, thus a correlation of zero, can be assumed. Some sources suggest using some other value for the correlation coefficient [110, 111]. The values and statistics (μ as mean value and CoV as coefficient of variation) of each random variable for stability analysis were assumed from the literature [84, 89, 112] and are shown in Table 2.1. As the levee was constructed from materials from an undefined borrow site, the mean values of the levee soil parameters were obtained during the deterministic design

Table 2.1. Parameters and the statistics used for slope stability analyses.

Material	γ [kN/m^3]	ϕ [°]		c [kPa]		k_x [m/s] (Mean)		k_y/k_x [-]
		μ [kPa]	CoV [-]	μ [kPa]	CoV [-]	SDC1	SDC2	
Levee Body	18	26	0.15	2	0.3	1×10^{-8}	1×10^{-8}	0.5
Crown and berm	20	30	0.12	1	0.3	1×10^{-4}	1×10^{-8}	0.5
Foundation soil	19	36	-	0	-	1×10^{-5}		0.5
Distribution	constant	normal		log-normal		constant		constant

phase of the levee, such that the stability criteria were met (Table 2.3) and represent the minimum required values that the materials must have to deterministically ensure slope stability.
Two stability design cases (SDCs) were analysed regarding hydraulic conductivity, one where the crown/berm is constructed from a more permeable material, and the other where the whole levee is homogeneous, i.e. the crown/berm and the body have the same conductivity.
Hydraulic conductivities for the subsoil were obtained from correlations with CPTu tests, while the hydraulic conductivities for levee materials were determined from deterministic steady seepage analyses, as minimally required to maintain hydraulic stability of levee in terms of the critical exit hydraulic gradient and free water surface position. To assess the sensitivity of the slope stability to the hydraulic conductivity of the levee body material, an arbitrary value of two orders of magnitude was selected since the range of reported hydraulic conductivity's CoV is too great to assume a value (30–750%) [29], while the foundation's and crown/berm's conductivities were kept the same as those defined for each SDC. For the piping analysis, the statistics of the hydraulic conductivity of the subsoil for case study location were estimated from the correlation with the CPTu test and assumed a log-normal distribution [113, 114]. Since the CPTu showed a mixed subsoil profile with lenses of fine-grained soil, the profile was idealized to just one layer with one highly variable hydraulic conductivity. The distribution was described by the median (1×10^{-5} m/s) and the extremely high CoV due to the soil profile idealization by averaging over the whole CPTu profile. However, if it is assumed that the water flows around the fine-grained soil lenses, the conductivity distribution can be defined only for the sandy material, where the median is similar (3×10^{-5} m/s), but the variation is significantly decreased. Taking this into consideration, the piping calculations were conducted for two piping design cases (PDCs)—first (PDC1), where the subsoil is modelled as a homogeneous soil layer with highly variable hydraulic conductivity estimated from CPTu data for every material in the subsoil, and the second (PDC2), where the hydraulic conductivity of the layer was estimated only from the CPTu data for sand. Parameters chosen for piping analyses are shown in Table 2.2.
The hydraulic anisotropy ratio, defined as the ratio of the vertical to horizontal conductivity, can vary over a wide range of values [115]. As the levee materials are usually compacted dry of optimum [116], and soils dry of optimum have lower hydraulic anisotropy [117], the used anisotropy ratio values are reduced mean values from the literature [115]. The relative density

Table 2.2. Parameters and their statistics used for piping analyses.

Material	k_x [m/s] (Mean)		D_r [%]	k_y/k_x [-]
	Median [m/s]	CoV [-]		
	PDC1			
Foundation soil	1×10^{-5}	32.5	80	0.5
	PDC2			
	3×10^{-5}	5.0		
Distribution	log-normal		constant	constant

(D_r) has been obtained via correlation with an SPT test.
The distribution of the hydraulic conductivity was defined through the median instead of the mean value since the parameter values vary over a few orders of magnitude, so the median was more intuitive and simpler to obtain as it is the geometric mean of the available data.

2.4 The Probabilistic Analyses Background

The methodology for the development of fragility curves for levee stability implies that the proper stress state, as well the proper water pressure state, is established.
To obtain the appropriate stress state for the slope stability analyses, the methodology suggests conduction of the load deformation total stress analyses. Since soil plastification is not relevant to this study, the linear-elastic constitutive model was used, and this required input of soil stiffness and unit weights, as well Poisson's ratio, whose variation was not considered, even though it may have had some effect on the results [118]. Further, for the design situations, which include water level up to the top of levee crown, numerical analyses were carried out, including commonly used boundary conditions of properly defined hydraulic heads on the riverside and landside. However, if the water level is higher—if surge overflow is considered—the stress analyses should be supplemented with the additional boundary shear stress along the crown and landside slope. Given that this aspect goes beyond standard analyses, a cautious evaluation of these shear stresses is required. The boundaries of both analyses were defined far from the levee region, enough to not affect the results. The constraints of load deformation analyses consisted of fixing movement of lateral soil elements of the model in the horizontal direction, and the bottom elements in two perpendicular directions. Seepage analyses require only hydraulic boundary conditions, which in this case consist of constant or varying hydraulic head values applied on lateral boundaries and on the top boundary of the model, up to the required height. During surge overflow, the water velocity increases down the slope until a terminal velocity is reached at equilibrium between water momentum and slope frictional resistance, after which

the flow becomes steady and the velocity can be calculated by the following equation:

$$v_0 = \left[\frac{\sqrt{\sin\Theta}}{n}\right]^{3/5} \cdot q_0^{2/5}[m/s] \tag{2.3}$$

where v_0 [m/s] is the steady flow velocity, Θ (°) is the landside slope angle, n [-] is Manning's coefficient, and q_0 (m^2/s) is the steady discharge [73]. For supercritical flow which develops on the landside slope, Figure 2.5, Hewlett, Boorman, and Bramley [119] proposed a value of Manning's coefficient of $n = 0.02$, relevant for slopes of 1:3.

The discharge over the levee crown can be calculated using the equation for flow over a

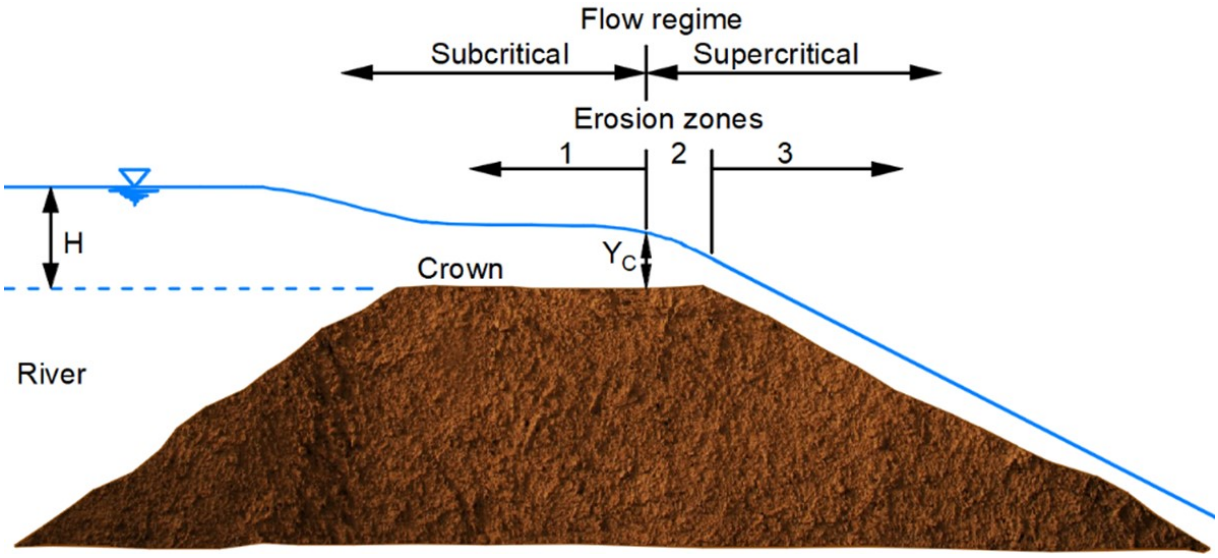

Figure 2.5. Flow regimes during overflow of a dam, redrawn from [1].

broad-crown weir, which gives slightly conservative results due to not taking into consideration frictional losses [72]:

$$q = \left(\frac{2}{3}\right)^{3/2} \cdot \sqrt{g} \cdot h_1^{3/2}[m^2/s] \tag{2.4}$$

where g (m/s^2) is the gravitational acceleration and h_1 [m] is the upstream head (elevation over the levee crown). If steady flow is assumed, the discharge is constant along the slope. Therefore, the height of water perpendicular to the slope in the steady, uniform flow area for unit length of the levee can be calculated from Eqs. (2.3) and (2.4) as:

$$h = \frac{q}{v_0}[m] \tag{2.5}$$

Finally, when steady, uniform flow is reached, the shear stress from surge overflow is equal to:

$$\tau_0 = \gamma_w \cdot h \cdot \sin\Theta[kPa] \tag{2.6}$$

where γ_w (kN/m^3) is the unit weight of water. Eq. (2.6) conservatively overestimates results since the resulting pressure is a little bit higher than the pressure in area above the steady flow [94]. Such calculated shear stress is applied along the crown and landside slope, as shown in Figure 2.6 for the case study numerical model. With the full stress state properly defined, for all

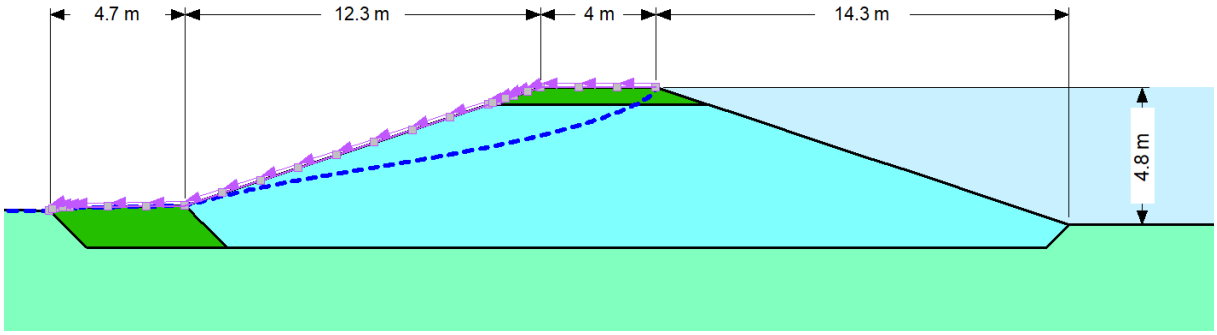

Figure 2.6. Numerical model for analyses of case study levee.

water levels including the surge overflow, stability analyses aim to find the critical slip surface out of the number of generated slip surfaces. To generate several slip surfaces, as well as to evaluate their safety margins, this study adopted a "Grid and Radius" method incorporated into the commercial software GeoStudio [120]. With this method, a grid of slip centres and a grid of slip tangents are created, and these define the number of analysed slip surfaces. However, a larger number of defined slip surfaces yields much longer calculation times, and conducting a single deterministic analysis prior to the probabilistic analyses is recommended. This analysis was conducted with a large grid covering a large area for potential slip surface centres, and a relatively large tangent grid to also cover a large range of possible surface depths. After the critical surface was found, the grid size and number of centre points and tangents were reduced around the critical surface point and tangent, to make smaller, denser grids and possibly find more critical surfaces around the original critical surface, while also minimizing the run time of the probabilistic calculations. This does not guarantee that the critical surface—defined in this case as the surface with maximum probability of failure—will be the same one as the deterministic critical surface, but it is a reasonable starting assumption that it will at least be close to the deterministic surface.

For the probabilistic slope stability analyses, four random variables were assigned, and these include cohesion and angle of internal friction for both levee body material as well the crown road base and berm material. The variability of the soil can generally be modelled by a random field described by the CoV and scale of fluctuation [84]. As opposed to the creation of random fields, the method used in this study sampled a random variable for each material only once and then applied it to all the slices found in the corresponding material. This kind of simulation usually gives conservative results. Within this study, the number of Monte Carlo trials was sufficient to obtain a relatively constant value p_f for each water level, which has been estimated at 15 000.

Table 2.3. Deterministic safety factors for the case study levee, exposed to various design situations.

Design Situation				Safety Factor
Low water	Riverside	Static	Drained	1.4
		Seismic (475-year RP)	Undrained	1.1
	Landside	Static	Drained	1.4
		Seismic (475-year RP)	Undrained	1.1
High water	Riverside	Static	Drained	1.6
		Seismic (475-year RP)	Undrained	1.6
	Landside	Static	Drained	1.3
		Seismic (475-year RP)	Undrained	1.1
Rapid drawdown			Drained	1.2

In regard to piping mechanism, for each hydraulic head difference, 25 000 Monte Carlo simulations were performed using an excel spreadsheet and its built-in random number generator function.

As the aquifer thickness is required for the Sellmeijer rule, two runs were carried out with minimum thickness from soil investigations to values after which further increasing of thickness no longer affected results. Therefore, aquifer thickness in numerical analyses ranged from 5 to 50 m.

2.5 Results and Discussion

2.5.1 Fragility Curves for Levee Slope Stability

To serve as a benchmark for the full probability analyses results, results of semi-probabilistic analyses adopted in Eurocode 7 are shown in Table 2.3. The analysed numerical model included idealized subsoil layering with mean values of both hydraulic and strength parameters, determined from the laboratory and transformation model data. Based on the Eurocode 7 design approach 3 (DA3), the design strength parameters were obtained from characteristic values by applying prescribed PSFs. Several design situations were analysed by following relevant norms and guidelines for geotechnical design [28, 121–123], with stability evaluation for both riverside and landslide slopes in drained and undrained conditions. The slope stability was assessed by the means of the LEM utilizing the pore pressure distributions from seepage analyses.

Deterministically obtained factors of safety are higher than unity ones, with a safety margin from 10 to 60%, indicating the stable levee slopes for all relevant design situations. However, these analyses neglect the variability of strength parameters as the ones governing the obtained

safety values. Therefore, full probabilistic analyses were conducted to develop fragility curves for the levee's landside slope stability.

Figure 2.7 shows the fragility curves for the levee's landside slope stability, through the relation of the hydraulic head on the river side vs. probability of failure. As the case study levee crown also acts as a road base, the crown material, constructed up to 0.5 m above the 100-year return period high water, consisted of coarser material mixed with fines. Therefore, the hydraulic conductivity of this layer is higher than levee body material conductivity, so when the water goes over the 100-year water level, the free water surface shifts towards the landside slope yielding a more unfavourable situation. The presented fragility curves were developed for steady seepage and include stability evaluation for levee material conductivity of 10^{-8} m/s and for increased conductivity of 10^{-6} m/s, while the crown material conductivity was kept constant for each SDC. The curves with higher p_f, marked in blue, refer to the levee constructed with the more permeable crown layer (SDC1), while the curves with lower p_f, marked in red, refer to the crown constructed of same permeability material as the levee body (SDC2). For the 100-year water level event, at 139.21 m a.s.l., there was an abrupt increase in p_f for the case with the more permeable layer on top, while the curve smoothly increased for the case of homogeneous levee. While the curves of SDC1 show an approximate linear trend, the SDC2 fragility curves show a bilinear trend, with the intersection at head value of around 143 m a.s.l. The point of slope change indicates the sudden shift from deeper (> 2 m) to shallower (< 0.7 m) slip surfaces, which do not exist for SDC1 as there is a slow transition from deeper to shallower surfaces. The increase in the levee body conductivity by two orders of magnitude (1×10^{-6}) at first had a slight positive effect for SDC1 because of the smaller difference in conductivities, but afterwards the negative effect was evident for both design cases. Further, considering that high-water events are usually of limited duration, preventing the development of a steady seepage, the fragility curves were further evaluated with consideration of transient seepage for a high-water event duration of 5 days. Failure probabilities for transient situations, up to the crown height, are shown in Figure 2.8. Even though the discrepancy in curves representing different levee conductivities is very low for 5-day high water duration, it should be noted that the time required to numerically reach steady seepage with hydraulic conductivity 1×10^{-8} m/s is higher than 500 days, while for 1×10^{-6} m/s levee conductivity it is less than 50 days. The fragility curves for the varied statistics of strength parameters are given for various CoV values obtained by reducing the standard deviation. For both friction angle and cohesion, the CoVs are halved. Figure 2.9 shows that, by lowering the friction angle's standard deviations, the stability increased up to a certain hydraulic head value (marked with a point on the curves), after which the stability was reduced when compared to the original case with non-reduced variability. Such behaviour is expected since less variability means less probability of obtaining lower strength values, but also less probability of obtaining higher strength values which increase stability. Thus, for lower head values, when the slope is deterministically stable, less variability is favourable, while for higher head values, when the slope is deterministically unstable (or in

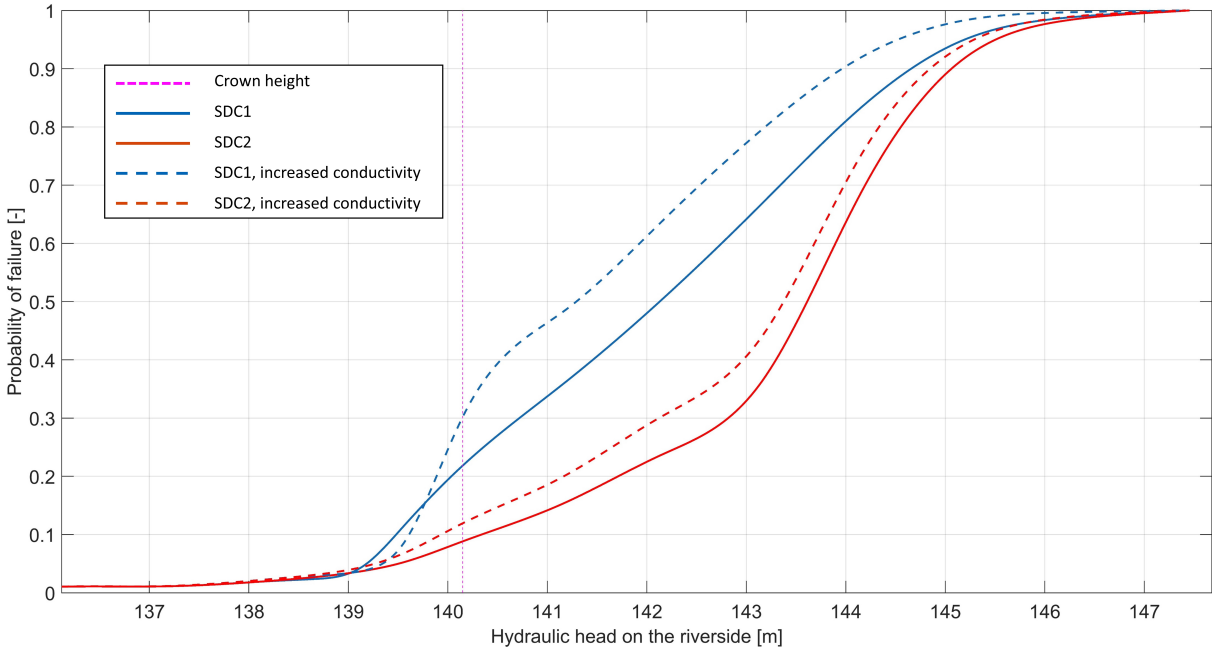

Figure 2.7. Fragility curves for landside slope stability with respect to varying hydraulic conductivities.

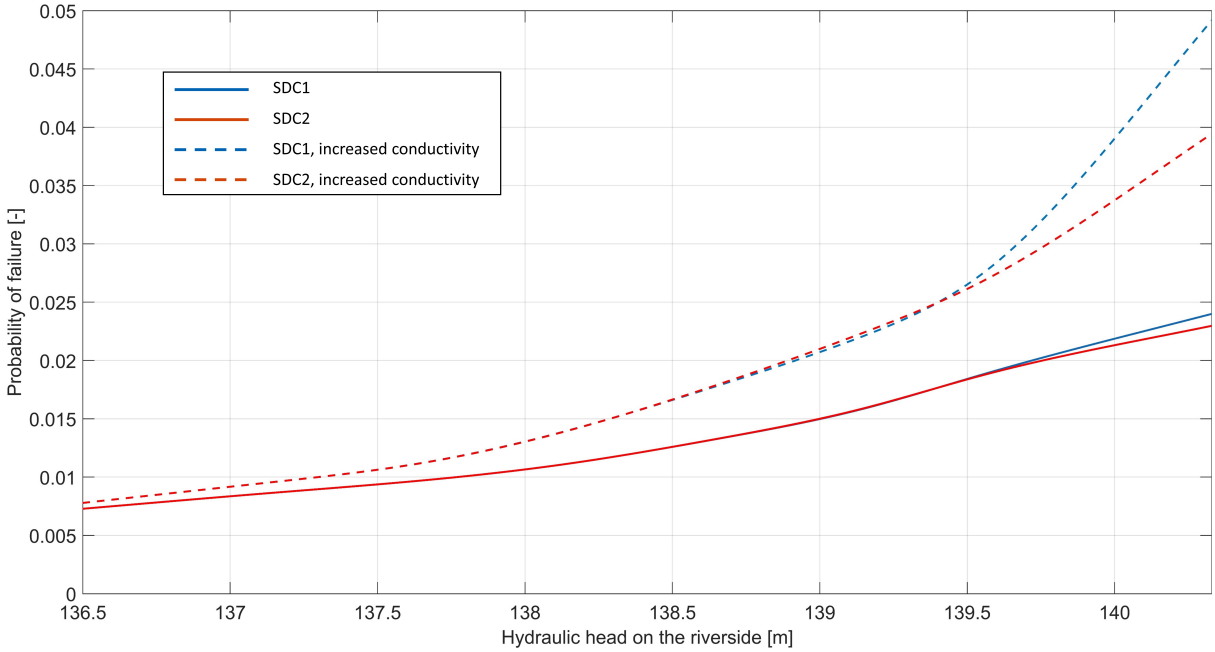

Figure 2.8. Fragility curves for transient seepage of 5-day duration.

equilibrium), less variability is unfavourable. It should be noted that for higher variability the distribution was truncated for a range of realistically possible values, while for lower variability the range was limited by the distribution itself and is lower than the truncated range for higher variability. For cohesion, the curves are practically unchanged, thus no point is marked on the corresponding curves in Figure 2.9. Figure 2.10 shows the relation between reliability indices and probabilities of failure, for both calculated indices and their theoretical values for normally distributed safety factors. The figure shows results of the analysis with reduced friction angle

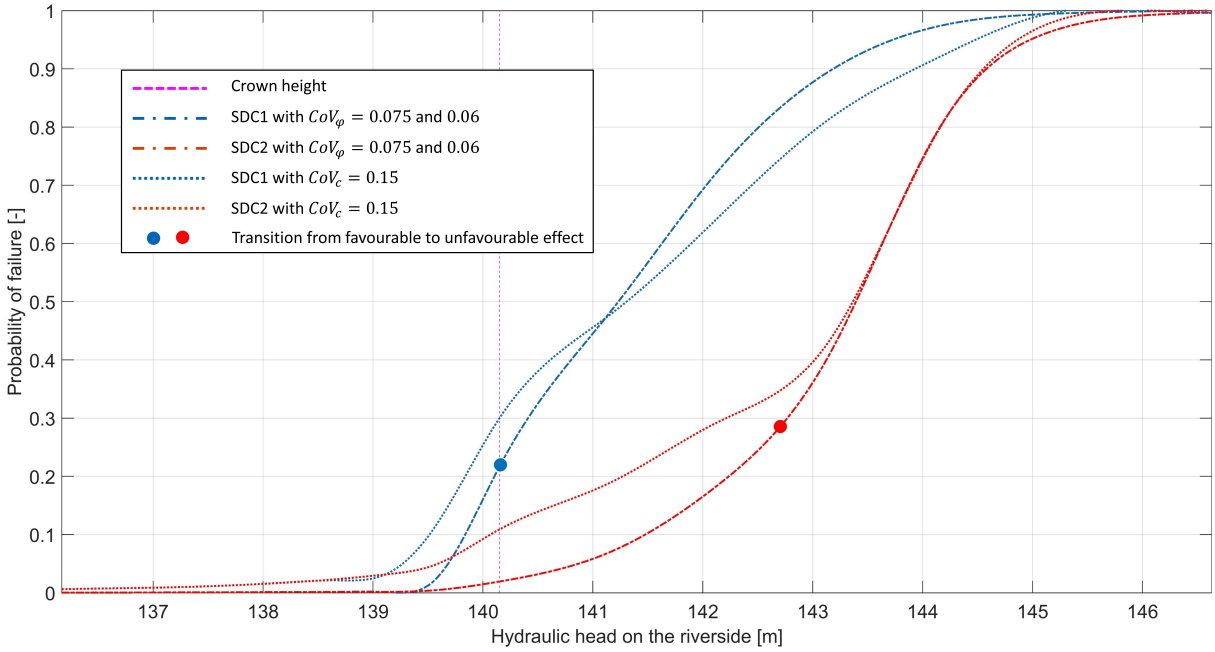

Figure 2.9. Fragility curves for reduced variability of strength parameters.

variability, but all other calculations yielded similar curves. The reliability indices of critical slips were calculated as:

$$\beta = \frac{\mu - 1}{\sigma} \tag{2.7}$$

The numerically obtained curve shows very good concurrence with the theoretical value up to $\beta = 2.7$, which indicates that the safety factor follows a normal distribution. For lower p_{fs} (higher β), the numerically obtained curve deviates from the theoretical one, which might indicate that for lower probabilities of failure the safety factor no longer follows a normal distribution.

2.5.2 Fragility Curves for Internal Erosion (Piping)

The piping analyses included hydraulic conductivity as a random variable, whereas simulations were conducted for two piping design cases (PDC1 and PDC2), depending on the procedure used to obtain the hydraulic conductivity distributions and statistics.

Additionally, to investigate the influence of aquifer thickness on the results, piping calculations included the deterministic variations of the thickness, starting from a 5 m value identified by the investigation works, to the value after which further increase does not affect the results (i.e., 50 m for the given analyses). Furthermore, the effective grain size d_{70} was varied between the minimum and maximum values (150-430 μm) which were used for the development of the Sellmeijer's model [51]. To assess the validity of the results obtained by Sellmeijer's equation, the levee and the subsoil geometry and parameters should fall within certain limitations for which the procedure is developed. Following the suggestion to apply the Sellmeijer's procedure only if the thickness of the aquifer is less than the seepage length [93], the maximum aquifer thickness

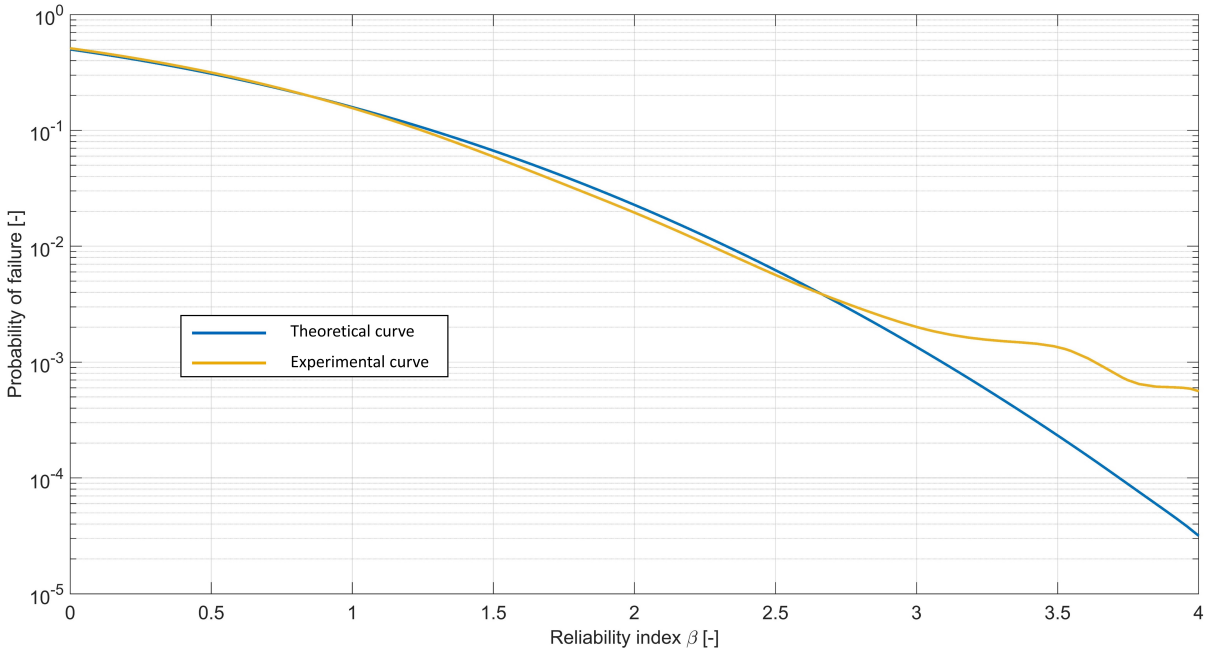

Figure 2.10. Probabilities of failure and respective reliability indices for levee slope stability.

of 35 m should actually be considered for the case study example. The curves in Figures 2.11 and 2.12 show the probability of failure for the water rising to the top of the crown for PDC1 and PDC2, respectively; however, for the specified seepage length, the actual hydraulic head for which the formula still applies is around 1 m below the crown. The "real value" fragility

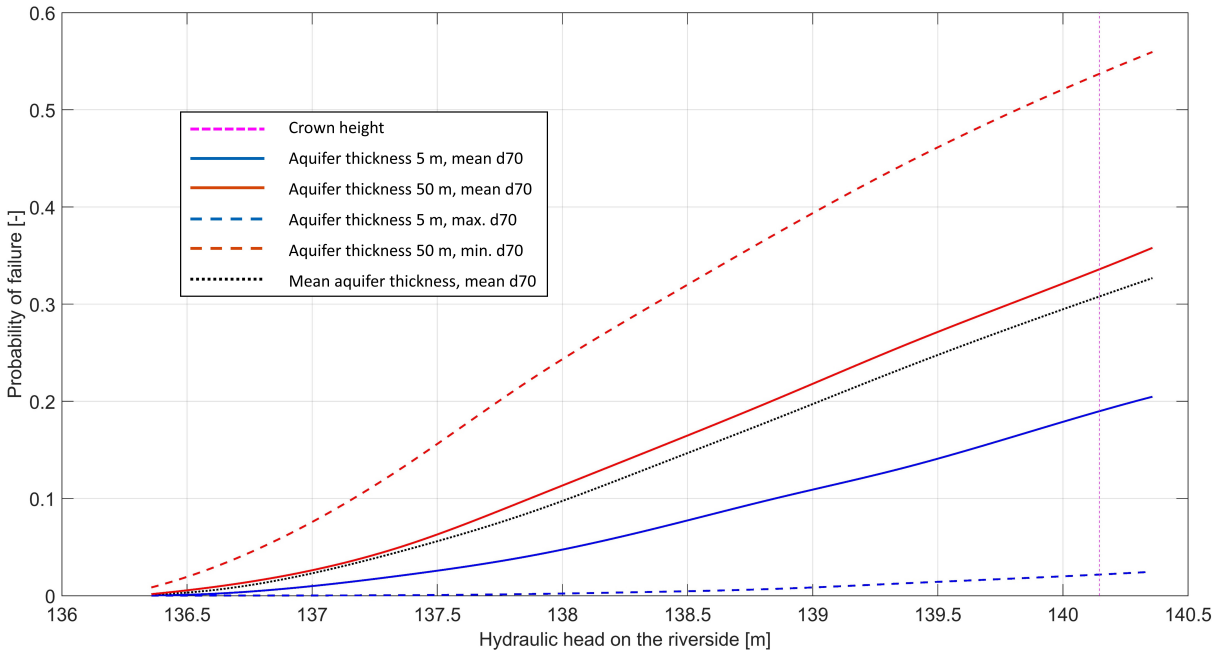

Figure 2.11. Probabilities of failure and respective reliability indices for levee slope stability.

curves for the analysed section are somewhere between the two extreme curves (dashed lines), which vary from p_f of only few percent up to the p_f of 50% for PDC1 and 75% for PDC2. This clearly demonstrates that quantities and quality of in situ and laboratory investigations, required

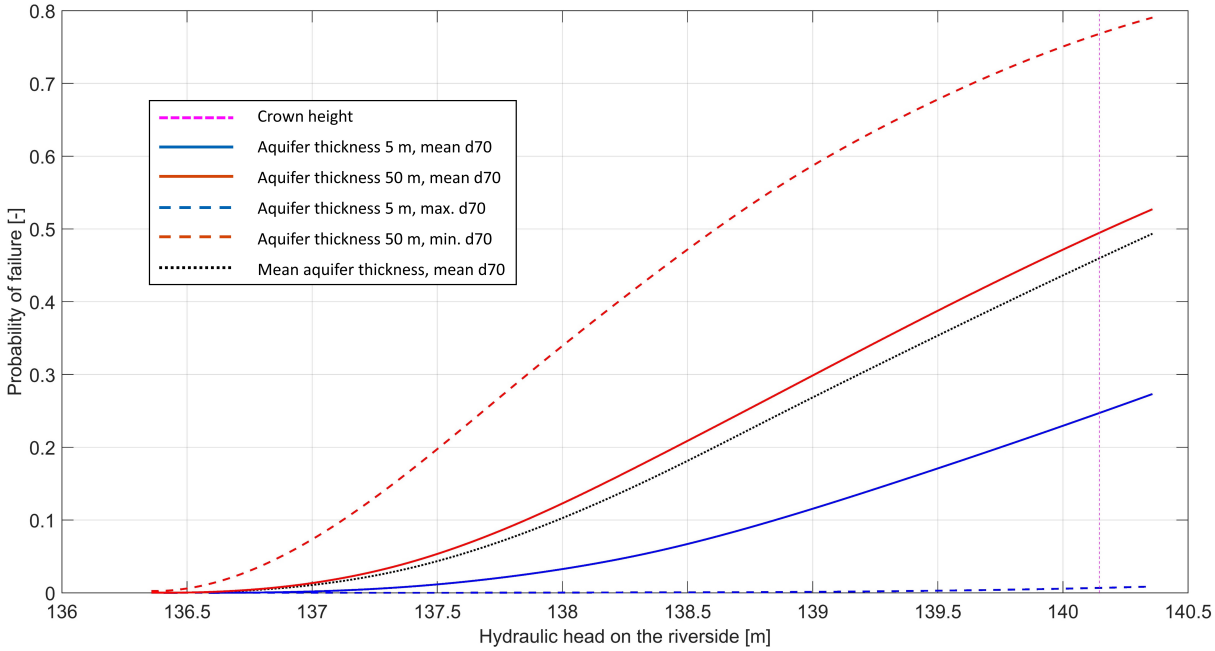

Figure 2.12. Probabilities of failure and respective reliability indices for levee slope stability.

to estimate the key parameters—i.e., aquifer thickness, d_{70}, and hydraulic conductivity are of paramount importance. Otherwise, the p_f for the backward erosion piping failure mechanism cannot be reliably estimated using the Sellmeijer 2-force rule. However, development of the shown curves provides a valuable insight into the effect that certain parameters have on the p_f. By analysing the mean curves for both design cases, as show in Figure 2.13, it can be expected that for smaller variations of the hydraulic conductivity, the probability of failure decreases in the lower range of hydraulic heads, but afterwards it drastically increases instead. The reason for this is the change in mean value which, even though is very subtle, significantly affects the results and seems to have much more impact on the p_f than the actual variability of the parameter. Overall, by utilizing USACE [90] classification and considering the 100-year flood event (139.21 m a.s.l.), the case study levee fits into the "hazardous" performance regard-ing piping mechanisms if the mean fragility curves are considered. Regarding the slope stability, for the worst-case scenario of steady seepage, the case study levee fits into the "poor" performance category. If the fragility curves for transient seepage of 5-day duration of the high-water event are analysed, then the probabilities of failure for slope stability in-dicate the levee have "below average" performances. With a lower variable friction angle, the situation significantly changes in favour of both SDCs, where the levee performance would be classified as "above average", while for the less variable cohesion the situation remains almost unchanged.

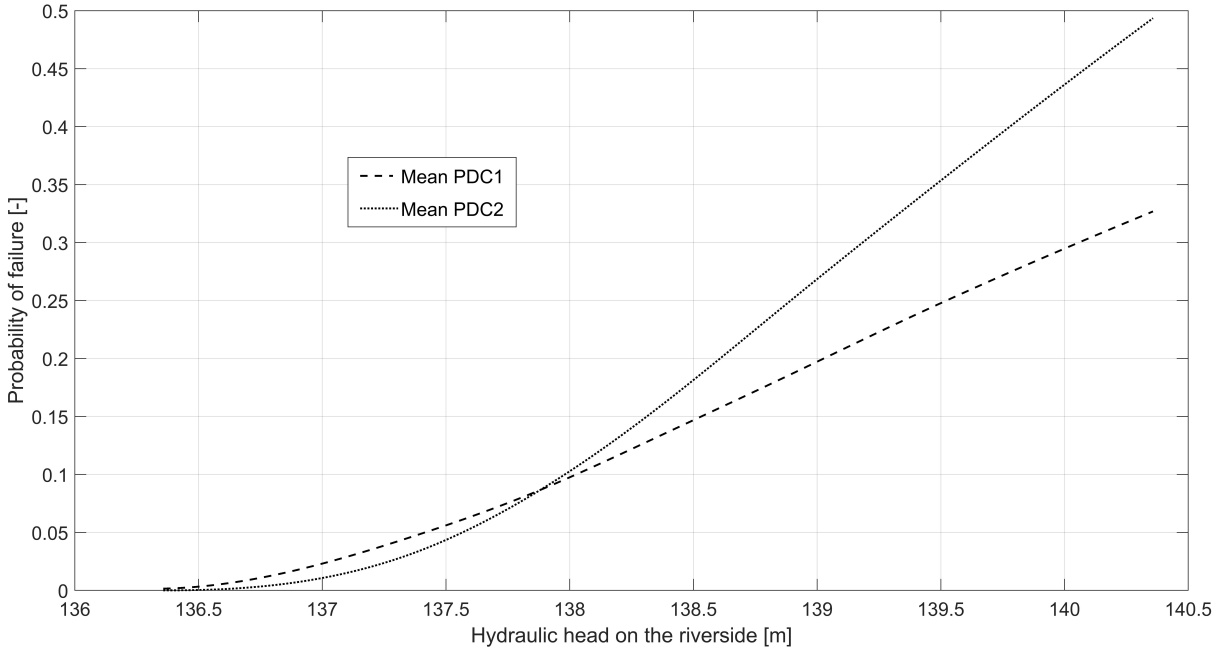

Figure 2.13. Probabilities of failure and respective reliability indices for levee slope stability.

2.5.3 Discussion on Calculation Assumptions and Recommendations for Future Work

Several assumptions are considered for the sake of calculation simplification and/or because of lack of data. These assumptions, as well their effect on the calculation results, are discussed.
Considering that the levee will be constructed of material of an undefined borrow site, there are no soil investigations to compute its scale of fluctuation, which is therefore assumed as infinite, meaning that all points in the soil region have the same properties. This yields conservative reliability calculations of levee stability. Additionally, the hydraulic conductivity is assumed as constant, and only the effects of its mean value, without inherent variability, are investigated. To consider the variability of hydraulic conductivity, with extremely high range of CoV values as reported by Baecher and Christian [29], a random field seepage analysis should be implemented if Monte Carlo procedure is utilized.
Further, water table on the landside of the levee was fixed at the levee landside toe level and this raised the free water surface inside the levee body during the high-water event. Such a realistic assumption results in higher probabilities of failure. Further, this study considered water to affect slope stability only in terms of pore pressures which lower the shear strength of the material. However, rising and lowering water levels induce cumulative internal erosional effects, eventually leading to levee material degradation. Since this effect is more pronounced with an increasing number of flooding events, numerical models which consider the internal erosion propagation caused by water flow through soil [62, 78, 80, 100–102] and its effects on mechanical and hydraulic properties [79] should be implemented in future probabilistic studies of levee stability.

Slope stability analyses were conducted with rising water levels until certain failure was reached. van der Meer, ter Horst, and van Valzen [58] note that levees can endure an overflow of 1 l⁄s (litre per second) if grass-cover is installed atop the crown and landside slope. However, it is unlikely that the landside slope with a clay and grass-cover will fail at discharges of less than 30 l/s [58]. If the latter is considered as representative for the case-study levee, and by utilizing Eq. (2.4), such discharge occurs at a water height of around 7 cm above the crown, which means the slope would actually fail before reaching the hydraulic heads used for slope stability calculation during the overflow.

This probabilistic study calculates levee slope stability by utilizing finite element and limit equilibrium analyses, coupled with Monte Carlo simulations to determine the probability of failure. For each slip surface, a fixed number of calculations was used (in this case 15 000) with randomly sampled soil parameters according to the assigned distributions, providing the p_f of each slip surface. The slip surface with the highest p_f was then pinpointed as the critical slip surface. However, such a procedure might underestimate the probability of failure of the levee slope, as it considers only specific slip surfaces one by one, without considering the possibility of a different slip surface occurring for each different set of soil parameters. Running the multiple deterministic analysis with variations of soil parameter values will lead to different critical slip surfaces. A combination of shear strength parameters may generate deeper surfaces, while others may generate shallow ones. Thus, imposing a slip surface onto a set of parameters, instead of determining the slip surface based on the parameters, will yield a lower p_f. Combining the various deterministic critical slip surfaces from one Monte Carlo simulation would be a collection of the most critical slip surfaces for each set of random variables realizations and would result in the probability of failure of the levee, instead of a specific slip surface. The quantitative effect of this change in probability calculation procedure could be investigated in future studies.

2.6 Conclusions

To provide the probabilistic evaluation of stability and piping as a failure mechanism which lead to the larger levee breaches, this study proposes a methodology for the development of fragility curves which give an insight into the probability of failure for identified mechanisms with respect to the riverside water level, including the overflow surge. As the variability of soil parameters, resulting from inherent soil variability, measurement error and transformation uncertainty govern the shape of fragility curves, the necessity for proper selection of each parameter statistic is stresses out. The methodology for development of stability fragility curves is based on the fusion of different types of numerical analyses including the total stress load deformation analysis to obtain a reliable levee stress state and seepage analysis to obtain distribution of pore water pressures. The results of these two analyses feed into the probabilistic LEM analysis. Considering how computationally expensive Monte Carlo simulations are, the presented

methodology minimises this disadvantage by combining the numerical analyses with LEM, which has the effect of decreasing the critical failure surface determination time. The necessity of separate stress analysis is additionally emphasized when overflow surge is considered, where equivalent shear stress, caused by water flow, should be applied. For the probabilistic evaluation of piping mechanism, the closed-form analytical Sellmeijer 2-force rule is the one being dominantly used in many state-of-the-art levee risk assessment methodologies.

The methodology was applied to a case study location of River Drava levee, a site which has shown a continuous trend of increased water levels in recent years. From the resulting fragility curves, it can be noted that the permeable crest layer affects stability substantially in cases where the water rises enough to start flowing through it. However, this effect becomes less notable as the ratio of the crown to body conductivities approaches 1. Moreover, if the duration of the high-water event is small enough so that it cannot achieve steady seepage through the levee, the effect also becomes less notable. Considering the soil variability, smaller variability offers increased stability up to a certain point, after which it has unfavourable effects. For the SDC1, this point was found at the crown height, but for SDC2 it was found only at hydraulic heads more than 2 m above the crown.

Regarding piping, even though values for parameters which were not available have been assumed based on correlations and recommendations, meaningful conclusions can still be obtained from the constructed curves. It has been shown how much the results can vary with changes to the investigated parameters—i.e., hydraulic conductivity statistics, effective grain size d_{70} and aquifer thickness, which emphasizes the importance of gathering relevant data for analyses. Additionally, the reduced variability of the hydraulic conductivity shows a favourable effect until a certain head height which depends on (not exclusively) d_{70} and aquifer thickness. After that point, the p_f increases. Since the mean value also changed together with the CoV, the effect shown in Figure 2.13 cannot be completely attributed to the change in variability, but by knowing the amount of change in each statistic their relative contribution is implied.

Since the proposed methodology includes several assumptions for the sake of calculation simplification and/or because of lack of data, this paper discusses them. However, with the lack of reliable data, conservative assumptions were usually made (e.g., higher soil parameter variability, longer flood duration, higher water levels, etc.). When each assumption introduces a small conservative effect, the effects stack and the probability of failure could be overestimated. With more data regarding variability of the levee and foundation soil's parameters, water levels and their durations, more reliable probabilistic analyses can be conducted.

Chapter 3

Fragility Curves for Slope Stability of Geogrid-Reinforced River Levees

Authors:
Nicola Rossi, Mario Bačić, Meho Saša Kovačević, Lovorka Librić
Paper status:
Published, https://doi.org/10.3390/w13192615

3.1 Introduction

River levees for flood protection are structures usually made from earthfill material, and their cross section can be made up of multiple distinct parts, which serve specific purposes in the protection from high waters. However, as Wang, Wang, and Zhang [20] noted, levees cannot completely exclude flood disasters, and living behind a levee poses unique flood risks since levees are designed to reduce the impact of a flood event at a certain scale.
Their stability is mostly affected by the material used for the levee body, the foundation material, and is also a function of the water level on the riverside. Often, due to cadastral parcels owned by the investor, stability cannot be ensured for required crown heights corresponding to defined return periods of flood events by using conventional solutions due to the need of building steep slopes to fit the levee into the parcel width. This issue is commonly solved by introducing ground reinforcement techniques that allow for steeper slopes. One common technique in such structures is the reinforced fill built by placing geosynthetic layers during the construction or reconstruction of a levee. The use of geosynthetic materials generally in reinforced earth structures started to increase after 1971 when the first geotextile reinforced wall was constructed in France, and their beneficial effect was noticed. At a later date, around 1980, geogrids were developed [2]. Nowadays, geosynthetics are widely used in various fields of geotechnical engineering, such as shallow footing to increase bearing capacity and decrease settlement [124–126], retaining walls [127–129], and road construction [130, 131]. When used

in levees, their benefit has also been shown in decreasing settlement of levees on soft soil [132] and increasing slope stability [133], or both. Their effects have been studied under undrained [134, 135], partially drained [135], and drained [136] conditions, during and after embankment construction. Hird and Kwok [134] studied the stress distribution in the geosynthetic element depending on its stiffness, and the strength and stiffness of the embankment material. As the levees can be made from various materials, Balakrishnan and Viswanadham [137] studied the tensile load-strain behaviour of geogrids embedded in different soil types and under variable normal stress. Other ground reinforcement methods can also be combined with geosynthetics. For example, Zheng et al. [138] have used stone columns in conjunction with geosynthetics to achieve stable embankments on soft soil and have studied their interaction.

Studies have shown the stability benefit of using geosynthetics to ensure embankment stability, as well as the economic advantages, with the help of limit equilibrium based methods [64, 139, 140] and numerical methods [135, 141, 142] in 2D and 3D [143], physical models [144], as well as various other methods mentioned by Tandjiria, Low, and Teh [145]. In practice, the most used method is the limit equilibrium due to its simplicity, despite all the limitations and assumptions, which has shown good performance in real-life problems [145].

The introduction of geosynthetics for stability, mostly geogrids, is significant not only because it means a higher stability, but also because it is a reinforcement element which can be made from various materials (polyester, polypropylene, polyethylene, polyamide, polyester, and polyvinyl chloride) [146], and whose characteristics can be controlled during their production, which in turn means a higher reliability in their parameters' values and less variability. Nevertheless, some variability within geogrid parameters can still arise from various sources, namely biases regarding strength reduction factors, which consider installation damage, creep, and durability.

As Rowe and Soderman [139] stated, geosynthetics can fail by two mechanisms, either on the soil–reinforcement interface, or internally as the rupture of the reinforcement element itself. To resist the tensile rupture of the element, the resistance is straightforwardly calculated by using the material's parameters and the cross section. To resist pull out, multiple effects are in place, whose relative contribution to the total pull-out resistance effect has been studied by various authors [144, 147, 148]. When such elements are placed within a levee, a few failure modes can be expected, namely internal, external, and compound [149], as shown in Figure 3.1. Internal stability refers to slip surfaces which pass entirely through the reinforcement layers, which means that the reinforcement failed either by tensile rupture, or by pull out. External failure refers to deeper slip surfaces which go around all the reinforcement layers. The compound failure is the most common type, where the slip surface goes around and through various reinforcement layers. On top of those mentioned failure modes, if the spacing between neighbouring reinforcement layers is too big and secondary reinforcement is not provided, failure can initiate by soil sliding between those layers, which then leads to a global failure. Thus, geogrid reinforced slope sections usually consist of primary or principal, and secondary or intermediate, geogrid layers [2, 149–151]. Failure of the slope can also occur without the need

of reinforcement failure, i.e., if the reinforcement is a low stiffness geosynthetic whose failure strain is much larger than the strain at which the slope fails, then the whole slope might fail without reaching any of the previously defined geosynthetic failure mechanisms [139]. Which failure mechanism will occur in a levee highly depends on the cross section of the levee and whether it is a newly constructed levee or a reconstructed one, because these parameters will dictate the placement of geogrids. Even though levees are characterized by a number of failure

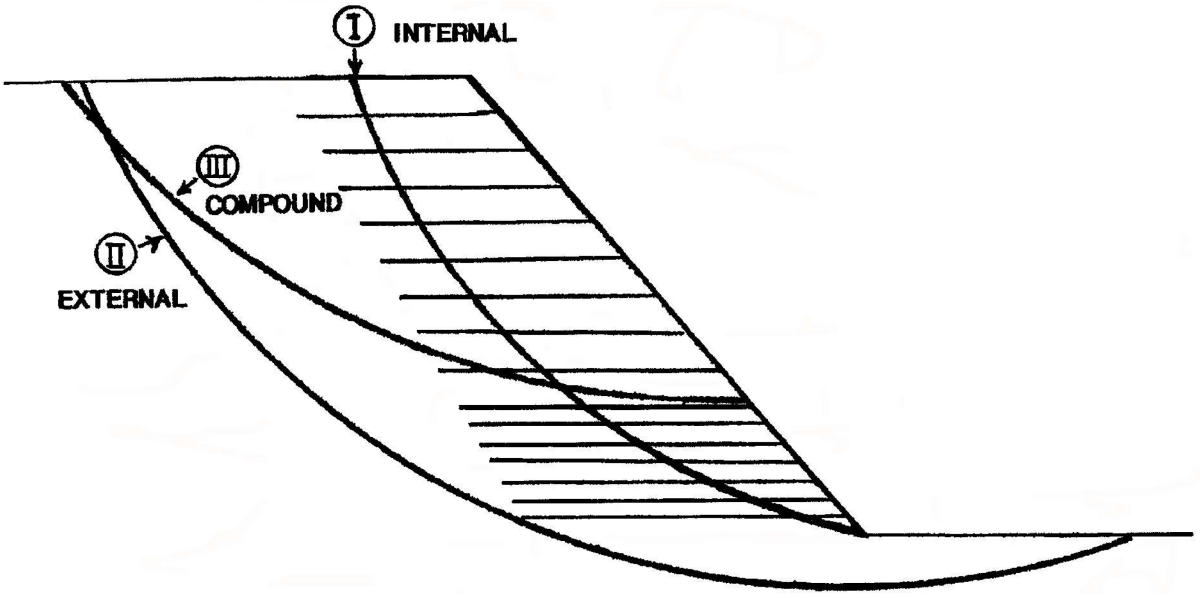

Figure 3.1. Failure modes of reinforced slopes [2].

mechanisms [24, 152], and that about half of earth embankment failures occur as a result of processes related to piping [153], this study considers only the slope stability of a reconstructed and additionally reinforced river levee. The primary purpose of this study is to investigate the sensitivity of reinforced levees to rising water levels and uncertainties in geotechnical materials, while also promoting the usage of probabilistic analyses which can take those uncertainties into consideration. Thus, probabilistic analyses are conducted with the objective of quantifying the effects of uncertainties related to geogrid reinforcement on the slope stability of levees, and to construct fragility curves which show the probability of failure of the levee for any water level. Such probabilistic slope stability analyses can be conducted using numerous methods [36, 37, 48, 65, 70, 76, 154–156]. In this study, the limit equilibrium method is adopted due to its simplicity and wide usage in geotechnical practice, while results are further processed with programmed probabilistic methods to find the probabilities of unwanted behaviour of the levee subjected to various water levels with steady state conditions. The statistical techniques and probabilistic methods used in this study are the Response Surface Method (RSM) and the First Order Reliability Method (FORM), which have been programmed with MATLAB. The variability values of random variables used for probabilistic calculations are selected as reported in literature. Since the considered sources of variability of geogrids include the long-term degradation, and no seismic event is considered, the conditions considered for the whole levee are

drained. The case study is described in Section 3.3.
Fragility curves, which will be constructed as a result of this study, are curves showing the conditional probability of an unwanted behaviour occurring as a result of increasing the design event intensity. Their usage in civil engineering began in, at least, 1980 with the work of Kennedy et al. [32] related to the safety of a nuclear power plant. Later, their usage in flood protection started in 1991 with a USACE Policy Guidance Memorandum [33], followed by a further explanation in a 1993 USACE Engineer Technical Letter [34], as reported by [35]. Today, their usage in slope stability is widespread [35–37], with regards to seismic events, rainfall, and rising water level.

3.2 Methodology

In this study, the Hasofer–Lind method is employed [157], also known as the First Order Reliability Method (FORM), together with the response surface method (RSM) for approximatively calculating the reliability of the flood protection embankment. The RSM is a statistical technique used to approximate the response of a model to input variables by using a suitable function when the true relationship is unknown. The approximation is done by fitting the selected function to the original model evaluated at multiple sample points, i.e., the coefficients of the function are determined by an error minimization technique. It is chosen as a relatively simple tool to complement the FORM by defining the required performance function. In this study it is used to construct an n-dimensional surface which approximates the response of the levee, where n is the number of random variables, based on known function values and on regression analysis. The surface used in this study is a quadratic function defined by a second-order polynomial, as shown in Eq. (3.4). The coefficients of the function are obtained by minimizing the error between the original and approximated functions [158]. After that, the probability of failure is obtained through FORM optimization. The FORM is an upgrade to the First Order Second Moment (FOSM) method with its geometrical interpretation of the reliability index, which is invariant to the performance function format. To employ it, the first step is to convert all random variables to independent variables in the standard normal space with zero mean and unit standard deviation, and the performance function needs to be known. It offers a solution which defines the reliability index (β) as the shortest distance from the failure function (defined by RSM and the performance function) to the origin of the standard variable space, which is the mean of the joint probability distribution, and is the most efficient method for estimating p_f for problems involving one dominant failure mode [159]. Rackwitz [160] noted that, for 90% of all application, the FORM fulfils all practical needs, and its numerical accuracy is usually more than sufficient. Since all the random variables are normally distributed and independent, the transformation to the standard normal space is simply done by Eq. (3.1) [161].

$$\overline{x_i} = \frac{x_i - \mu}{\sigma} \tag{3.1}$$

where ($\overline{x_i}$) is the standard normal variable value, μ the mean value of the original variable, and σ the standard deviation of the original variable.

The first step in the analyses is to determine the number of random variables to be used, and their respective statistics. The mechanisms of failure of the geogrids are the rupture of the elements, or the pull out of the grid from the soil. Regarding the tensile strength, as there are three rows of geogrids reinforcing the body, the ultimate tensile strength of each of them is simulated as an independent random variable. The interaction between reinforcement and soil depends on various factors, including grid parameters such as roughness, grid opening dimensions, thickness of transverse ribs and deformability characteristics, as well as soil parameters such as friction angle, grain size distribution, particle shape, density, water content, cohesion, and stiffness [2]. For the pull-out parameters in this study, the soil–grid interface friction is taken as a fraction of the soil internal friction angle, while the cohesion is ignored. As the soil–grid interface friction depends on the friction angle of the material which covers the grid, the internal friction angle of that material is also taken as a random variable. Thus, a total of 4 random variables are considered (Table 3.3). Since there is no face anchorage, the sliding of the soil on the soil–grid interface can happen on either end of the grid, i.e., inside the body or at the face. Throughout the analyses, a specific soil-grid friction ratio is kept constant to investigate the behaviour at various ratios. The analyses are performed for three design cases with different interface friction, named here as SIF (small interface friction), MIF (mean interface friction) and HIF (high interface friction). Sia and Dixon [162] analysed the variability of interface strength parameters between soil and geotextiles or geomembranes in coarse- and fine-grained soils. In this paper, the ratio is held constant as a deterministic parameter. For the MIF case, a contact friction angle of 2/3 ϕ is used, which is the recommended conservative value for geosynthetics [2]. This is closely in agreement with values obtained by Yu and Bathurst [163] who used a reduction factor applied to the tangent of backfill friction angle of 0.5–0.8, with the best agreement between pull out tests and numerical model results being 0.67 or 2/3. Other studies propose different values, e.g., Ferreira et al. [133] define the interface friction angle as 6/7 ϕ, while Jewell [164] takes a factor of 0.8 as the "direct sliding coefficient" as a value to "safely encompass most practical cases". In this study, the factor 0.67 is used as the mean value but applied directly to the friction angle instead of its tangent (which is equivalent to applying a factor of 0.63 to the tangent). For the other two cases, SIF and HIF, interface friction ratios of 0.5 and 1 are used, respectively.

Next, an arbitrary number of different deterministic slope stability analyses are conducted for each water level by varying the random variables' values. In this study, this is achieved with the help of Latin Hypercube simulations, which varied the grids' strength for each chosen friction angle. All the variables' values are then transformed into the standard normal variable space by Eq. (3.1), and the resulting safety factor is corrected accordingly with the appropriate performance function, as follows. The performance function is defined for two cases and shown in Eqs. (3.2) and (3.3), one for failure condition where $FS = 1$ (ULS), and one for an arbitrary safety factor value of $FS = 1.5$. The "probability of failure" calculated for the second

case actually refers to the probability of reaching the defined threshold. When the performance functions defined by the left and middle terms in Eqs. (3.2) and (3.3) are equated to zero, this becomes the limit state function which defines failure or unwanted behaviour. Deterministic slope stability analyses, as well as steady seepage analyses, are conducted using Slide2 v9.009, Rocscience Inc , Toronto, Canada.

$$g(\overline{x}) = F_S - 1 = 0 \tag{3.2}$$

$$g(\overline{x}) = F_S - 1.5 = 0 \tag{3.3}$$

Such defined groups consisting of standard normal variables' values and the respective performance function values for each water level are fitted with a polynomial shown in Eq. (3.4) [165].

$$g'(\overline{x}) = c + \sum_{i=1}^{N} b_i x_i + \sum_{i=1}^{N} \sum_{j=1}^{N} a_{ij} x_i x_j \tag{3.4}$$

The $g'(\overline{x})$ symbolizes an approximation of the real performance function, where c, b, and a are its coefficients, N is the number of random variables, and x the random variables' values. The fitting is done in MATLAB by minimizing the sum of squared residuals with the *lsqcurvefit* function, where the value or the performance function and the random variables are known. The results of such minimization are the coefficients c, b, and a for a polynomial, which approximates the performance function in the vicinity of the design point (1 or 1.5). Now that the coefficients are known, a constrained optimization (minimization) is run. What we are searching for is the minimal value of the Euclidean norm of the standard normal variables which satisfies the condition that $g(\overline{x})$. This is done by minimizing the vector of standard normal variables $\mathbf{x}_i$ with the constraint $g(\overline{x})$, by using the MATLAB function *fmincon*.

$$\beta = \sqrt{\mathbf{x}_i' \cdot \mathbf{x}_i} = min \tag{3.5}$$

The result is, (1) the reliability index β defined as the shortest value of the radius vector $\mathbf{x}_i$ which defines the limit state function, and (2) the standard normal variables' values x_i which give the previously defined distance. After a few iterations, these values converge towards the true limit state function. When the difference between two iterations becomes negligible, the procedure stops. This is usually achieved within 2–4 iterations for this study. Each iteration contains new deterministic slope stability analyses with new random variables' values, which resulted from previous iterations. To calculate the probability of failure from the resulting reliability index, the cumulative standard normal distribution is calculated for the reliability index with inverted sign. As the optimization needs a set of starting values, they are varied for the same calculation to check for the robustness of the result and for local minima. Another quality check is made by plotting surfaces in a 3-dimensional space by ignoring 2 of the random variables. To accept the result, not only is a small change in consecutive iterations needed, but also the quality

of regression be-tween the real performance function and the approximated one, as shown in Eq. (3.6) [56], needs to be ≥ 0.95.

$$R^2 = 1 - \frac{\sum_{i=1}^{r}[g(\overline{x}) - g'(\overline{x})]^2}{\sum_{i=1}^{r}[E[g(\overline{x})] - g(\overline{x})]^2} \rightarrow 1 \tag{3.6}$$

where $E[g(\overline{x})]$ is the expected value of the performance function, simply taken as the arithmetic mean of all the deterministic performance function values. On top of that, the mean square error (MSE) is also calculated by Eq. (3.7), and the results varied between 5×10^{-6} and 2×10^{-19}. The whole process is repeated for various water levels, and fragility curves are constructed.

$$MSE = \frac{1}{n}\sum_{i=1}^{n}[g(\overline{x}) - g'(\overline{x})]^2 \rightarrow 0 \tag{3.7}$$

The previously discussed methodology for the development of fragility curves for levee stability, summarized in Figure 3.2, requires the proper water pressure state to be established. For the design situations which include water level up to the top of levee crown, numerical analyses include commonly used boundary conditions of properly defined hydraulic heads on the riverside and landside. However, as Librić, Kovačević, and Ivoš [166] found in their study, the overtopping of the case study levee has a high risk exposure compared to other risks, thus overflow is also considered in this study. Overtopping (i.e. overflow) is usually a result of a high-water event (surge), or it can occur due to wave overtopping. The combined effect of surge and wave overflow is discussed by many authors [73, 74, 94]. However, for the river levee considered, only a surge type of overflow is relevant. When the water level rises higher than the crown, the stress analyses are supplemented with the addition-al boundary shear stress along the crown and landside slope. Additionally, a trapezoidal stress is applied over the crown during overflow to simulate water pressure, corresponding to the height of water on the upstream side, and to the water height on the down-stream side calculated by Eq. (3.10). Given that this aspect goes beyond standard analyses, a cautious evaluation of these shear stresses is required. The boundaries of both analyses are defined far from the levee region, enough to not affect the results. Seepage analyses require only hydraulic boundary conditions, which in this case consist of constant or varying hydraulic head values applied on lateral boundaries and on the top boundary of the model, up to the required height. During surge overflow, the water velocity increases down the slope until a terminal velocity is reached at equilibrium between water momentum and slope frictional resistance, after which the flow becomes steady and the velocity can be calculated by the following equation:

$$v_0 = \left[\frac{\sqrt{\sin\Theta}}{n}\right]^{3/5} \cdot q_0^{2/5}[m/s] \tag{3.8}$$

where v_0 [m/s] is the steady flow velocity, Θ [°] is the landside slope angle, n [-] is the Manning's coefficient, and q_0 (m^2/s) is the steady discharge [73]. For supercritical flow, which de-

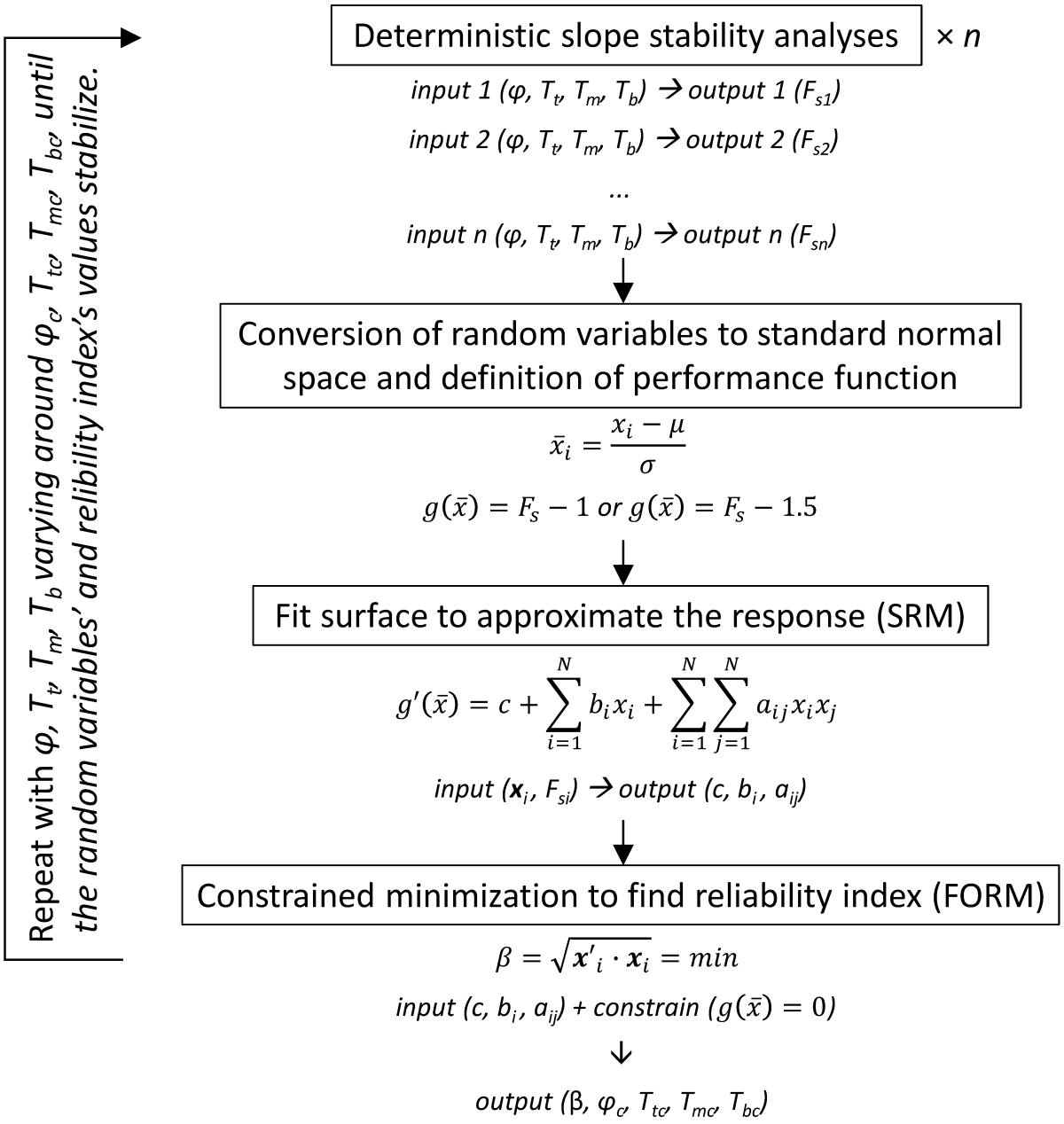

Figure 3.2. Flowchart of the applied methodology.

velops on the landside slope—as shown in Figure 3.3—Hewlett, Boorman, and Bramley [119] proposed a value of Manning's coefficient of $n = 0.02$, relevant for slopes of 1:3. The discharge over the levee crown can be calculated using the equation for flow over a broad-crown weir, which gives slightly conservative results due to not taking into consideration frictional losses [72]:

$$q = \left(\frac{2}{3}\right)^{3/2} \cdot \sqrt{g} \cdot h_1^{3/2} [m^2/s] \tag{3.9}$$

where g $[m/s^2]$ is the gravitational acceleration and h_1 [m] is the upstream head (elevation over the levee crown). If a steady flow is assumed, the discharge is constant along the slope. Therefore, the height of water perpendicular to the slope in the steady, uniform flow area for

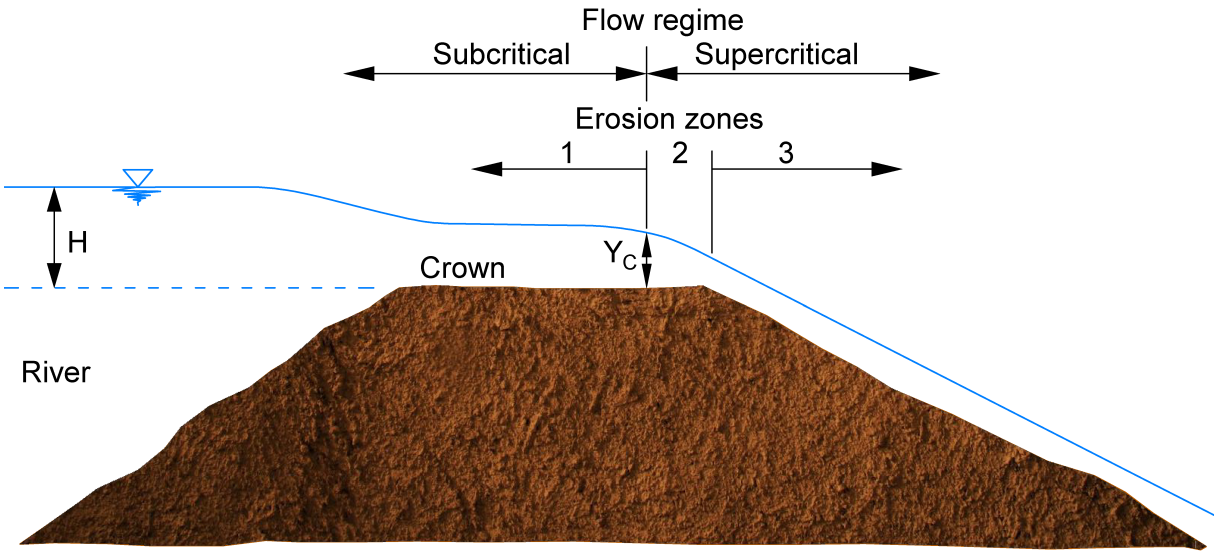

Figure 3.3. Flow regimes during overflow of a dam, re-drawn from [1].

unit length of the levee can be calculated from Eqs. (3.8) and (3.9) as:

$$h = \frac{q}{v_0}[m] \tag{3.10}$$

Finally, when steady, uniform, flow is reached, the shear stress resulted from surge overflow, is equal to:

$$\tau_0 = \gamma_w \cdot h \cdot \sin\Theta[kPa] \tag{3.11}$$

where γ_w $[kN/m^3]$ is the unit weight of water. Eq. (3.11) conservatively overestimates results, since the resulting pressure is a little bit higher than the pressure in area above the steady flow [94]. Shear stresses calculated this way are applied along the crown and land-side slope, as shown in Figure 3.4 for the case study numerical model. Stability analyses aim to find the

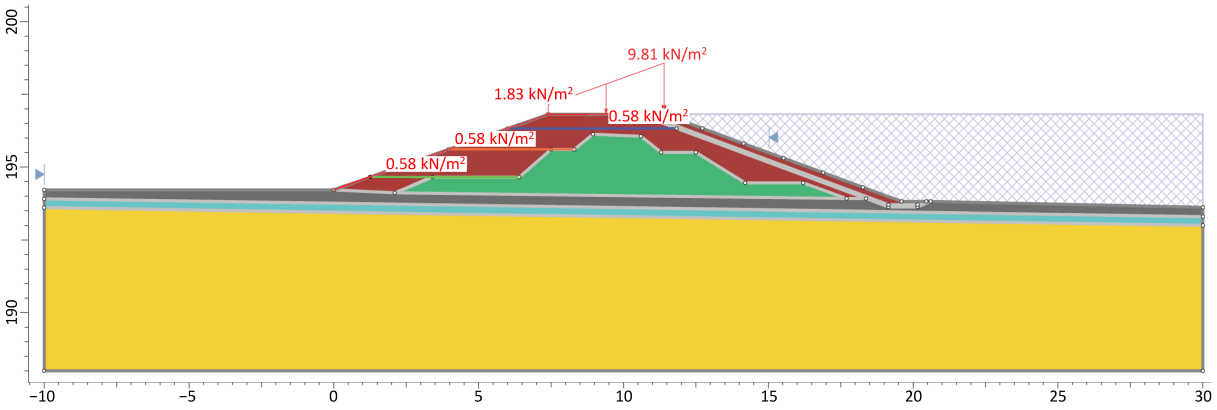

Figure 3.4. Numerical model for analyses of case study levee.

critical slip surface by using a population-based stochastic algorithm, Cuckoo Search, which searches for non-circular slip surfaces, together with Monte Carlo optimization to potentially find even more critical surfaces [167]. All the slope stability analyses are deterministic with

values of the four random variables previously described varied over appropriate ranges, while probabilistic analyses are conducted after the results of deterministic analyses are obtained. The variation is manually performed for the friction angle, while for the geogrids it is performed with the help of Latin Hypercube simulations. It was initially conducted over a range of $\pm 3\sigma$ with steps of 1σ to detect the approximate location of the design point and was then corrected to small-er steps closely spaced around the design point.

3.3 Case Study

River Drava, with the overall length of 710 km, flows from Italy to eastern Croatia where it merges with Danube, and is historically known for major flood events [106], where prominent events occurred in last several years. For this case study, a reach of a 3.7 km long section of flood protection embankment running from Otok Virje to Brezje on the Drava River in Croatia is analysed. The reach lies on sediments from the Holocene period. They are mostly sediments of the first alluvial terraces of Drava, composed of large amounts of sand and gravel, which at places surpass 100 m in depth. Closer to the surface, layers of silty material can be found.
In 2012, a water level of 1000-year return period was measured in the Drava River, which caused the overflow of the embankment over a length of more than 1 km, and breaching over a length of 50 m, causing huge damages to the surrounding area. Since the original embankment was built in 1968 with the design high water level from 1965 [168], a reconstruction of the existing embankment is required for raising its crown height to new design water levels. The new required height corresponds to the new 100-year return period water level +1 m, which is between a few centimetres and 1 m above the old crown. Raising the height also implies a widening of the embankment cross section, which can be accomplished in three ways: by keeping the existing embankment on the landward side of the new one (i.e., reconstructing towards the river side), keeping the existing embankment on the river side (i.e., reconstructing towards the landward side), and by coinciding the existing and new axes (i.e., reconstructing on both sides). The selected reach for this case study is defined by the reconstruction direction and subsoil stratigraphy—the reconstruction on both sides is chosen. A situational view of the embankment section on the Drava River is shown in Figure 3.5.
To prove the stability of the newly reconstructed embankment in all the relevant de-sign situations, calculations are made using deterministic limit equilibrium analyses, and all according to valid norms for geotechnical design, i.e., EN 1997-1:2012 Eurocode 7: Geotechnical design—Part 1: General rules and its respective Croatian national annex for static design situations, EN 1998-1:2011 Eurocode 8: Design of structures for earthquake resistance—Part 1: General rules, seismic actions and rules for buildings and its respective national annex for seismic design. The analyses resulted in the deterministic safety factors shown in Table 3.1. It can be seen that safety factor values for all design situations are acceptable. The reconstruction of the levee is made with well graded gravel (GW by USCS classification). Since gravel is highly permeable, GCL

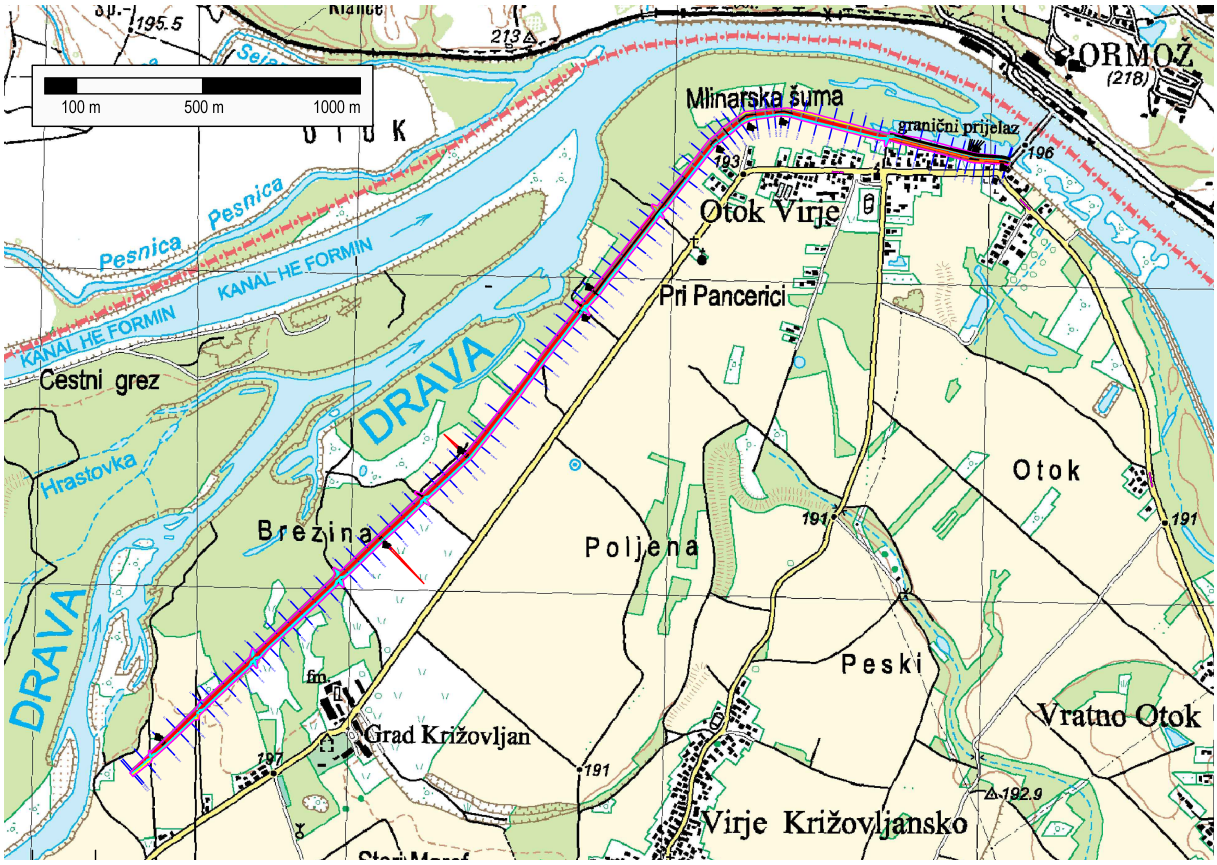

Figure 3.5. Situational view of the levee section.

membranes are used to make sure the free water surface stays inside the levee body during high water events. Suzuki et al. [169] performed field and laboratory tests with various types of GLC to find their effect on the stability of the embankments. However, since the GCL in this study is located on the riverside of the levee, while the stability of the landside is analysed, their effect is not relevant for this study. Other than that, the body is further strengthened using TENAX TT 045 GS, HDPE uniaxial geogrids. The embankment's cross section used in calculations is shown in Figure 3.6. Geogrids are placed on 0.7 and 0.9 m distance from one another to fit the height of the embankment, while the maximum suggested height for reinforced slopes as per [151] is 1 m due to local face stability. This way, local face instabilities are partly mitigated. Instabilities on the landside may also be initiated by surface erosion during overflow. The resistance against such action can be increased by placing a reinforcing layer of standard geosynthetics or other specific products [170] such as biopolymers [56, 57] over the slope, but in this case, there is no such additional protection. The same applies for the riverside slope where surface erosion might be caused by the flow of the river and during the rapid decrease of water level in the river (RDD).

Table 3.1. Deterministic safety factors for the cross section of interest in various design situations.

Design Situation					Safety Factor[1]
Reconstruction on both sides of the existing levee	Low water	Riverside	Static + traffic	Drained	1.79
			Seismic (475-year RP)	Undrained	1.47
		Landside	Static + traffic	Drained	2.18
			Seismic (475-year RP)	Undrained	1.48
	High water (100-year RP)	Landside	Static + traffic	Drained	1.72
			Seismic (475-year RP)	Undrained	1.49
	Water at crown height	Landside	Static + traffic	Drained	1.66
	RDD	Riverside	Static	Drained	1.21

[1] Analyses are made using EC7, DA3, thus the minimum required safety factor is 1.

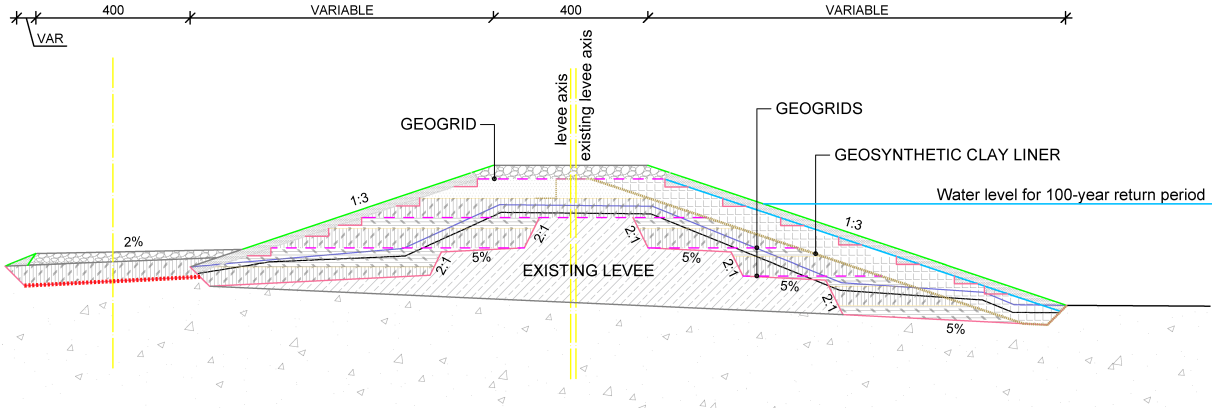

Figure 3.6. Levee cross section.

3.3.1 Variability of Materials' Parameters

Deterministic parameters for all soils are carefully chosen from the available laboratory and field data conducted by the authors of this paper. The mean values of geogrid parameters are taken from the manufacturer's specification sheet. Statistics for the parameters assigned as random variables are chosen from literature. Table 3.2 shows the design values of deterministic parameters for each material, while Table 3.3 shows the statistics of the random variables. As all three grids inside the embankment are the same, their statistics are also the same, but each grid is modelled as an independent random variable. The statistical parameters for the geogrids are determined as follows. The mean value is taken from the manufacturer's specification sheet where the characteristic value is divided by a series of factors, namely the factor for installation damage (RF_{ID}), creep (RF_C), and degradation due to chemical and/or biological processes (RF_D), to obtain a design tensile strength of 18.5 kN/m. To transform the manufacturer's proposed long term design strength into a random variable, it is first multiplied with the mean

Table 3.2. Deterministic values of parameters.

Material	USCS Symbol	ϕ_d [°]	c_d [kPa]	γ_d $[kN/m^3]$	k [m/s]
Reconstruction material	GW	Random	0	20	2.5×10^{-2}
Existing body	SM	25.1	1.6	19	1.4×10^{-5}
Thin surface layer	MI	18.8	3.3	19	5×10^{-6}
Second thin layer	SP–SM	25.6	0	19	4.7×10^{-4}
Foundation soil	GP–GM	28.4	0	19	8.6×10^{-4}
GCL[1]		-	-	-	1×10^{-7}

[1] GCL is only relevant in seepage modelling

Table 3.3. Statistics of random variables

Material	Tensile strength [kN/m]		Friction angle [°]	
	Mean	CoV	Mean	CoV
Geogrids	19.06	0.122	-	-
Reconstruction material	-	-	35	0.1
Distribution	Normal		Normal	

values of bias factors for installation damage ($\mu_{X_{ID}}$), creep (μ_{X_C}) and durability (μ_{X_D}), whose statistics are determined from literature [26, 171–173] to obtain the mean, while the CoVs of different bias factors are together taken as the CoV for tensile strength (Eq. (3.12)). Theoretically, this is valid for uncorrelated log-normal random variables, but with small CoVs it is sufficiently accurate for uncorrelated normal random variables [174]. Since the durability factor is mostly project-specific, it is taken with an arbitrary $CoV = 0.1$ [172]. Chosen statistics for all factor's bias values are shown in Table 3.4. The chosen geogrids are made from HDPE (High Density Polyethylene), which showed the lowest mean and CoV of the bias factors values, and their statistics are found to be independent of soil type [172]. As the random variables of the geogrids are normally distributed [172] and uncorrelated, the simple conversion to standard normal variables as shown in Eq. (3.1) can be employed.

$$CoV = \sqrt{CoV_{X_{ID}}^2 + CoV_{X_C}^2 + CoV_{X_D}^2} \tag{3.12}$$

Since partial factors in various design approaches are calibrated using reliability analyses [175], the mean friction angle of the reconstruction material is left at its characteristic value and the variability is applied to it, while all the other deterministic values are factored using partial factors from Eurocode 1997 DA3.

Table 3.4. Statistics for reduction factor's bias values

Statistics	X_{ID}	X_C	X_D
Mean	1.03	1	1
CoV	0.06	0.036	0.1

3.4 Results and Discussion

During slope stability calculations at higher water levels, small variations in random variables' values resulted in shallow and deep sliding surfaces with highly different safety factors, such as those shown in Figure 3.7. In such cases, the shallow and deep surfaces are separated, and two probabilities of failure are calculated, one pertaining to the shallow sliding and the other to deep sliding. Fragility curves are then constructed for two limit states defined by safety factors 1 and 1.5 (LSF10 and LSF15 respectively), for both types of failures. Figure 3.8 shows the resulting fragility curves for the two limit states, for varying water levels from the toe to the crown of the levee (located at 196.8 m.a.s.l.), and over to simulate surge overflow. The water level is increased until almost certain failure is ensured. However, Rackwitz [160] noted that FORM works well only for sufficiently large reliability indices, which he defined as $\beta > 1$, as otherwise it might not be the best linearization point [176], which in this case corresponds to water level of around 200.5 m.a.s.l. for LSF10, and 196 m.a.s.l. for LSF15. The curves used to fit the points are represented by general sigmoid function with the following equation [177]:

$$f(x) = p_{f,min} + (p_{f,max} - p_{f,min}) / \left(1 + 10^{[(\overline{H}-x)\cdot k]}\right) \tag{3.13}$$

where $p_{f,min}$ and $p_{f,max}$ are minimum and maximum values of the function respectively, $\overline{H}$ the mean hydraulic head, and k is the slope of the curve at the mean value. The curve is fitted to the points using least-squares. By using such a function, a curve can be defined even by not having the whole range of points from zero to one probability of failure. As can be seen from the figures, for the cases where the limit state function is defined by $FS = 1.5$ (LSF15), the probabilities of failure occur over the whole range, and certain limit-state behaviour with probability of one is already reached at the crown water level. For the limit state function defined by $FS = 1$ (LSF10), the maximum calculated probabilities of failures reach from around 65% to as low as 10%, while the rest of the curve is based just on the fitting to those smaller values.
From the diagrams it is seen that with increasing interface friction, the distinction between shallow and deep surfaces starts to show earlier, i.e., at lower water levels, for LSF10. For $\delta/\phi = 0.5$, the distinction occurs at $p_f > 0.3$, for$\delta/\phi = 0.67$ at $p_f > 0.05$, and for $\delta/\phi = 1$ at $p_f > 0.002$. Regardless, this effect never reached water levels as low as the levee crown for this case. For the LSF15, the distinction occurs at lower water levels rather than higher and is not so large, which is the reason why it is not noticeable on the normal scale. Also, the interface friction in this regard does not have any noticeable effect in this case. At water levels where there is

no distinction between deep and shallow surfaces, this happens because of two reasons. One is that all the failures occurred as either deep or shallow failures, and the other is that there is little distinction between safety factors of deep and shallow surfaces. The first reason indicates that the curves are constructed for the stability of the slope regardless of the failure mode, as long as all the surfaces followed the same mode. Only when different modes appear, the curves become separated.

Even though the diagrams for both limit states seem to merge at lower water levels, obviously

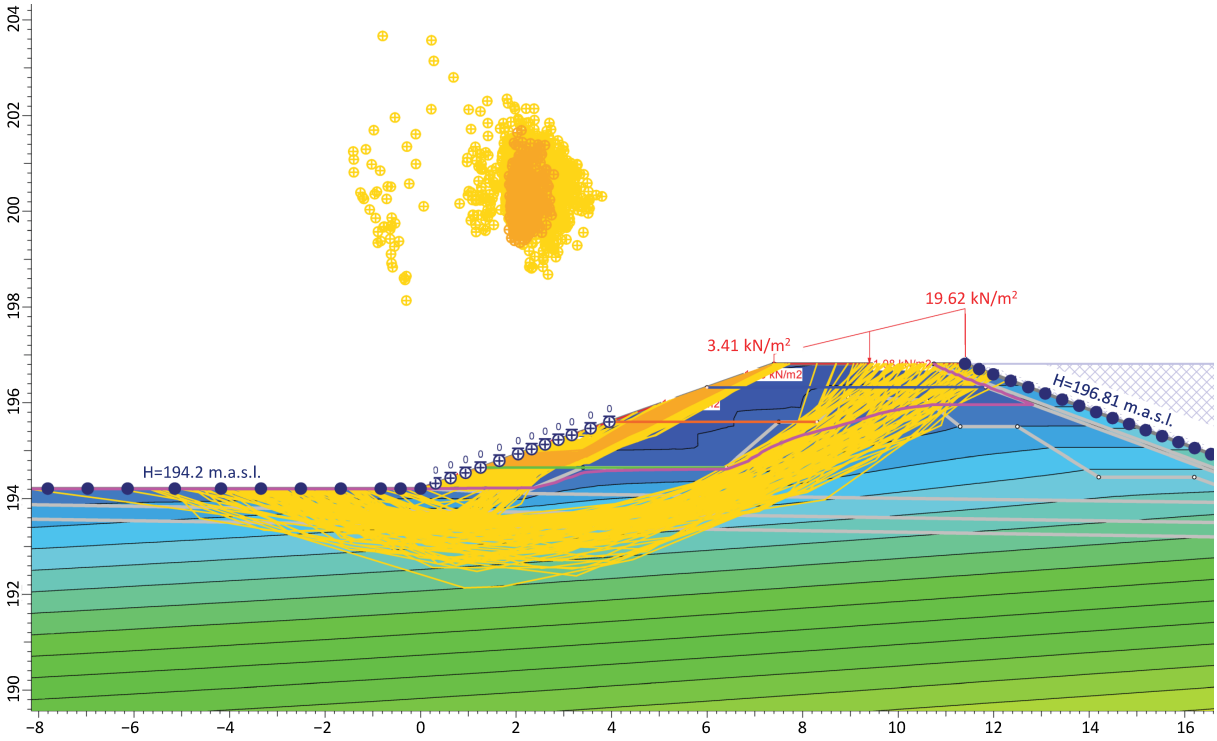

Figure 3.7. Shallow and deep surfaces on a characteristic slope stability analysis.

this is not the case because the diagrams refer to different limit states which cannot be achieved with the same strength parameters for a specific water level. Thus, Figure 3.9 shows the diagram in a logarithmic scale to see the difference at lower water levels. The LSF15 points can still be approximated as relatively good by the same sigmoid function. For LSF15 the probability of failure starts to noticeably increase only after the water level reaches circa 60% of the levee height. On the other hand, the LSF10 points have a worse fit which is caused by the fact that the p_f stays almost the same for water levels between 0 and the levee crown, and start to substantially change only for the surge overflow. Thus, to fit the LSF10 points, the first point referring to a no-water situation is ignored. The reason for the constant probability of failure is that the parameters needed to achieve the defined limit state are such that they produce small slip surfaces on which water has no effect in this case. This means that regardless of the water level up to the crown, the p_f of the levee stays the same. It can be noted from the figures that deeper failure surfaces are generally less likely to occur during failure than shallower surfaces. This is certainly conditioned by the fact that the levee body through which the deeper surfaces

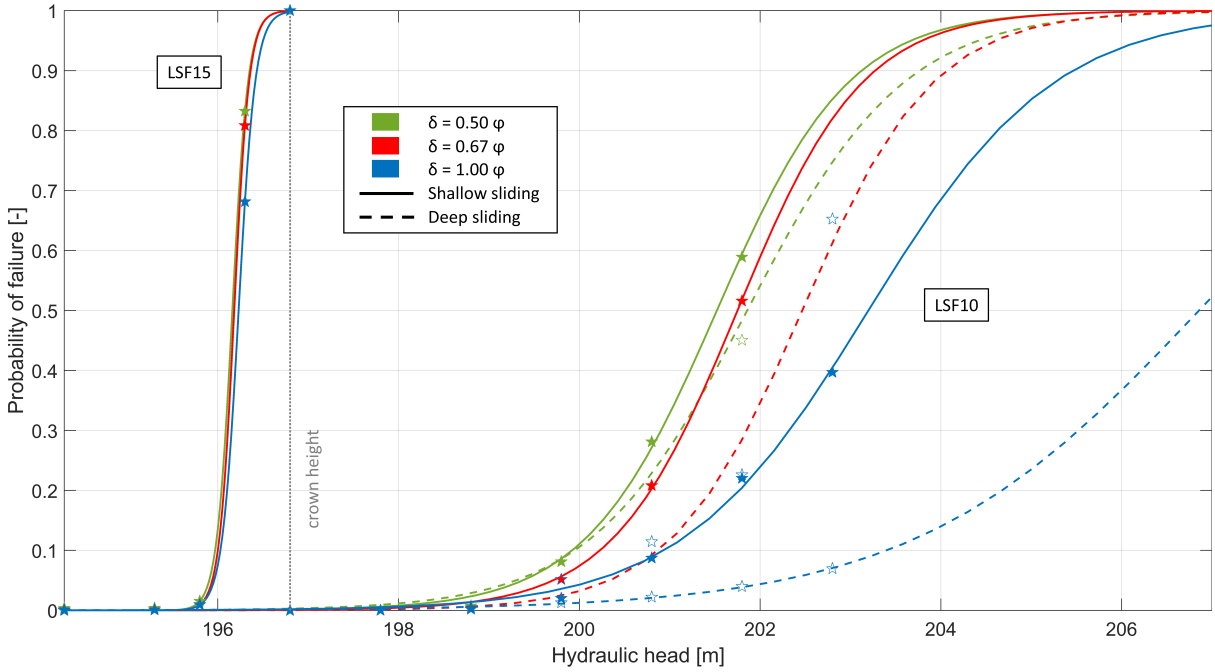

Figure 3.8. Fragility curves for LSF10 and LSF15, for shallow and deep surfaces, and all interface friction angles.

pass has been modelled as a deterministic material. An interesting thing to note for the minimum friction LSF15 case is that the points which refer to deep surfaces show a slight decrease of p_f with the increase of the water level at the beginning of the curve. This means that for the lower water level there is a higher probability that the levee will fail overall, than there is for the higher water level that the levee will fail through deep sliding. The reason for such behaviour is because, for the smaller water level, no deep surfaces are found. For other interface friction angles, these two values are quite similar.

While interpreting the results of computed conditional probabilities of failure, it must be kept in mind that they are calculated based on only one point closest to the origin, de-fined by the reliability index. This implies the linearization of the limit state function for integration below the standard normal joint distribution, which can lead to an overestimation or underestimation of the real probability, depending on the true shape of the limit state function [161]. To investigate their shapes, 2D representations of the limit state functions for mean interface friction, and for LSF10 and LSF15, are shown in Figure 3.10, where the black lines represent LSFs for soil internal friction and top grid strength as random variables, red lines LSFs for soil internal friction and middle grid strength as random variables, and blue lines LSFs for soil internal friction and bottom grid strength as random variables. The rightmost curves correspond to higher water levels, decreasing towards the leftmost curves. The circles in Figure 3.10 represent the standard normal joint distribution, i.e., each circle corresponds to one standard deviation. From the figures it can be seen that LSFs are slightly curved in either direction, without any notable trend, thus giving mixed results in terms of conservativeness. However, the effect of linearization is not expected to be high in most cases due to the curvatures being relatively mild. Similar

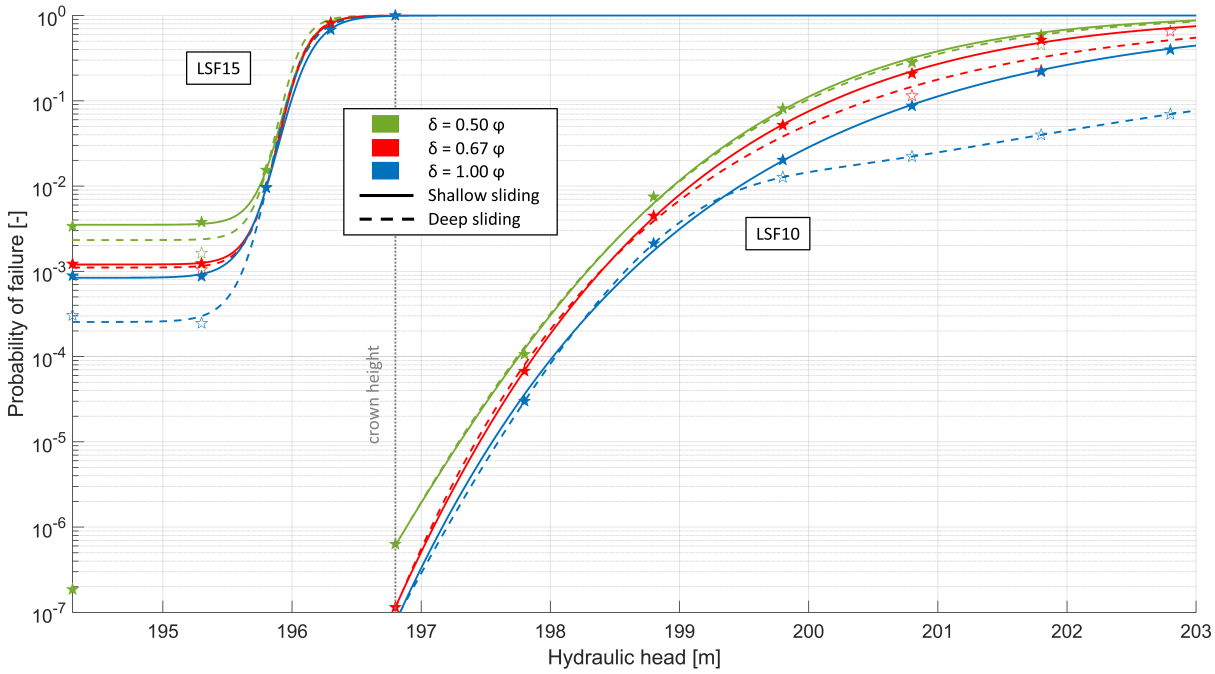

Figure 3.9. Diagrams shown in logarithmic scale.

shapes are noted for all interface friction angle values and are not shown here. To better investigate the effect of increasing reliability with increase of interface friction ratio, defined as δ/ϕ, graphs are plotted in Figure 3.11 showing these trends for LSF10 with the normalized reliability index on the vertical axis. The normalized reliability index is simply the reliability index for the mean interface friction ratio for each respective water level subtracted from the reliability indices at other friction ratios ($\beta_n = \beta - \beta_{0.67}$). This way all the curves are translated over the vertical axis for better comparison. From Figure 3.11 two characteristics are noticed, one being that the trend is approximately linear, changing from a power law for the lower water levels (i.e., higher β, lower p_f) to a positive parabola for the higher water levels (i.e., lower β, higherp_f). The second relates to the increase of steepness of the curve from lower to higher water levels, which is more pronounced on the higher friction ratio than on the lower. Also, the same increasing effect is seen for deeper versus shallow surfaces for the same water level (the two highest curves). For the LSF15 case (not shown on figures), even though some differences apparently exist between p_fs for different friction ratios, there are no visible trends, except for the deep sliding curve being steeper than the corresponding shallow sliding curves. To analyse the sensitivity of the slope stability to each of the defined random variables, 2D sections of the response surfaces through the design point are plotted on Figure 3.12. For each graph, one variable of interest is varied in the vicinity of the design point, while the other random variables are held at their respective design point values. The horizontal axes on the graphs are normalized such that the design point value is at zero and show the number of standard deviations away from the point. In other words, the curves are shifted from values obtained through Eq. (3.1) to align all the design points at zero. This helps comparing the trends of the response surface at

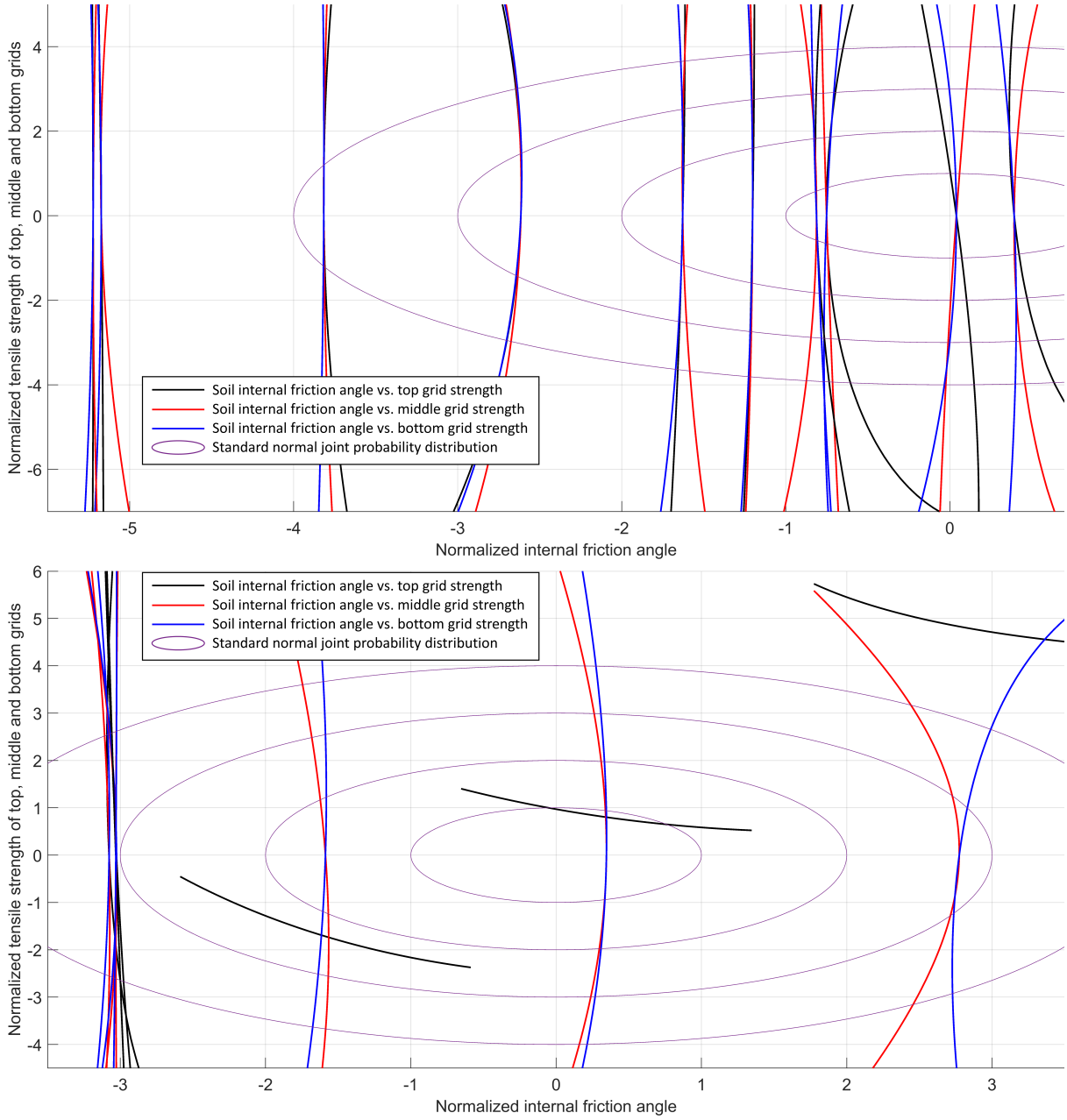

Figure 3.10. Limit state functions for LSF10 (top) and LSF15 (bottom).

various water levels. From the response surfaces, it is found that two main trends exist, namely parabolic (positive or negative) and linear. This is of course constrained by the function used to approximate the response surface (Eq. (3.4)), which is a quadratic polynomial. It is intuitive that the increase of any strength or resistance parameter's value causes the stability of a slope to increase by increasing the safety factor. However, some curves shown in Figure 3.12 seem to contradict this statement as they are parabolas which have maxima and minima at, or close to, the design point. This is just an apparent problem caused only by the chosen approximation function and does not show any inconsistencies considering the friction angle because all the maxima are found on the right side of the design point, while all the minima are found on the left side, and the curves are fitted to the data by their in-creasing parts. This mostly occurred

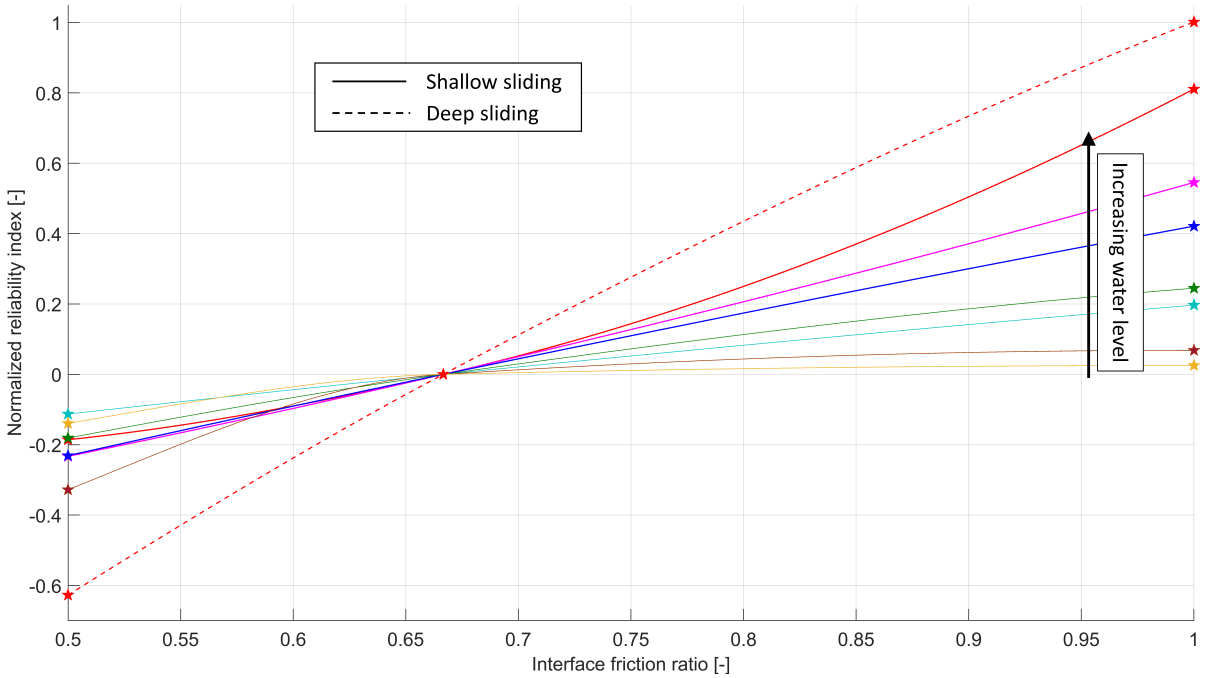

Figure 3.11. Trend of reliability index increase with increase of interface friction ratio for LSF10.

when smaller friction angles did not have a distinction between deep and shallow sliding, but higher friction angles did have it. In those cases, a sudden increase in safety factor occurs and a parabolic response surface cannot be generated with the whole range of data for deep sliding. This means that to achieve a good fit of the data to a parabola, one needs to discard all but the closest sample points on either side of the design point, while only keeping all the points on the opposite side. An example of such situation is shown in Figure 3.13. It is obvious that a higher order function should be used to approximate such data. It could be argued that if only a narrow range of data around the design point is used, then there would be no need to approximate the da-ta using higher order function. While this may be true in some cases, in other cases the range which would be needed to avoid higher order functions is relatively narrow, and would complicate the analysis to find values only inside that narrow range.

For the geogrids' tensile strengths, the trends are generally constant, which means they do not affect the safety factor. However, there are multiple increasing curves, and others which actually do show a decrease of the safety factor with a strength increase. Regarding the latter, it should be noted that the range of safety factors on Figure 3.12 for the grids is from 0.95 to 1.05, and thus such trends cannot be deemed as true trends. They can instead be attributed to data scatter in both deep and shallow surfaces, as well as to the shape limitations of the selected approximation function. This data scatter occurs mostly for the bottom and middle grid layers, and only at the higher end of friction angles. In the same region of friction angles, the top grid's strength start showing a linear to parabolic trend, as shown in Figure 3.14. This kind of data, however, also did not cause any inconsistencies with results, as the design point tensile strengths are practically at the mean values for most cases (Figure 3.15).

With each increment in water level there is change in probability of failure/reliability index,

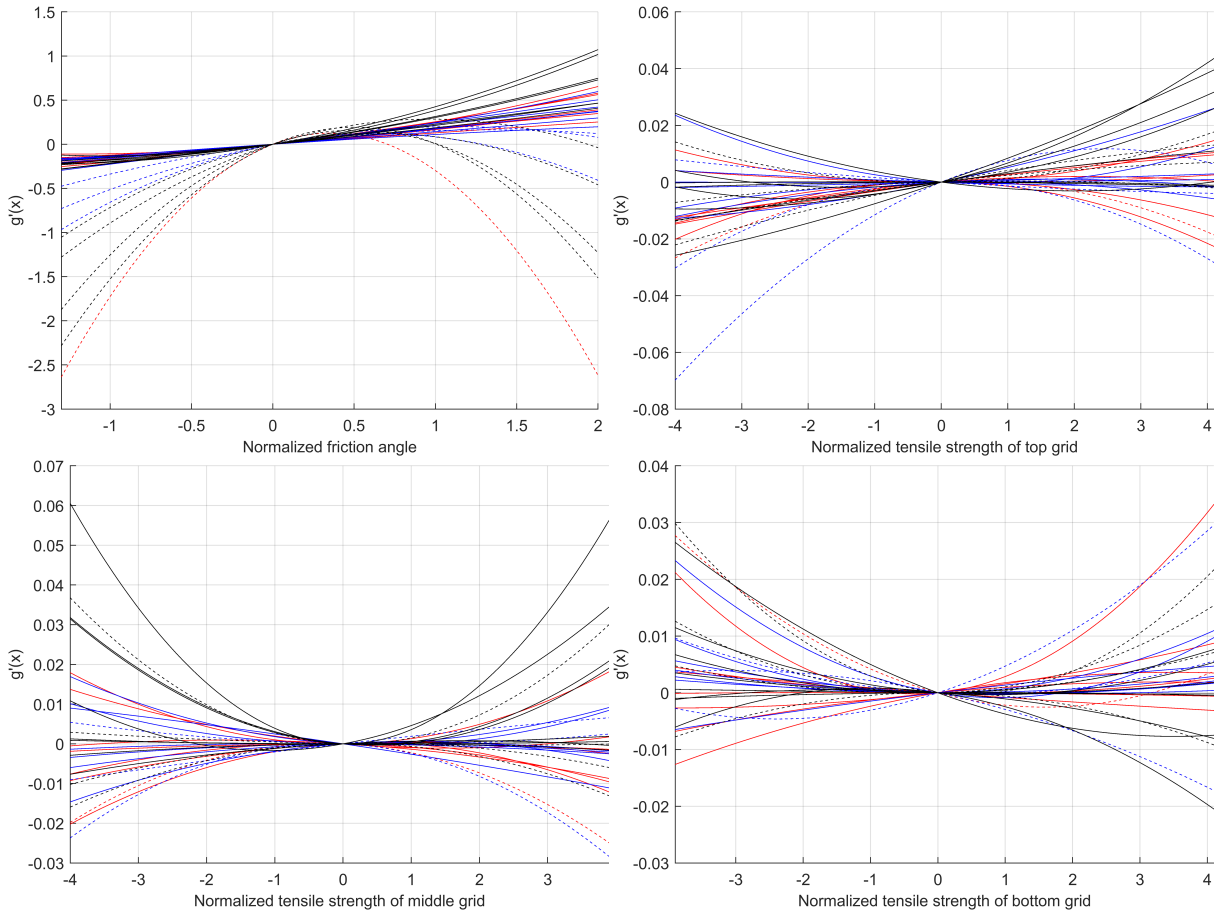

Figure 3.12. Trends of the response surface around the design point for LSF10 for low (red lines), mean (blue lines) and high interface friction angle (black lines), with full lines representing response for shallow sliding, and dashed lines for deep sliding.

which is caused by the different critical values of random variables needed to reach a specific LSF at that specific water level. Even though the critical values differ when the same water level is evaluated with different interface friction ratios, because the difference is not large, Figure 3.15 shows the mean critical value of each random variable. Figure 3.15 is a representation of Eq. (3.5), where the total reliability index can also be calculated for each water level by knowing the corresponding critical values of each random variable. Even though Figure 3.15b shows a decrease in critical tensile strength for the LSF15 at hydraulic head near 196 m.a.s.l. compared to lower heads, the reliability index still decreases (Figures 3.8 and 3.9) due to an increase in critical friction angle. On the other hand, the critical value for the LSF10 shows practically no change with the increase of water level. This is also true for both LSFs for the middle and bottom grids.

To investigate the relative contribution of the uncertainty of each random variable to the total uncertainty, the direction cosines (or sensitivity factors) are calculated as the ratio of each random variable's critical value to the reliability index. The squared sensitivity factors give us the values of interest [30]. For all interface friction angles (low, mean, high) for LSF10, the

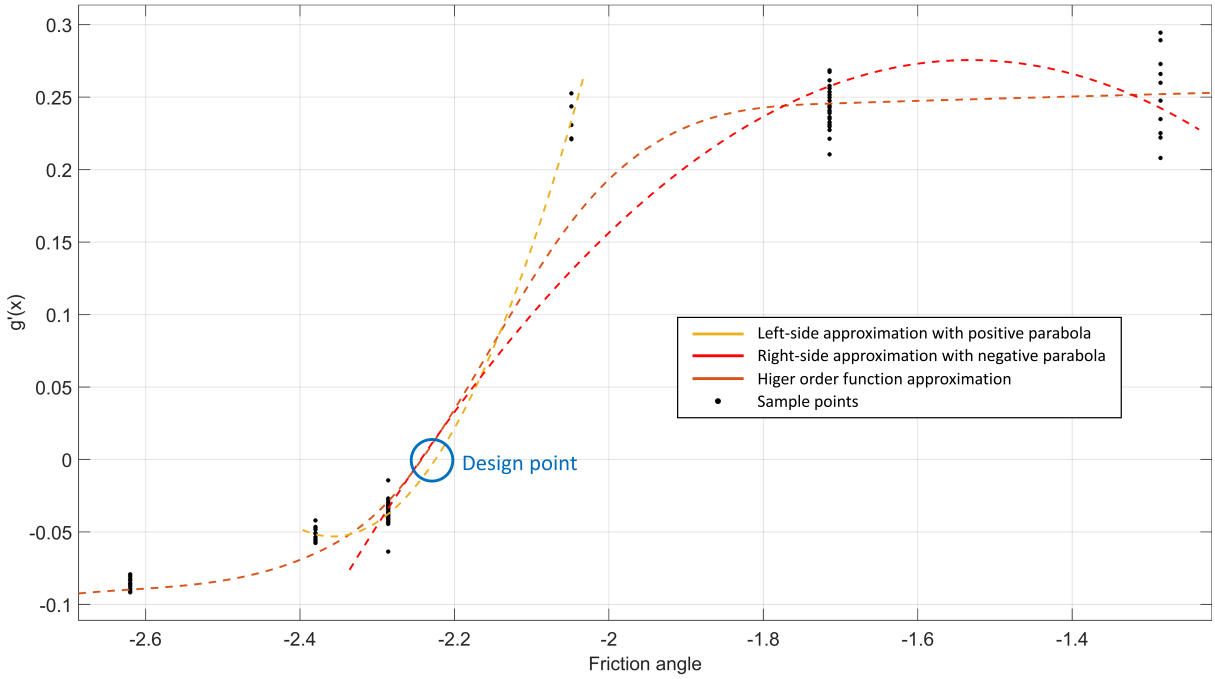

Figure 3.13. Situation where a cubic equation would be more appropriate (on the horizontal axis an interval of $0.1 = 0.35°$).

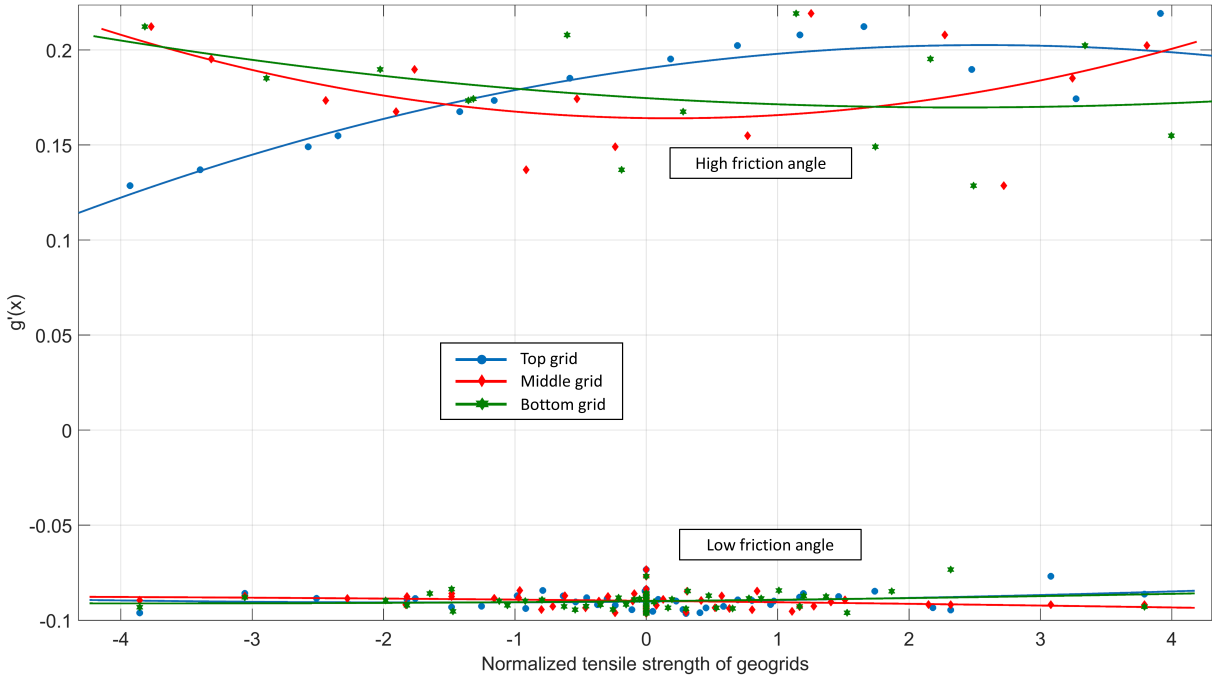

Figure 3.14. Effect of tensile strength of all geogrid layers on the performance function for mean interface friction angle, for two different values of reconstruction material friction angle.

contribution of the internal friction angle is >99.84%, with a mean value of 99.97%. The small remainder (<0.15% of total uncertainty) belongs to all three layers of geogrids, with almost 3/4 of that belonging to the top grid, and the rest somewhat evenly distributed between the middle and bottom grids. For LSF15, the relative contribution of the internal friction angle decreases

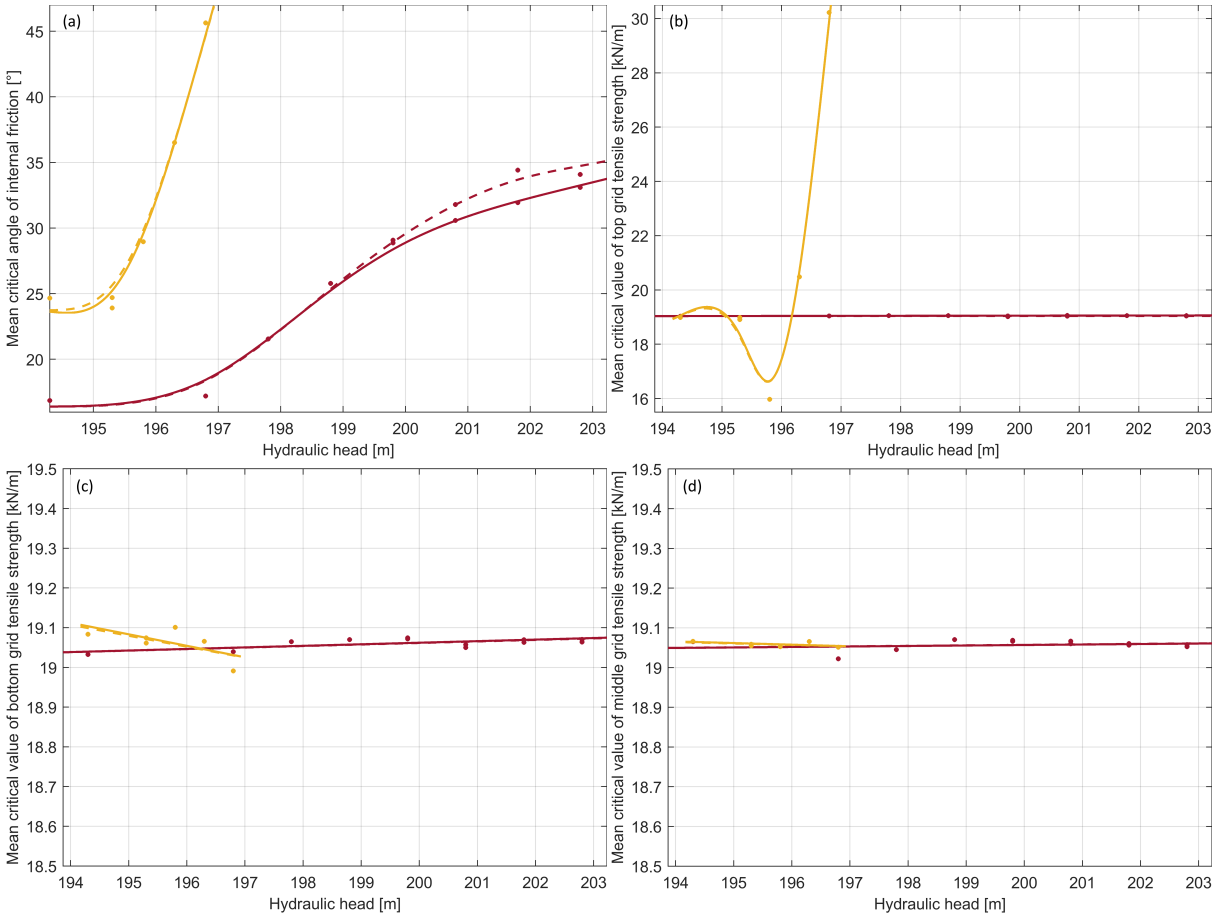

Figure 3.15. Critical values of random variables for various water levels; (a) friction angle (top left), (b) top grid (top right), (c) middle grid (bottom left), (d) bottom grid (bottom right); dark lines represent LSF10, light lines LSF15, full lines shallow sliding, and dashed lines deep sliding.

with the increase of water level, from almost 100% to 17%, while the rest is attributed to the top grid, as shown in Figure 3.16. The middle and bottom grid's contribution stayed close to zero at all times.

3.5 Conclusions

It should be noted that conclusions drawn from this study are only valid for systems similar to the analysed levee, where local face stability in ensured between geogrid layers, and where there is no anchorage on the front face, which would increase stability even more at the cost of additional material for the anchorage. From the presented results, a few conclusions can be drawn:

- Close to the ULS, at higher water levels (in this case $p_f > 0.002$), small variations in random variables cause deep and shallow sliding surfaces with highly different safety factors and p_fs. With the increase of interface friction angle, the water level at which

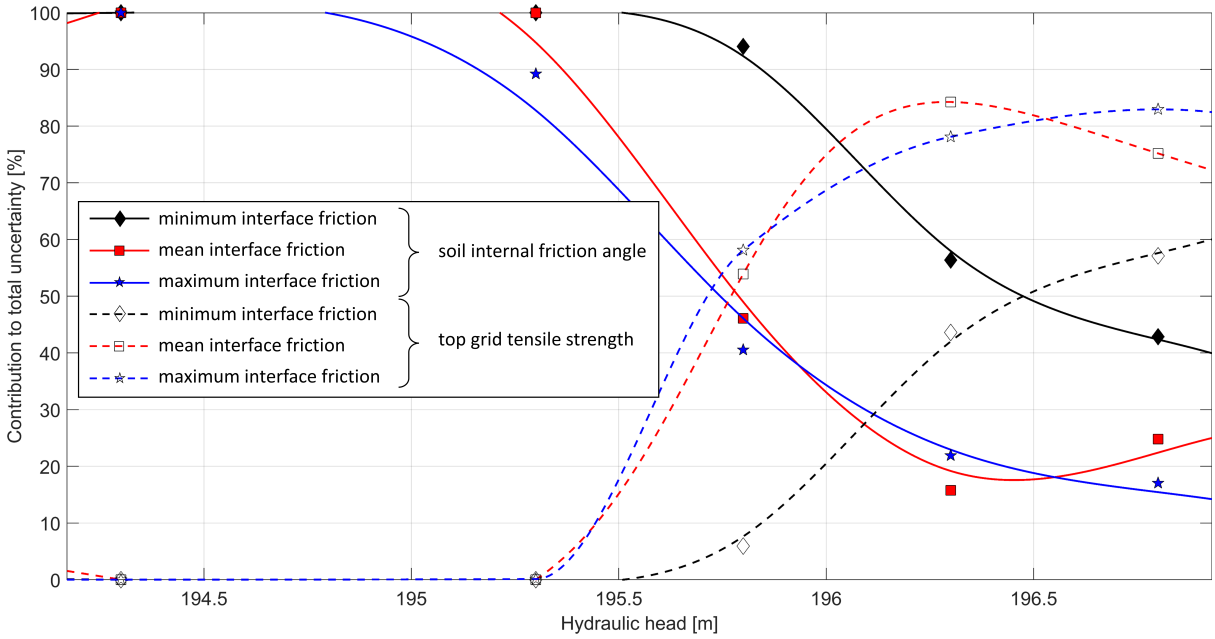

Figure 3.16. Relative contribution of internal friction's and top grid's uncertainty to total uncertainty for LSF15, for all three interface friction angles (full lines refer to internal friction angle, dashed lines refer to top grid).

this distinction becomes visible decreases. Farther from the ULS, this effect occurs at low water levels rather than higher, and the interface friction doesn't have any noticeable effect on the occurrence. Shallow sliding is shown to be more likely to occur for both limit states.

- Linearization of the performance function required for calculation of the probability of failure with the FORM does not influence the results greatly as the curvatures of the limit state functions are generally not large.

- The increase of reliability with increase in interface friction ratio is approximately linear in proximity of the ultimate limit state, with higher steepness for higher water levels. Also, deep surfaces seem to have a steeper curve than shallow surfaces. This is not true farther away from the ULS.

- Constant, linear, and parabolic trends, and those of higher order, are found for the performance function dependency to the reconstruction material friction angle and to the geogrid layers. The order of the function tends to increase with water level, i.e., with probability of failure. The higher order trends occur mostly for deep sliding when a sudden increase of safety factor occurs as a result of small increase in friction angle of the levee body. For this reason, quadratic functions should be used with care, and perhaps a function with an inflection point (e.g., cubic function) should be employed in some cases.

- The internal friction angle contributes almost completely to the total uncertainty when close to the ULS (the contribution of the grids is negligible). However, it seems that

geogrids placed near the top contribute the most out of all the geogrids. The contribution of the internal friction angle seems to diminish going farther away from the ULS (e.g., LSF15), and it transfers to the grid placed near the top, while the other grids' contribution remains negligible.
This importance of the top grid, however, needs to be considered carefully, because in this study the top grid is the only one that goes from one slope of the levee to the other, while the middle and bottom grids are only placed on one side. The relative contribution might be different in case all grids are the same length.

- The reason for the grids' extremely low contribution to the total uncertainty lies with the small variability of their tensile strengths. But as seen in the LSF15 case, as the required critical tensile strength reaches the actual tensile strength, their variability has more effect on the stability, which indicates a way of determining the required strength for each grid layer. Moreover, since the increase of both the soil friction angle and the soil-grid interface friction individually tend to generate deeper surfaces, it is implied that a balance between these parameters can be found. Both procedures would lead to a balanced reinforced slope design with regard to geogrid rupture strength and geogrid pull out.

At this time, deterministic analyses are still the dominant type of analyses when it comes to designing levees for flood protection in terms of slope stability. These calculations require safety factors >1 to be acceptable by definition of the safety factor. However, it is rarely deemed acceptable to reach safety factors around one, and higher values are often targeted. This study deals with slope stability of a geogrid reinforce levee in a probabilistic manner, and shows trends in the response of the levee and behaviour of the reinforcement components for two target safety factors of one and 1.5. Even though some trends are not as clear as others, and/or they are not quantitatively defined, and for which further investigations are needed, the identified trends might still serve as guidelines for design and can be loosely interpolated (where applicable) to increase understanding of the system behaviour for a targeted safety level.

Chapter 4

Methodology for Identification of the Key Levee Parameters for Limit-State Analyses Based on Sequential Bifurcation

Authors:
Nicola Rossi, Mario Bačić, Lovorka Librić, Meho Saša Kovačević
Paper status:
Published, https://doi.org/10.3390/su15064754

4.1 Introduction

There are many types of levees being constructed, considering their different cross sections and the materials used for each part of the levee. This also includes the subsoil on which they are constructed, as the behavior of the levee is also affected by it. Each of these components is susceptible to some factors that may or may not be controlled, such as locally available materials, construction space requirements, ULS and SLS requirements, local practices, etc. Combinations of those factors yield the many different cross sections that can be encountered. Such variations may even occur within a single levee, which is why levees are often divided into what we call "reaches" when conducting analyses. Reaches are segments of a levee that have similar characteristics such that they can be considered using one single cross section [24]. These cross sections are often defined by 5 to 10 parameters selected based on theoretical and empirical prior knowledge and experience, without looking too much into it. However, if we were to describe any section uniquely and use advanced constitutive laws such as the Hardening Soil model, then even a simplified geometry (including the subsoil) would require over 100 parameters, which can be geometrical, physical, mechanical, or hydraulic. Granted, most of those parameters do not have a noticeable effect on the desired quantity (such as deformations), but a relatively quick preliminary analysis might indicate some parameters that may be overlooked

and, more importantly, detect the relative importance of each one so the analyst knows where to focus. These parameters and their order of importance may change with any specific case being analyzed and with the response parameter of interest. In contrast to determining the factors that affect the levee's response to high-water events, Mirosław-Świątek et al. [52] showed a method for determining the effects of eight groups of factors, defined by factor types, on the technical condition and safety of levees after a period of exploitation, based on experts' opinions.

This paper presents a methodology for an efficient evaluation of the important parameters that affect the behavior of all the levees found within a specific area of interest so that further analyses may be conducted based on the obtained results of the presented methodology. The methodology relies on statistical techniques for the design and analysis of experiments. Generally, to design an experiment, one needs to know what is to be studied; that is, to have a clear statement of the problem and objectives, how will the data be collected, and how the data will be analyzed [178]. The type of experiment required for detection of the key parameters is called factor screening, and in this study we will specifically focus on the sequential bifurcation (SB) method. Designs of experiments can be generally divided into classical and sequential designs. Classical designs focus on creating one big experiment that answers some specific questions, i.e., the whole experiment setup must be known in advance before starting. On the other hand, sequential design starts with one smaller experiment, and the knowledge gained from its results is used to "adjust" the parameters of the later experiments. One such method is the SB method developed by Bettonvil [54] in his doctoral thesis in the field of economics. Throughout the years, SB has been improved within various fields of study, and other variants have emerged, such as the extension by Cheng [179] where the response is allowed to be stochastic and subject to significant error, and then the controlled SB (CSB) [180], the CSB-X [181], the fractional factorial CSB (FFCSB) [182, 183], the use of second-order metamodels in SB as explained by Kleijnen [53], as well as the multi-response SB (MSB), which allows for a simulation to have multiple response types [184, 185]. However, the authors did not come across the usage of the SB within the field of geotechnics. The SB method is a similar idea to the binary search in computer science, which divides a sorted array into two halves in each iteration and eliminates one (even though SB does not necessarily eliminate one in each step). In the SB, the elimination of one (or none, or both) of the halves is controlled by a control parameter, Δ, set in advance, which can be chosen arbitrarily by the analyst's judgement, or by techniques described in the mentioned papers. On top of that, SB also identifies the magnitudes of each effect. The goal of this study is to identify the most important parameters of the levees, within a large area of interest, that affect their behavior, but also contain enough information to describe the different cross sections we may encounter. These parameters will be later used to create generalized predictive models to predict the behavior of levees during high-water events based on monitoring data. The methodology is demonstrated on Croatian levees in areas prone to floods, sometimes with catastrophic outcomes [186, 187], which are also being managed with very limited funds. As many of these levees were constructed when height requirements were

substantially lower than today's standards, many are being reconstructed and many more are waiting their turn. This methodology is the first step in generalizing the levees' behavior in the analyzed area, which would help improve decision-making before, during, and after high-water events.

4.2 Methodology

The methodology presented in this study is based on a popular factor screening method—the sequential bifurcation (SB)—with slight changes to the procedures, coupled with statistical analyses and complex geotechnical numerical analyses. The results indicate a list of factors which are found to be most important in the behavior of levees, with regards to the observed mechanisms. The importances are given as percentages for a specific factor's effect on a specific mechanism. However, when conducting analyses it is always useful to consider the previous knowledge and local expertise regarding the subject, and thus this list is not exclusive.

4.2.1 The Sequential Bifurcation Procedure

The classic SB method relies on the assumption that the metamodel that simulates the system's behavior is linear, as shown in Equation (4.1), where y is the response, β represents the model parameters, x represents the independent variables that are then coded, and e is the error. Each of the selected variables (parameters, factors) is observed at two levels, which are encoded as 0 and 1 based on the effect that the value has on the response; i.e., if the value decreases the response, it is coded with 0, and if it increases the response, it is coded with 1. This leads to the second assumption of the SB method, which states that the signs of the model parameters are known. In other words, for each levee parameter, we must know its effect on the response. In accordance with this assumption, the function is assumed to be monotonically increasing. Otherwise, some effects may cancel each other out within the SB groups and may thus go unnoticed.

$$y = \beta_0 + \sum_{j=1}^{k} \beta_j x_j + e \tag{4.1}$$

SB starts with two analyses, which consist of one where all the parameters are set to the "high" value coded with 1, and the second where all are set to the "low" value coded with 0. Continuing after the first two runs, the factors are then split into groups labelled w_j, where j indicates that the first j out of the k parameters is set to the "high" value, while the rest $(k - j)$ are set to their "low" values. Each group's effect is compared to the parameter Δ to check whether the effect is important or not. This continues until the groups are reduced to individual factors and all groups are exhausted. Thus, during the SB, the model parameters β are estimated for groups

of factors and for single factors, as shown in Equation (4.2), where $j \neq j'$.

$$\widehat{\beta_{j'-j}} = \frac{(w_j - w_{j'-1})}{2} \qquad \widehat{\beta_j} = \frac{(w_j - w_{j-1})}{2} \tag{4.2}$$

If the previous assumptions are satisfied, the first two runs should yield the highest and lowest values of all subsequent runs. However, it is not uncommon to be uncertain about some factors' effects and encode them incorrectly. In such cases, Kleijnen [53] suggests excluding these parameters from the SB analysis and analyzing them individually (in groups of 1). Instead, Oh et al. [182] in their version of the SB, suggest conducting a preliminary fractional factorial design of resolution III to identify the sign of each effect, then perform the SB with all the correctly encoded factors first, and then with the others. Due to the efficiency of the SB method, in our case, the identification of the eventually incorrect signs is done with just the SB method itself. If some factors are incorrectly labelled, the results of the first two analyses will not be the minimum/maximum, but will be higher/lower than the same runs with correctly labelled parameters. The amount by which they would differ depends on the cumulative importance of the incorrectly assigned factors. Figure 4.1 shows the estimated response of the "all high" and "all low" runs for two situations with increasing number of incorrectly assigned factors, for a general case of SB. In one situation, the first incorrectly encoded factor is the most important one, with each subsequent incorrectly encoded factor being the second most important one, and so on until the least important one is reached (termed "decreasing" in the figure). The second situation is the opposite (termed "increasing" in the figure). The realistic situation where seemingly random errors in factor encoding exist is found between these boundary curves. Firstly, all factor combinations that yield results on the right side of the curve-pair intersections, where the "minimum" response is higher than the "maximum", are immediately obviously incorrect. For the left part, if we define the parameter Δ as a fraction of the difference between the first two SB runs, which means it is a function of the incorrectly assigned factors, then the Δ is lower when there are more incorrectly assigned factors, which makes it more likely for SB to identify those parameters that yield a response lower than the "all low" run or higher than the "all high" run. The high and low values of such parameters should be switched. This is all done to avoid effect cancellation, which is a main concern in SB. However, as found by Dean and Lewis [188], cancellation occurs very rarely under effect sparsity, which states that a system is mostly controlled by main effects and two-factor interactions. This ties in with the third and final assumption of SB—heredity—which states that if a factor does not have an important main effect, then it also does not have important interactions. This means that all the important interactions are found only between the parameters that have important main effects, and no significant interaction exists between a detected and undetected factor.

From Equation (4.2), it can be seen that, to estimate a factor, say factor 6 out of 10, one would need to perform an analysis with the first 6 factors at their high values and the rest on low, then use the results from the analysis where the first 5 factors are at the high values and the

rest on low, to subtract one from the other and get the effect of only factor 6 being at the high value. This works for systems that are truly linear. Wan et al. [180] used an approach where the groups consist of having only the parameters of interest at their high values, which directly estimates their effects. The latter is implemented in this study. It seems that the standard method of estimating a group's or single factor's effect is to have it on "high", while all the others are on "low". However, due to the complex stress–strain behavior of levees, the situations with all the factors at "low" and with all the factors at "high" produce completely different behavior mechanisms. Since we are interested in predicting what happens at the "high" values, we instead use the approach of estimating the factor importances by having those factors set to their "low" values, while all the others are on their "high" values. This way, we do not observe how much a group or single factor increases the response compared to the situation of all on "low", but how much that group or single factor decreases the response compared to the situation of all on "high". In our case, these two situations are not equivalent. However, certain responses are better observed in one way, and other responses in the other way, so in this study both are implemented, as described later in this section.

Figure 4.2 shows the structure of the described sequential bifurcation method with the required analyses and decisions to be made in each step.

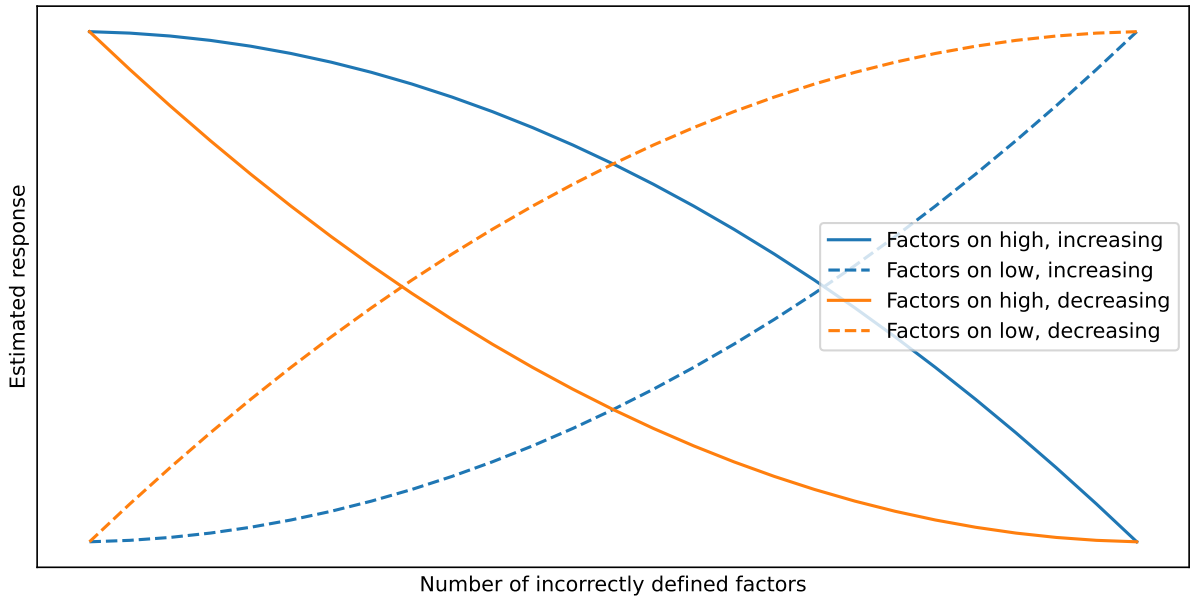

Figure 4.1. Bounds of the first two analyses in the SB method.

4.2.2 Implementation

The first step in the implementation of this methodology is to define the area of interest based on the problem of interest, i.e., which structures to consider in this factor screening analysis. The covered area (or structures) may be defined in terms of geographic locations, a specific class

First two runs "All high" run (w_k, all factors coded with 1): gives max. deformations, max. gradients, min. factor of safety

"All low" run (w_0, all factors coded with 0): gives min. deformations, min. gradients, max. factor of safety

$$\Delta = (w_k - w_0) \times 0.05$$

Middle runs Take a list of factors from the queue and set all of these factors to either $+$ or $-$, depending on the selected approach, while all the rest are set to the opposite sign. After performing the analysis, the result is the group's effect, $w_{j'-j}$, where j' through j are the parameters set to the selected level, with all the others set to the opposite level.

Check if the specific list (group) of factors is important by comparing the results: $w_k - w_{j-j'} \geq \Delta$ or $w_{j'-j} - w_0 \geq \Delta$. If the group is important, divide the list of factors into two lists, and add them to a LIFO (Last-In-First-Out) queue, such that the first list to be analyzed always contains factors of assumed higher importances. Optionally, the effect of the other half of the original list can be checked by superposition and either discarded if it seems to be not important or left as it is if it seems important. Repeat until the queue contains lists of length 1.

End runs When the list contains only one factor, it is set to either $+$ or $-$, while the rest are set to the opposite sign. Its effect is estimated by: $w_k - w_i \geq \Delta$ or $w_i - w_0 \geq \Delta$, where w_i is the response for that single factor set at that specific level, with the rest set at the opposite level. Repeat until the queue is empty.

Figure 4.2. Structure of the described sequential bifurcation method.

of structures if some classification exists, same owners and managers, or any other specific criteria. In our case, the problem of interest is the identification of the key factors affecting the levees' behavior with regards to several limit states, and thus our structures of interest are river levees found across various locations. The next step is to define all the parameters that may be used to describe the more or less complex geometry of these levee sections—the geometric, hydraulic, physical, and mechanical parameters of each component, as well as the relevant hydrological and hydrogeological data. The parameters must be chosen based on the desired complexity of the models, and again the problem of interest that defines the parameters required to conduct the analyses. Then, the data should be gathered from all relevant sources: project designs, field and laboratory investigation works, technical drawings, jurisdictive institutions, etc. Often, the data are incomplete, i.e., not all parameters are available for all the sections. In such cases, they can either be estimated based on experience and knowledge of local regulations and/or practices, or just left blank, requiring work with less data.

When a database is formed from the gathered data, exploratory data analysis is conducted to facilitate further analyses. This includes factor normalization to overcome impossible or

unrealistic combinations that result from a random selection of factors' values, finding factor correlations, and data transformation. The factors are normalized with regard to other factors of the same type (geometric, hydraulic, physical, mechanical). Most geometric parameters are normalized to the levee height or crown-width. Some physical and mechanical parameters that need to be in specific relation to other parameters are also defined this way, e.g., hydraulic conductivities and Young's moduli of the various components.

After having each parameter defined in the desired units, the range bounds of each factor for the analyses need to be defined. For some parameters which may not be available, such as flood durations and inundation time, the bounds can be estimated from experience. For the available parameters, the bounds are first taken as the extreme values of the gathered data for each parameter and are set as the two levels of each. However, it should be noted that if the levee's behavior is not linear, then the selected range may greatly affect the calculated model parameter β. Additionally, some factors may display lower or higher effects only due to their ranges being smaller or larger in comparison to other factors' ranges [189]. For example, if the levee height is varied within a small range, say ± 0.25 m from a mean value, while berm width is varied in a large range, say 1–5 m, then the berm width might show higher importance than the levee height, which would generally not be expected when searching for parameters that affect levee behavior. Thus, it is important to clearly define the purpose of conducting these analyses. One purpose may be to deepen the understanding of the behavior of levees in general, and the other to detect the parameters that have the most effect on the behavior of levees found within a specific area of interest. In the latter case, the ranges chosen based on the data gathered within that area intrinsically contain information about the importance of parameters in the area, i.e., parameters which we should focus on. Now, if we look again at the previous example with the latter purpose in mind, then the fact that the SB identified the height as unimportant and the berm width as important means that we should focus more on the berm width, because all the levees are practically the same height, so a mean value could be a good enough representation. However, even by using the normalized values, the ranges may be too large such that using the extreme values can still yield numerical model failures due to unrealistic parameter combinations. Additionally, the highly non-linear nature of the levees' behavior may cause the linear metamodel of SB to be unfit for this system if the behavior cannot be linearized over the selected ranges. Because of this, data transformations are used to create reduced ranges if needed, as follows. First, all of the heavily skewed data are transformed by logarithmic, square root, or Box–Cox transformations to make the data symmetrically distributed around the mean. Then a normal probability distribution is created for each parameter by setting $\pm 3\sigma$ of the transformed variables as the ranges bounds, and then selecting the new ranges as $\pm 1\sigma$ away from the mean, which is either the value between the range bounds or the 50th percentile. The average of the range bounds is used when the data are approximately uniformly distributed. The real parameters are then found by reversing the transformed values of $\pm 1\sigma$. With this method, the whole range of identified parameters is

covered, which is important because there are no outliers in these data, only extreme but realistic values. For data that look normally or uniformly distributed, the transformation step is skipped.

Now, with the defined ranges, factor screening analyses using the described SB method are conducted. The factor Δ used to decide whether a factor or a group is important is usually a fraction of the value of the response type/performance-measures (cost of the supply chain, cycle-time of a system, deformations of a system, etc.). However, the decision can also be based on multiple responses. This study utilizes the described SB procedure, and multiple responses are observed simultaneously only when all the factors had equal effect signs for both responses (which does not require the usage of MSB), while for other response variables of interest, separate SB analyses are conducted. Through the responses of interest, all the relevant geotechnical analyses are considered—deformation analyses through the maximum model deformations (regardless of the location of its occurrence in the section; D), flow analyses through the exit hydraulic gradients (G), and safety analyses through the factor of safety (F). Since a goal of this study is to identify parameters that may be used to create predictive models that will rely on monitoring data, one more response variable is added. This response is the horizontal deformation at a specific point in the levee section (the landside part of the crown in this case; Ux), because it is a quantity that can be directly measured by conventional monitoring, which is one of the main aspects of levee safety control and management. The horizontal deformations of a specific point are observed simultaneously with the model deformations. Other similar responses can be added based on the available monitoring equipment, such as piezometer results, etc. Finally, the model deformation, the deformation at a specific point, and the gradient are observed by comparing the effect of each parameter at its low value with all the others at their high value, while the factor of safety is observed by comparing the parameter's high value with all the others at their low value. The reasoning behind the way the factor of safety is observed is that often the slip surface generated by the strength reduction method (SRM) coupled with the previous flow–deformation analyses with all the parameters set to their high values (lowest factor of safety), develops as a shallow slip surface that does not encompass the levee at all, but forms within the channel or river slopes. On the other hand, the slip surface generated with all the factors set to their low values (highest factor of safety) develops as a larger surface that encompasses the levee body. By turning a group or single factor to its high value while all the others are on their low values, it is more likely that the generated surface will encompass the levee.

It should be noted that the parameters identified as important will vary depending on the stress/strain component of interest and its location in the levee section.

4.3 Case Study

For this study, 16 levees were considered, and from each, 1–14 cross sections. The chosen levees were all found in Croatia and varied from segments of only a few hundred meters in

length to over 10 km. Their positions are shown in Figure 4.3. In total, 91 different cross sections were taken for the statistical analysis. The criteria for choosing the cross sections were that each cross section must have some specific geometry compared to other cross sections of the same levee, and/or in the same way have specific subsoil conditions. The criterion for saying that something is "specific" compared to other sections was a subjective choice based on the analyst's experience. Some levees simply contain less variability in their geometry, subsoil stratigraphy, and material parameters due to the construction methods, locations, and lengths. Because of this, for some levees it was possible to identify more specific-sections than for others. To uniquely define a levee section consisting of the foundation soil, a relatively thin surface soil layer, an impermeable levee core, the levee's body, and two berms, 102 parameters have been identified, which may be divided into three groups, as shown in Tables 4.1–4.3, while the general geometry in Figure 4.4 also shows all of the geometric factors. Out of the 91 levee sections analyzed, not all sections contained all of the mentioned components, but instead contained different combinations of them. The numbers of levee sections containing each specific component along the levee body and foundation soil are shown in Figure 4.5. All of the geometric factors with the unit of length were normalized to either the crown height from the landside toe, or to the crown width, with three exceptions being: the crown width of the core, which was normalized to the levee width at the core height; the thickness of the top soil layer, which was not normalized; and the channel width, which was also not normalized. Some mechanical factors have also been normalized. These are Young's modulus of the core, normalized to the modulus of the levee body, and the vertical conductivities of the core and both berms, which were normalized to the vertical conductivity of the levee body. For each factor in the tables, the sign of their effect is mentioned, where the plus ($+$) or minus ($-$) signs indicate which of those operations (increase or reduction) on the factor's value increased the responses. The increase in a response is here defined as the change towards a more unfavorable value. The indicated signs are the ones used to obtain the highest and lowest responses for the appropriate runs and response types.

The ranges for the factors were determined from statistical analysis. As previously described, SB takes only the limiting values of the ranges, i.e., the minimum and the maximum. A combination of only the observed extreme values often leads to unrealistic levee section and material parameters, and if numerical analyses are used to obtain results, this leads to numerical problems and thus results are impossible to acquire. Additionally, the relationships of deformations and other responses to all the input parameters are highly non-linear, similar to the function of safety factors shown in Rossi et al. [190]. Since the SB is based on a linear meta-model, this would cause the model to be unfit for the data and as a result give incorrect factor importances. To get around this problem, in this study, the ranges were reduced as previously described (the data in the ranges were already normalized prior to the reduction). The only exception to the described reduction method is the water level on the land side, where one value was taken at the surface level (as it is the most commonly used value in numerical analyses),

Table 4.1. Common physical, mechanical, and hydraulic parameters.

Physical & Mechanical		Hydraulic	
unit weight	$- \; - \; - \; -$		
porosity	$+ \; + \; + \; +$		
cohesion	$- \; - \; - \; -$ [1]		
friction angle	$+ \; + \; - \; -$ [2]		
dilatation	$- \; - \; - \; -$ [3]	vertical perm.	$+ \; + \; + \; +$ [5]
Poisson ratio	$+ \; + \; + \; +$	anisotropy	$+ \; + \; + \; +$
OCR	$- \; - \; - \; -$		
Young's modulus	$- \; - \; - \; -$		
unload./reload. modulus	$- \; - \; - \; -$		
power *m*	$- \; - \; - \; -$ [4]		
	D Ux G F [6]		D Ux G F

[1] Except for the foundation soil, where the effect is $+ \; + \; - \; -$; [2] Except for both berms, where the effect is $- \; - \; - \; -$; [3] Except for the foundation soil, where the effect is $- \; - \; - \; -$; [4] Except for the levee body and core, where the effect is $+ \; + \; - \; -$; [5] Except for the land. berm ($- \; - \; - \; -$), top soil ($+ \; + \; - \; +$), found. soil ($- \; - \; - \; +$); [6] Response types: "D"—deformations, "Ux"—crown displacement, "G"—hydraulic gradient, "F"—factor of safety; The responses are increased by either increasing ($+$) or reducing ($-$) the factor's value.

and the other value as the median of all the other observed values. In this way, we obtained much more realistic levees, while also reducing the range covered by the function, which can thus be better linearized. However, care must be taken not to reduce the range too much in order for the results of the numerical analyses to be distinguishable enough from one another and not fall within errors contained in the results of each analysis.

The soil's behavior was modelled using the Hardening Soil model (HS), which requires both Young's modulus and the constrained modulus, with no fixed relationship between them. Due to some limitations imposed by the HS model, some combinations of these two moduli are not possible. In such cases, various modifications to the parameters are possible, where some compromises need to be made. Due to the loading conditions, where an existing levee is pushed by water loads, focus may be put more on shear-hardening than on compression-hardening, which is represented in the HS model by Young's modulus. Thus, the choice is made to set the constrained modulus equal to Young's modulus, which complies with the limitations. It should be noted that even though 102 parameters were identified, only 101 were varied, while one—the water level—was kept constant at the crown height because it is the main action on the levee and its variation should be included in later analyses anyway. This means that all of the factors' effects are, in this phase, determined only for the most critical water level. There may be some complex factors to analyze, one of them being the thickness of the top layer. The reason for its complexity is that an increase it may have a favourable effect when, e.g., the conductivity and Young's modulus of the top layer are larger than their foundation soil counterparts, but have an unfavourable effect in the opposite case. Such factors should either be isolated and analyzed separately, or left in the analyses and be kept in mind during the analysis of the results. The

factors' effects should always be arranged such that the "all-low" run gives the lowest possible response and the "all-high" run the highest possible response.

To model the levee sections' response to the input variables, fully coupled flow-deformation analyses were conducted to analyze the stress–strain behavior, and safety analyses based on the SRM to find the factor of safety, both conducted with Plaxis 2D, 2019. Because many numerical analyses are required to make a factor screening experiment, Python programming

Table 4.2. Specific geometric parameters.

Component	Geometric Parameters	D	Ux	G	F
Levee body	waterside slope	−	−	−	+
	landside slope	+	+	+	+
	crown width	−	−	−	−
	crown height from waterside toe	+	+	+	+
	crown height from landside toe	+	+	+	+
Impermeable core	waterside slope	−	−	−	+
	landside slope	−	−	−	−
	crown width	−	−	−	−
	crown height from landside toe	−	−	+	+
	core position within the body [1]	+	+	−	+
Landside berm	height	−	−	−	−
	width	−	−	−	−
	slope angle	+	+	+	+
	berm angle	+	+	+	+
Waterside berm	height	+	+	−	−
	width	−	−	−	+
	slope angle	+	+	+	+
	berm angle	+	+	+	+
Surface layer	thickness	+	+	+	−
Foundation soil					

[1] − moves the core towards the water side, and + towards the land side.

Table 4.3. Geometric and hydraulic parameters not associated with any specific material.

Geometric					Hydraulic				
river depth	+	+	−	−					
river bank slope	+	+	+	+					
river dist. from waterside toe	−	−	−	−	landside water level	+	+	−	−
channel depth	+	+	+	+	inundation time	+	+	+	+
channel bank slope	+	+	+	+	duration of max. water level	+	+	+	+
channel width	+	+	+	+	height of water event				
channel dist. from landside toe	−	−	−	−					
	D	Ux	G	F		D	Ux	G	F

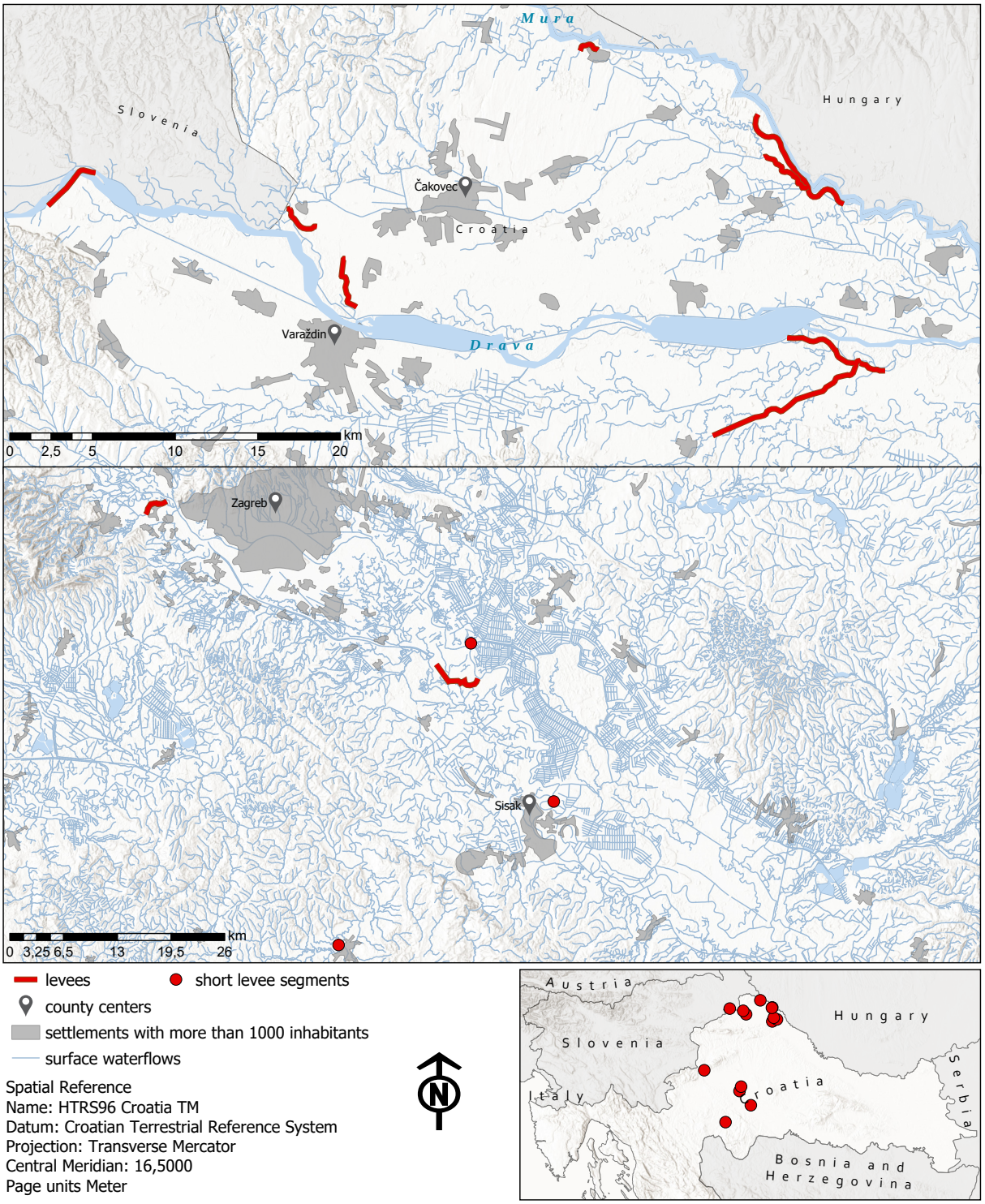

Figure 4.3. Map showing the locations of the chosen levees.

was used to automatically generate the models, set calculation parameters, run analyses, gather results, and decide what to do in the next SB step. For the SB method, it is unknown in advance how many runs it will take to finish, which, among others, depends on the chosen Δ and factor arrangement—the factors should be sorted by assumed importance, with the most important being at the end of the list. In this study, the Δ was chosen as 5% of the difference between

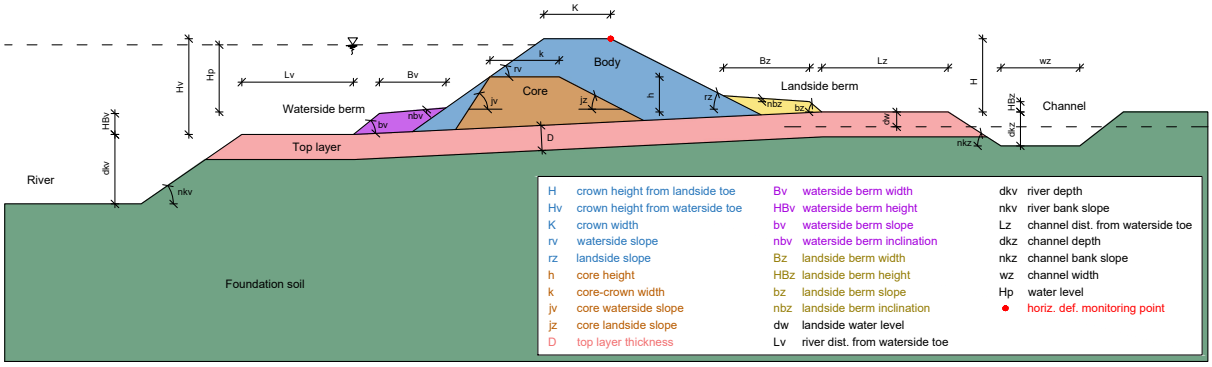

Figure 4.4. General model with identified geometric characteristics.

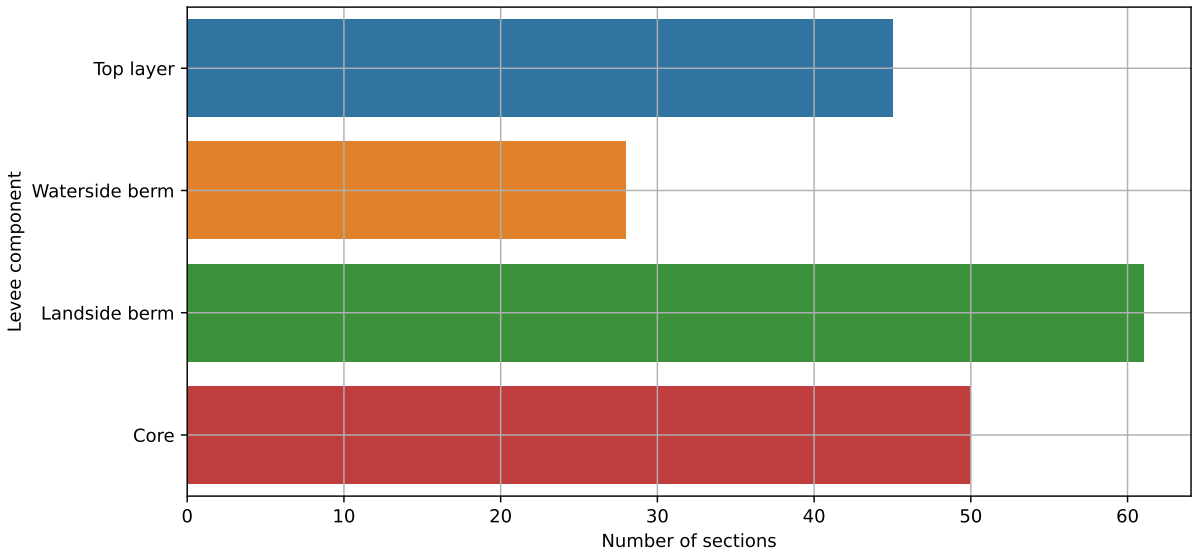

Figure 4.5. Number of each levee component found in the 91 analyzed cross sections.

the maximum and minimum values of the response type of interest. Due to the SB's efficiency, this procedure was applied multiple times, each time observing a different response. The reason these had to be separate analyses is that a handful of factors have reversed effects for different response variables (model deformations, exit gradients, factors of safety). These SB analyses for identification of the most important factors were performed for the most complex and the most simple levee geometries, i.e., the cross section containing the impermeable core, both berms, and the top soil layer (Figure 4.4), and the cross section containing only the homogeneous levee body and foundation soil, without all the other components. In total, 6 SB analyses were performed, 3 for each cross section, and the resulting number of runs varied from as little as 20 up to 100.

4.4 Results and Discussion

With the six conducted SB runs, it was found that the parameters' individual effects varied up to over 90%. From the direct results of the analyses and the sum of all the single effects, is seems as

though factor interactions reduce the individual effects when estimating the effect by how much the factors reduce the response, i.e., the sum of the effects of two factors is greater than the effect of those two factors acting together. If the model was indeed linear and interactions were unimportant, then superposition could be applied to get the lowest deformation from individual effects. However, this is not the case, and thus it is likely that some two-factor interactions are important to consider. Assuming the heredity assumption still holds, some of the identified factors must have an important interaction with another identified factor. The identified factors are shown in Table 4.4 (sorted by the effect on deformations). The table also shows for which response variable (mechanism) each factor is deemed important. As mentioned previously, the water level is not identified because it was kept constant at the crown height in these analyses. The Δ was set arbitrarily as 5% of the difference between the maximum and minimum runs' results.

By using the method of identifying incorrectly assigned factors described in Section 4.2, a few factors were identified for the different response variables, which were appropriately corrected for each analysis, which were then run again. Out of these factors, the most surprising were the friction angles of both the foundation soil and the top layer, which have reversed effects to the deformations, i.e., the higher friction angles yield higher deformations. After analyzing the specific factors, it is concluded that a possible reason for this behavior is the plastification of the foundation soils caused by the lower friction angles. Because the maximum deformations are in most cases found somewhere on the waterside part of the levee body, in the upwards and landside direction, the plastification of the foundation soils reduces the deformations at those places caused by the water pressure. Table 4.4 also shows the original ranges of the identified parameters found by analyzing the selected levee cross sections. These are the ranges which have been reduced by using the described methodology. Still, the results found in this study apply for the whole range, because the reduced ranges are all directly affected by the original ones. Levees whose geometric, physical, mechanical, and hydraulic parameters approximately vary from one bound to the other will have results similar to these, but if the values are only found within the ranges and the bounds are not actually part of the possible parameters, then the values will differ from the ones in this paper. However, the methodology can still be applied to find the parameters on which to focus for the levees found within an area of interest.

The identified parameters' importance, shown in percent effect, only holds for situations where all the other factors are at either end of their spectrum (most critical or least critical). This means that the percentages shown here are not fixed on a specific factor but can vary depending on the other factors.

It may look like there are some factors missing from the ones identified as important for the factor of safety, e.g., the strength properties of other materials. This is because, firstly, in the coupled flow–deformation analysis using the Hardening Soil model, plastic failure occurs on various occasions within the river and channel slopes. The safety analyses that come afterwards identify these positions as critical for stability failure, and a small failure surface develops at

these positions. Those failure surfaces are not affected by the levee and core materials. Using such analyses instead of simple slope stability analyses where a failure region can be manually defined is limiting in this regard, but they provide the most realistic results, even though it may be harder to analyze the results and retrieve the wanted data. This, however, can be partly mitigated by creating other analyses where such section components are missing, so that failure surfaces cannot occur in these positions. Also, additional parameters can be added to the list of important parameters based on theoretical knowledge, experience, etc.

A total of 24 parameters were identified as important by the 5% effect criteria, where 13 (more than half) were geometric characteristics, 4 were mechanical, and 7 were hydraulic. It can be seen from Table 4.4 that individual factors have the most effect on the maximum exit gradient, where the single most important factor has an effect of over 95%, while the most important factor in the deformation response type has an effect of around 60%.

Additional analyses were performed for a geometry that includes only the levee body and a homogeneous foundation soil, and the results are shown in Table 4.5. It can be seen that the strength parameters are indeed important for the stability analyses, now that the slip surfaces cannot develop away from the levee. It can be noticed from the table that for this simple situation no singular factors are identified as important for the hydraulic gradients; however, it is clear that instead the interactions are high, as there is a large difference between the “all maximum” and “all minimum” runs.

Finally, Table 4.6 shows the subset of the input parameters that are deemed important for the analyzed levees, as well as others that fall within the selected ranges, after modifications are made to account for prior experience and theoretical knowledge. The table contains the factors identified in Tables 4.4 and 4.5, and also includes the minimum number of parameters needed to describe a levee component if they are not already identified by SB.

Table 4.4. Identified important factors with main effects.

Factors		Percent effect [%]				Ranges	
	crown height from landside toe	52.9	59.5	96.7	24.0	0.5–7.3	[m]
LEVEE BODY:	vertical permeability	35.6	37.8	91.7	∼	1×10^{-8} to 5×10^{-3}	[m/s]
FOUND. SOIL:	Young's modulus	23.6	22.4	∼	∼	10–80	[MPa]
	water depth in the landside soil	21.3	12.0	79.4	12.0	0–5.5	[m]
CORE:	position inside the levee	20.6	24.3	∼	∼	−1 to 1	[%]
	crown height from waterside toe	18.8	20.8	∼	27.0	0.3–3.34	[%]
FOUND. SOIL:	unloading/reloading modulus	15.0	13.8	∼	∼	2–5	[MPa]
TOP LAYER:	vertical permeability	12.0	9.3	87.5	31.6	1×10^{-10} to 1×10^{-2}	[m/s]
LEVEE BODY:	waterside slope	9.7	5.8	∼	∼	0.18–0.55	[/]
CORE:	height	7.3	9.6	91.0	∼	0.3–0.9	[%]
LEVEE BODY:	Young's modulus	7.2	8.2	∼	∼	20–50	[MPa]
FOUND. SOIL:	friction angle	6.9	5.4	∼	19.8	21.9–42.4	[°]
FOUND. SOIL:	vertical permeability	5.5	7.9	94.3	∼	1×10^{-8} to 1×10^{-3}	[m/s]
	river depth	5.1	8.0	∼	∼	0.8–5.4	[m]
LEVEE BODY:	crown width	∼	6.0	91.7	∼	1.4–12.4	[m]
	inundation time	∼	∼	91.7	∼	1–6	[d]
CORE:	landside slope	∼	∼	80.5	∼	0.25–2	[/]
CORE:	vertical permeability	∼	∼	79.9	∼	1×10^{-10} to 5×10^{-5}	[m/s]
	channel width	∼	∼	32.9	∼	0.5–7	[m]
	duration of water event	∼	∼	19.4	∼	1–6	[d]
	river bank slope	∼	∼	∼	46.7	0.06–0.75	[/]
TOP LAYER:	thickness	∼	∼	∼	43.5	0.5–5.5	[m]
	channel depth	∼	∼	∼	35.2	0.8–2.4	[m]
	channel dist. from landside toe	∼	∼	∼	12.0	0–4.9	[%]
		D	Ux	G	F[1]		

[1] Response types: "D"—deformations; "Ux"—crown displacement; "G"—hydraulic gradient; "F"—factor of safety

Table 4.5. Identified important factors with main effects for the simple geometry.

Factors		Percent effect [%]				Ranges	
	crown height from landside toe	91.4	78.3	∼	43.0	0.5–7.3	[m]
LEVEE BODY:	vertical permeability	89.4	71.5	∼	40.2	1×10^{-8} to 5×10^{-3}	[m/s]
	crown height from waterside toe	83.2	37.4	∼	∼	0.3–3.34	[%]
	water depth in the landside soil	72.5	42.0	∼	52.5	0–5.5	[m]
FOUND. SOIL:	vertical permeability	70.0	42.0	∼	34.5	1×10^{-8} to 1×10^{-3}	[m/s]
LEVEE BODY:	landside slope	65.5	27.3	∼	∼	0.29–0.57	[/]
	inundation time	52.9	9.2	∼	∼	1–6	[d]
LEVEE BODY:	waterside slope	50.0	29.9	∼	∼	0.18–0.55	[/]
FOUND. SOIL:	anisotropy	34.7	∼	∼	∼	2–5	[/]
FOUND. SOIL:	friction angle	33.4	∼	∼	24.4	21.9–42.4	[°]
LEVEE BODY:	cohesion	27.5	27.0	∼	8.1	1–29.1	[kPa]
FOUND. SOIL:	unloading/reloading modulus	17.4	22.2	∼	∼	2–5	[MPa]
FOUND. SOIL:	Young's modulus	17.4	22.2	∼	∼	10–80	[MPa]
LEVEE BODY:	anisotropy	6.0	9.5	∼	∼	2–5	[/]
LEVEE BODY:	friction angle	5.2	∼	∼	∼	26–35	[°]
LEVEE BODY:	crown width	∼	16.3	91.7	∼	1.4–12.4	[m]
LEVEE BODY:	Young's modulus	∼	16.3	∼	∼	20–50	[MPa]
LEVEE BODY:	power m	∼	10.5	∼	∼	0.5–1	[/]
	duration of water event	∼	∼	∼	8.7	1–6	[d]
		D	Ux	G	F		

Table 4.6. Final selected important parameters.

Component	Parameter		
	Geometric	Physical/Mechanical	Hydraulic
LEVEE BODY	waterside slope crown width landside slope	Young's modulus cohesion friction angle power m	vertical permeability anisotropy
CORE	position inside the levee height landside slope crown width *		vertical permeability
TOP LAYER	thickness		vertical permeability
FOUND. SOIL		Young's modulus unload./reload. modulus friction angle	vertical permeability anisotropy
BERMS	landside berm width * landside berm height *		
GENERAL	crown height from landside toe crown height from waterside toe river depth river bank slope channel width channel depth channel dist. from landside toe water height *		water depth in the landside soil inundation time duration of water event

* Factors not identified by SB.

4.5 Conclusions

This paper presents a methodology for assessing the most important parameters affecting levee behavior within an area of interest, in terms of deformation, flow, and stability, but it is not limited to these mechanisms by any means. The methodology utilizes complex numerical analyses coupled with the sequential bifurcation method to identify these parameters. The first step requires the analyst to define the area of interest for which the analysis results will hold. Then a statistical analysis of all the desired levee parameters is done to identify the appropriate ranges, and then if needed, data transformation is conducted to modify the identified ranges. Analyses by SB are then conducted by using said numerical analyses and observing the desired response variable or variables. The results of analyses conducted by this methodology provide a list of parameters that should be focused on when analyzing the specific levees of interest and any levee whose parameters fall within the ranges specified by the analysts. These parameters (or factors) should not be confused with the parameters that in general are known—from theoretical knowledge, empirical data, and intuitively—to control any specific mechanism, but they are instead parameters which, for a large number of levees, are most important for the generalization of their behavior. They obviously do have some overlap, but failure to understand this point could lead to incorrect conclusions about the system. It should be noted that the methodology encourages adding parameters to the list that are not identified by the methodology but that the analyst deems important. The resulting list of important factors may be used for various purposes, some of which are: understanding the behavior of levees within the specific area of interest, creating models by using only the most important information, optimizing the field and laboratory investigations required for a specific project, and optimizing the control measures during and after construction. Results from this paper's case study are valid for any set of levee cross sections that are part of a larger set of levees, whose parameters can reach approximately the same values as the bounds specified in this paper. In any other case, the percentages would be misleading; instead, new analyses should be conducted following the same methodology. Further improvements can be made by defining the corresponding levee parameters as random variables with known distributions [84, 112, 156, 191, 192] and then conducting a variation of the SB method by Cheng [179], which allows for the output to be stochastic. This would surely affect the classification of the important parameters as their variations are taken into consideration, contrary to the analyses in this paper, where the inherent soil variation is considered negligible.

One of the biggest challenges regarding this methodology, besides the need for correct sign identification, is that some parameters change sign depending on other parameters' values. This means that it is impossible to assign a "correct" sign for these parameters' effects. If such parameters are known, they may be isolated and analyzed separately; otherwise, they are left in the analyses and should not have too much of an effect on the desired results.

Chapter 5

Machine Learning Tools for the Generalized Assessment of the Levees' Behaviour

Authors:
Nicola Rossi, Mario Bačić, Lovorka Librić, Meho Saša Kovačević
Paper status:
Draft

5.1 Introduction

Flood-causing high-water events are events that occur with some statistically expected frequency and have the possibility of causing large-scale disasters which bring direct and indirect losses to the community. According to Serinaldi et al. [4], between the 1994 and 2013 floods were the natural disaster with most occurrences out of all (not, however, the most damaging). Similar statistics regarding the destructiveness of floods can be found in literature, e.g. [5]. To mitigate the effects of high-water events in residential or other important areas, levees are built to confine the water to floodplains. Building levees, however, theoretically affects the hydrograph's shape differently at various locations relative to the levee, i.e. increase the peak water height ("stage") and velocity at the levee location, while different changes occur upstream and downstream [193]. Hydraulic modelling procedures also showed an increase, but with highly varying heights, which is also generally supported by empirical observations, as summarised by Heine and Pinter [194]. Climate changes also play a significant role in all of this, by having different impact on flood frequency and magnitude at different geographic locations [195]. Even though various measures exist to alleviate these effects, the safety requirements of the existing levees protecting residential and other important areas need to keep up with these changes, which often require reconstruction/enlargement. High-water events, being such a frequent event

with relatively short durations, with peaks of even shorter duration, can cause levees to fail by various mechanisms [24] during these short-timed events. Since levees are long linear structures whose construction depends on many criteria, among which are locally available materials, construction space requirements, ULS and SLS requirements, local practices and so on (some of which can or cannot be controlled), they also pass over highly variable subsoil stratigraphies (often alluvial deposits with high inherent variability). This obviously results in many different cross-sections, including the subsoil, and is often handled by probabilistic analyses which consider each parameter as a random variable with its probabilistic distribution [29, 30, 196, 197], with the geometry often being fixed. These analyses give valuable insight into the behaviour of levees, but often do not offer a level of generalization that would encompass large areas of interest. To predict deformations [198, 199], factors of safety [200, 201], hydraulic gradients [78, 79], and from them probabilities of failure or unwanted behaviour, the primary methods being used are numerical analyses. They are, however, inefficient when there is a need to evaluate these responses in very limited time periods, due to the need for data gathering, model creation, and analyses run times. Instead, they can be conducted prior to water-events by considering the most important variable-levee-parameters to accumulate a large quantity of data. The results can then be used to train machine learning models to find relations between input and output parameters, such that results may be obtained immediately upon request at any given moment, for any section whose parameters fall within the ranges defined for the numerical analyses.
To describe any levee section uniquely, in terms of both geometry and material properties, a large number of factors is required. In a recent paper, Rossi et al. [202] showed that out of over 100 parameters required to uniquely define a levee section, about one third are deemed important for the generalization of the levee behaviour, such that the variations of the other parameters can be ignored. This study continues on their findings and uses the selected parameters to create predictive machine learning models—to predict crown displacements, factors of safety of the landside slope, and exit hydraulic gradients. Machine learning for different types of assessment of earthen waterfront structures is readily being used in scientific investigations [45, 50, 51, 77], and back-analyses are conducted by single- or multi-target optimization algorithms [38–41, 203]. The methodology presented here is based on the Support Vector Machines (SVM) method for creating the models, and Particle Swarm Optimization (PSO) for optimizing them for conducting back-analyses. SVM was originally published by Boser, Guyon, and Vapnik [204] for classification purposes, and later extended to adopt regression too [205]. PSO was introduced by Kennedy and Eberhart [206] in 1995 as an optimization algorithm for continuous non-linear functions, born from the need of simulating social behaviour, and inspired by the behaviour of animal groups in nature. The algorithm has, despite its origins, been successfully applied in the field of geotechnics [42, 207]. The methodology is also an extension to the methodology presented in the recent paper by Rossi et al. [202], where the key levee factors were identified for the relevant geotechnical analyses performed on levees (deformation, stability and flow analyses). By using these parameters as input, numerical analyses are

run, and machine learning models are created to predict and control the behaviour of the monitored levees during high-water events. Back-analyses by optimization are used to assess the true parameters of the levee components in the case that deformation monitoring showed different displacements from the predicted ones. Figure 5.1 shows a flowchart with the steps of the whole methodology within a standard machine learning framework. The top part of the figure shows the steps of the methodology defined in [202], the two squared steps pertain to the ones discussed in this paper, and the last two steps written in red regard the validation with real-life data and deployment to existing management frameworks, which are yet to be applied on the developed models.
Employment of such models for the management of a large numbers of levees would minimally require a database of at least the most essential levees characteristics. Such databases are unfortunately still scarce.

5.2 Description of the Dataset

The dataset is composed of 1000 observations. Complex numerical analyses are used to generate the observations to simulate as realistically as possible the real-life behaviour of levees during the rising phase of a high-water events, from start until reaching a peak value, without the receding phase. The finite-element analyses consist of fully-coupled flow–deformation analyses in which the pore pressures and deformations are simultaneously developed in saturated and partially saturated soils in time [208]. After achieving equilibrium in the specified time, stability analyses are conducted with the Strength Reduction Method (SRM) with the soil in the state it is found in after the time-dependent deformations have developed. This gives realistic factors of safety of the levee and its surrounding area in the most critical point in time during the high-water events, i.e. the maximum water level. To consider the interaction between the deformations and the soils' strength and stiffness parameters, the Hardening–Soil model is used. The analyses are conducted in Plaxis 2D, 2019. In a recent study by Rossi et al. [202], out of the 101 parameters used to define a complex levee section, 34 parameters are found to be important for defining the levee sections and generalizing their behaviour, and so they are used in this study (called features in the machine learning terminology). Since different sections are considered which have more or less components—the impermeable core, the landside and waterside berms, a thin surface layer under the levee, the riverbed in the vicinity of the levee, and a channel on the other side—and these components affect the behaviour of the levee, the (non)existence of these components is also input as features in the model. From the results of these analyses, multiple outputs are observed and recorded:

- Horizontal displacements at one specific point on the levee crown (Figure 5.2).
- Maximum model deformations within the levee area (between the two toes), and its location.

- Maximum exit hydraulic gradient along the landside surface, and its location.
- Minimum factor of safety, and the location of the corresponding slip surface.

These observations are used to assess the behaviour of the levees. The slip surfaces resulting from load-deformation analyses with the SRM method manifest themselves and can be detected

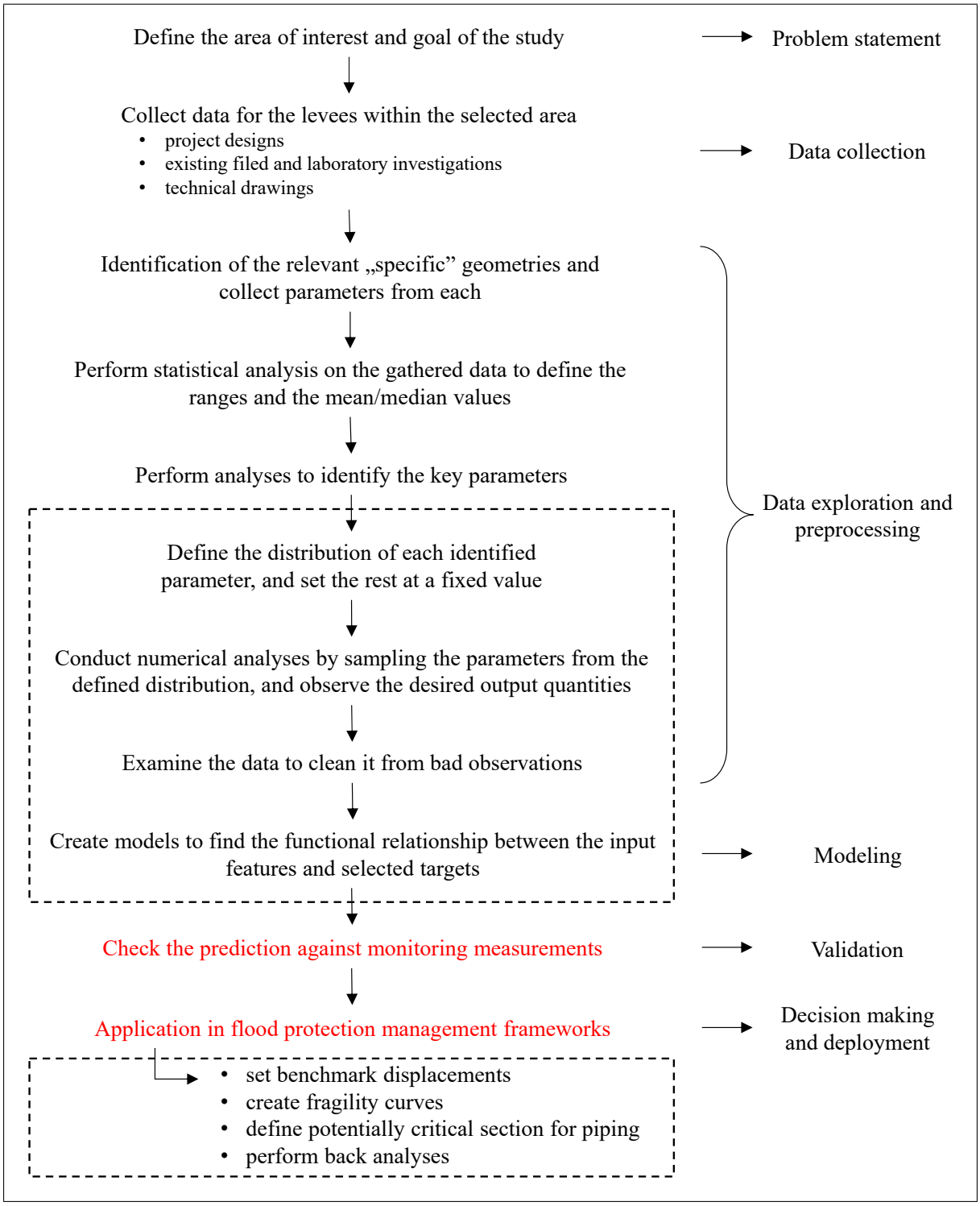

Figure 5.1. Flowchart of the presented methodology within a machine learning workflow.

by the a zone of large deviatoric strains. One limitation of the SRM method is that the slip surface cannot be forced on a location or shape of interest, such as, for example, looking for the minimal factor of safety of the landside slope using the limit equilibrium method (in which case the slip surface is contained within a specified area). Which means that often the critical surface does not even reach the levee, but forms within the river or channel slopes instead. This does show where the occurrence of the surface with the absolute minimal safety factor is going to be expected, but does not always tell about the stability of the levee itself. In any case, the locations of the critical slip surfaces are defined only by the levee components they encompass (where they start and where they finish), regardless of their shape and depth.
The locations of the maximum deformations are defined by four quadrants in each levee component above ground, and two parts for the components underground, as shown in Figure 5.2.
The hydraulic gradients are observed on the landside of the slope, from the top of the crown, to the end of the model, along the surface. This line is divided into four parts to categorize the location of the critical gradient occurrence. The locations are: the levee slope, the berm, the foundation soil next to the berm, and finally the slope of the channel (if it exists).
The materials' and geometric parameters used to construct the different levee sections are sam-

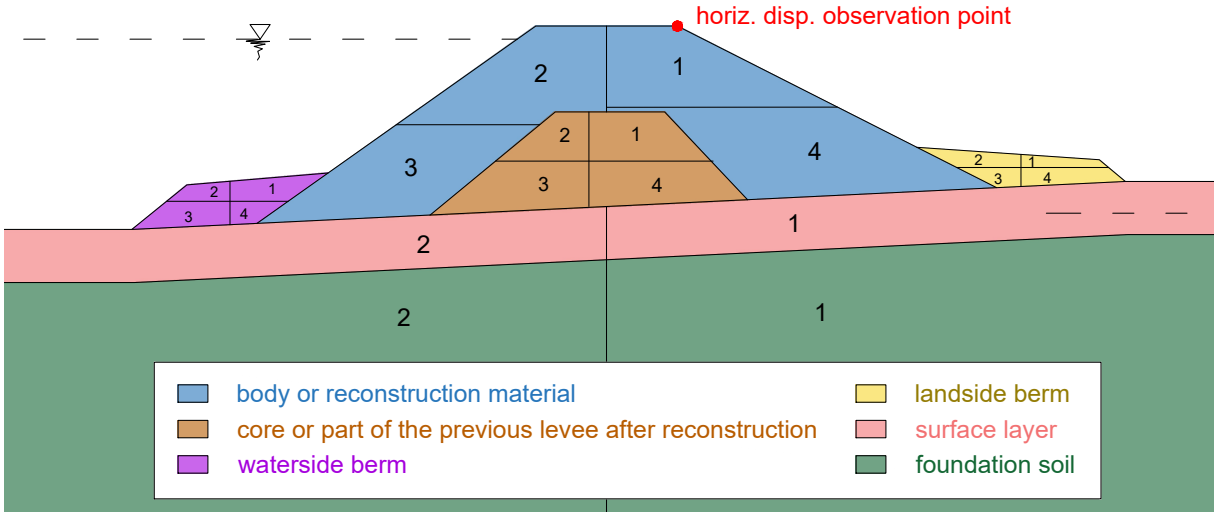

Figure 5.2. Quadrants for defining maximum deformation locations, with point for observing horizontal crown displacements.

pled from statistical distributions. The distributions are artificially created from the bounds of each parameter, which are found by a prior statistical analysis of the cross-sections of all the considered levees [202]. Many parameters contained extreme values found on only a handful of cross-sections, which consequently produce skew in the distributions. Because of that, to have all distributions close to normal, all the parameters have been transformed by log, square-root or boxcox transformations. This is done for most parameters, except some for which a uniform distribution is more natural. Sampling is then done by either normal or uniform distributions, and the parameters are afterwards transformed back to their original space. All the other parameters required to define the sections and materials' models, but which were found to be

unimportant, are kept at the mean or median values of their expected ranges or distributions. The ranges and the distributions of all the used parameters are defined in the dataset which is available at the end of this paper.

5.3 Data Exploration and Preprocessing

Before training any machine learning model, exploratory data analysis is performed to clean the data and prepare it appropriately for training. This chapter describes in detail the exploration and preprocessing which are common to all the models, and a short description of the additional works conducted for each model separately.
First, each feature defining the existence of a specific component is binary encoded with 0 for not existing, and 1 for existing. This added 6 new features to the 34 existing numerical features, which makes a total of 40 features for training. Outliers in the data are possible due to model failures and premature termination of calculations. Since no correlations are set beforehand between the various input parameters, there is the possibility of unreal parameter combinations, e.g. between internal friction angle and cohesion, which also yield results which are not of interest. Numerical issues are also of concern. So, first all of the unfinished calculations due to model-failures (regardless of the cause) where the reached time does not equal the defined high-water event duration are removed (a total of 12 observations). Attempts to detect outliers are then made by boxplots which define the expected range of the data by the observed percentiles. All data lying outside this range are potential outliers, which are then manually reviewed before removing them. By this method, only 2 observations are removed corresponding to extreme and unrealistic deformations, with 986 observations now remaining. After removing the bad observations caused by the mentioned errors, the dataset is split into train and test sets, with 70% of the data in the training set and the remaining 30% in the test set. This is done to make all the additional transformations and scaling fit to the data in the training set, which will be used to train the models, and then use the transformation and scaling parameters found in the training set to perform the same operations on the test set, which will be later used to validate the model. The target(s) are then transformed to better fit a normal distribution. For both the horizontal displacement of the crown and the factor of safety, this is achieved by single boxcox transformations. Figure 5.3 shows the original and transformed histograms of the horizontal crown displacement and the factors of safety, along with the corresponding p-values from a normality test [209, 210] and the λ values for the boxcox transformations. When using distance-based algorithms such as SVM, it is important to bring all the features on the same scale. Most often this is done by standardization or linear scaling between a minimum and maximum value. In standardization, the distribution of the data is inferred from the training set, then from each value the mean is subtracted, and the result divided by the standard deviation. In the “MinMax” scaling the minimum and maximum are also found within the train set, and each value in the train and test set is then scaled in between those values. Each feature is scaled by

either one of these scalers, except for the features which are already close to the desired ranges. Some features exist in the logarithmic scale, so they are first transformed by taking the natural logarithm of their values before scaling. The target is not scaled.

After getting the data ready, a preliminary SVM model for horizontal crown displacement

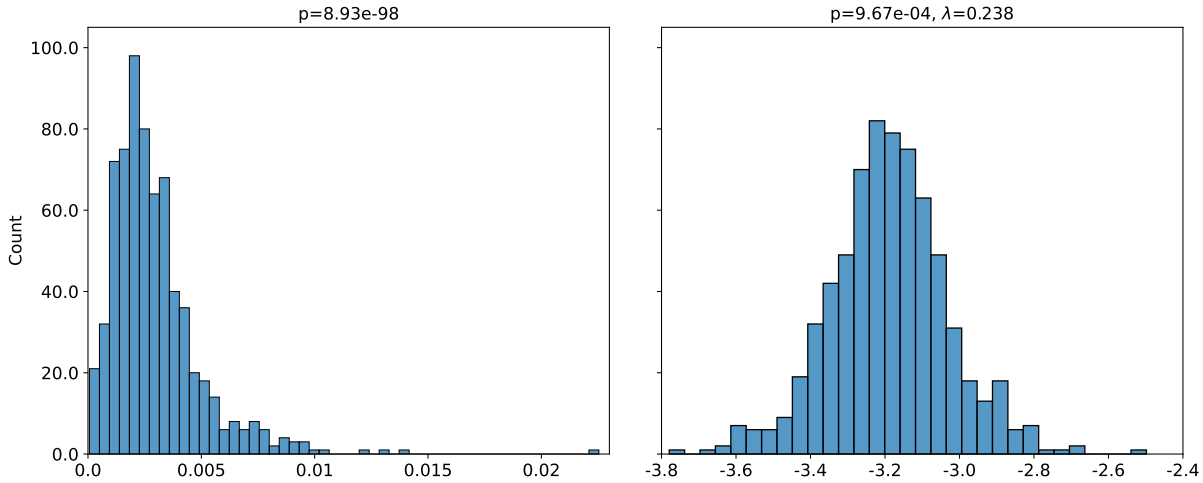

(a) Horizontal crown displacements

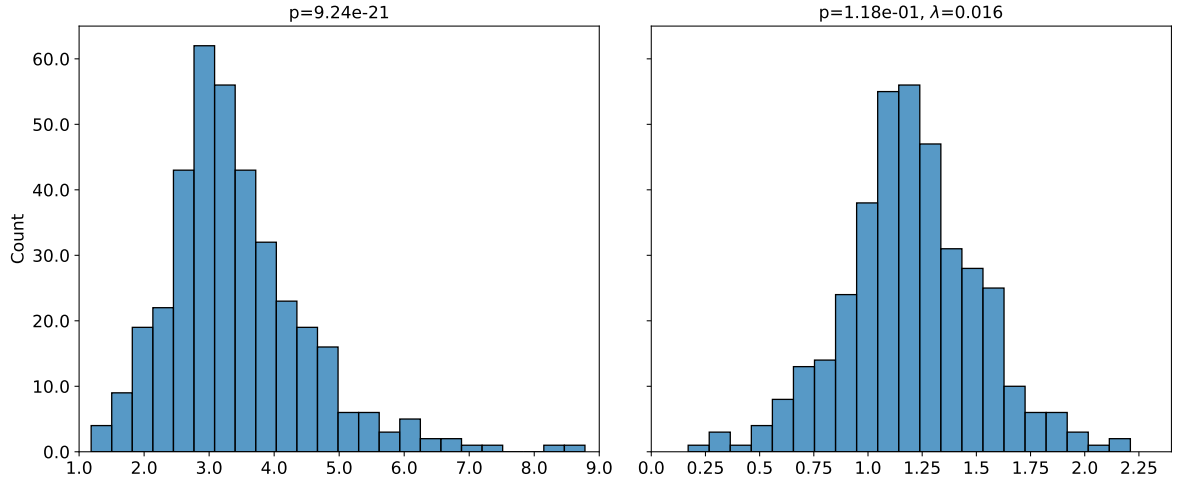

(b) Factors of safety

Figure 5.3. Histograms of the original (left) and transformed (right) targets.

prediction is trained using all the data and calculating the residuals. A simple plot visually showed the datapoints with high residuals which may be outliers due to various reasons. This way, 5 more observations are identified to be outliers, none of which corresponding to the minimum or maximum sampled values of any feature, and are removed after close inspection. The final datasets thus contain 688 observations in the training set, and 293 in the test set, for a total of 981 observations (only 19 observations removed, or 1.9% of the dataset size).

For the model predicting the factor of safety, other preprocessing was required. Due to the mentioned limitations in detecting the slip surfaces with the SRM, only a subset of the critical slip surfaces within the dataset developed through the levee body (see Section 5.5.6). That subset contains 542 observations. Since we are dealing with existing levees, only observations

of slopes with factors of safety over 1 are considered, which further reduced the subset by 4 observations. This datased is then split into train and test sets, again by 70%–30%, which yields 376 observations in the training set and 162 in the test set, and these are used for this model creation and validation.

For the hydraulic gradient prediction, two sets are used. Numerical analyses showed that in the majority of cases, 60%, the exit gradients were 0 or close to 0, while in the rest of the cases, 40%, they varied up to 15, resulting with a histogram shown in Figure 5.4 (the histogram is cut at 3 for readability, the values up to 15 are sparse). Because of this, a preliminary classification model is trained, to detect whether a section will experience an exit gradient greater or lower than a selected value of 0.1. For this model, no additional preprocessing is done, but it is worth mentioning that the train–test split is done by keeping the 60–40% ratio of the larger–lower than 0.1 gradient in both train and test sets. The second model is to be used only if the first model classifies the section as a candidate for developing large exit gradients. Thus, it is trained using the observations with gradients > 0.1, which is 388 observations. The gradients larger than 5 are removed, which is only 6 values (leaving 382 observations), which are probably data gathering errors due to local spikes in gradients around the water table. Train and test splits are for both models again done by 70–30% splits.

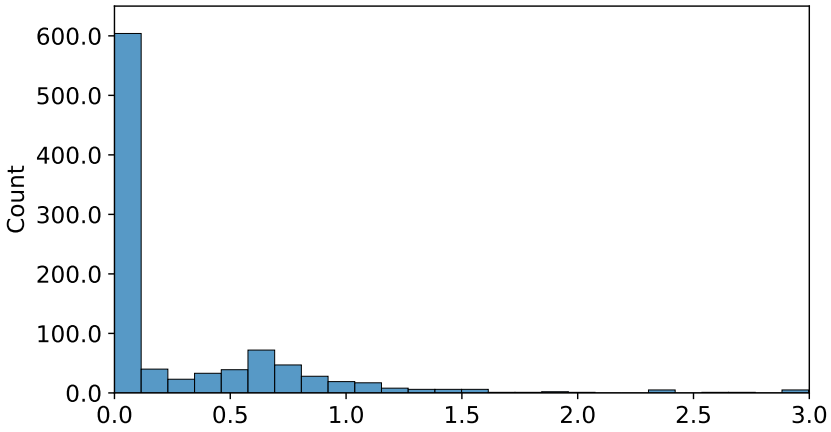

Figure 5.4. Histogram of hydraulic gradients, cut at 3

5.4 Model Training

The first model is trained to predict the horizontal crown displacements, based on the 40 features and 688 observations. Support Vector Machines are used for the model training, by searching for a linear hyperplane which best fits the data. Clearly this is not always possible in the space in which the data exists, and thus often some transformations are employed to bring the data to higher dimensions, where a linear hyperplane may be found. This is done by functions called "kernels", and the kernel used in this study is the Radial Basis Function (RBF). To fit the plane

to the data, SVM searches for support vectors. Each observation in the training set is deemed a vector in the feature space, any only a subset of them are selected as support vectors, which are the ones required to define the hyperplane with the various constraints. Additionally there are three hyperparameters which affect these constraints, the tolerated errors, the generalization capacity, and the complexity of the SVM models—γ, ϵ and C, and their optimum values are found from specified ranges. Cross-validation with 10 folds is used for the training, where the training set is additionally divided into 10 train and validation splits, and then training is done 10 times for each hyperparameter combination, each time on one of the 10 train sets and validated on the corresponding validation set. The hyperparameters' combination which yields the highest mean validation score from all the 10 sets is selected. The metric used for optimizing the hyperparameters is the coefficient of determination (R^2). This procedure is done to avoid overfitting, and multiple splits are required to avoid lucky splits. The highest score is obtained for the following hyperparameters: $C = 220$, $\gamma = 3 \times 10^{-4}$ and $\epsilon = 0.01$. After training, the model is evaluated by four performance metrics—the coefficient of determination (R^2), the mean squared error (MSE), the root mean squared error (RMSE) and the mean absolute error (MAE).

A second model is trained using the same procedure to predict the factors of safety of the slip surfaces fully or partly encompassing the landside slope. The model is trained on the previously described reduced dataset. This model used an additional feature compared to the previous, and that is the target of the first model, i.e. the horizontal crown displacement (total of 41 features). Since this model's intention is to predict the factors of safety for sliding, which always follows deformations, it makes sense to include the crown displacements as a feature. The model is based on the same setup as the first model, where the found optimal hyperparameters are: $C = 3.1$, $\gamma = 0.01$ and $\epsilon = 0.01$. The controlled performance metrics are the R^2 and the MSE.

The third model's focus is on the exit hydraulic gradients along the landside surface, from the levee crown to the end of the model, with a buffer of 20 cm in depth. As previously shown, before trying to predict the gradient values, first a preliminary classification model is built to detect which sections will or will not experience a potentially significant hydraulic gradient. This classification model is done by using SVM for classification which, similarly to the described SVM for regression, searches for a linear hyperplane, but one which is best at dividing the two classes, instead of fitting the data. The hyperparameters used here are C and γ, with the best value being 8 and 0.028 respectively. 5-fold cross validation is done, with evaluation by the Recall metric, defined by the ratio of true-positives to the sum of true-positives and false-negatives. This metric gives more focus on correctly predicting true-positives, which in this case is the group experiencing potentially large gradients, which means it tries to minimize the false-negatives (incorrectly predicting that a section will experience 0 gradients). In this case, as in many others, it is better to incorrectly predict that a section will experience potentially large gradients than not. The chosen model is then evaluated on the test set by the Precision, Recall, F1 score, and the confusion matrix from which the scores are computed, as well as the

Precision–Recall curve with the associated AUC (Area Under the Curve) score. The second, predictive model is trained on the small set of 267 observations (70% of 382), again using SVM for regression with the same setup as before. Unfortunately, the model was not able to predict the gradients in any sensible manner, so the results are not reported.

Oftentimes only the essential and most common geometric and physical-mechanical levee parameters are available from geotechnical reports, contrary to all the parameters used to train the described models. From the currently used parameters, the essential and most common ones are identified. New test sets are then created by keeping the identified parameters' values as they are, while fixing all the others to the mean or median values of the ranges and distributions used for training. Then, to test the models' application to more real-life situations where less data is available, both are subjected to the new test sets. These predictions are expected to be slightly worse than with all the parameters, but an acceptable performance would show that the models can be used even with lacking data about the levees. No additional training is done on these models, they are just applied to the new test sets.

During deployment of the predictive models in real-life scenarios, it has been described how they can be used to set a benchmark value for displacements to be compared with data from real-time monitoring. Measurements can, however, deviate more or less from the predicted value. After the flood event, new investigations can be conducted to detect the cause of the different behaviour—which may either be damage to some levee component, or simply an incorrectly assessed parameter value. For the latter case, model optimization is here used to find the values of the potentially unknown parameters based on the measured displacement on an arbitrary levee section. The Particle Swarm Optimization (PSO) algorithm is used, which is based on initializing a number of "particles" across the prediction plane, and searching for minima around each particle in random directions, and ultimately settle for the global minima of the whole "swarm" or particles. In each iteration the movement of each particle is influenced by its own local minima, and the global minima found by other particles. The behaviour is also affected by four hyperparameters—the number of particles n, the inertia weight w which controls the convergence of the particles to a specific solution, the cognitive parameter c_1 and the social parameter c_2, which respectively affect how much weight is placed on each particle's local minima, or the whole swarm's global minima. Their values are selected as $n = 30$, $w = 0.73$, and $c_1 = c_2 = 2.05$. The objective function to be optimized is the SVM model for displacement prediction. The performance of the model is evaluated by the square of the minimization error, $(f(\mathbf{x}) - u_{x,target})^2$.

5.5 Results and Discussion

5.5.1 SVM for Displacement Prediction

The results of the first model trained for predicting the levees deformations during the rising stage of high-water events is shown in Figure 5.5. The figure shows a color-density plot of the observed versus predicted values, the mentioned performance metrics realized on both the training and testing sets, and another color-density plot showing the residuals versus the predicted values. The values shown on the diagrams correspond to the boxcox-transformed values with the previously specified λ value, and as such the error metrics that have a unit of measurement also pertain to the transformed values. From the performance metrics it can be concluded that good quality predictions can be achieved through this model, and that no overfitting to the training data occurred. However, as can be seen from the histogram in the original scale in Figure 5.3, most displacement values fall within a 0–1 cm range, so any predictions of larger displacements should be carefully considered. The distribution of the residual errors shown on

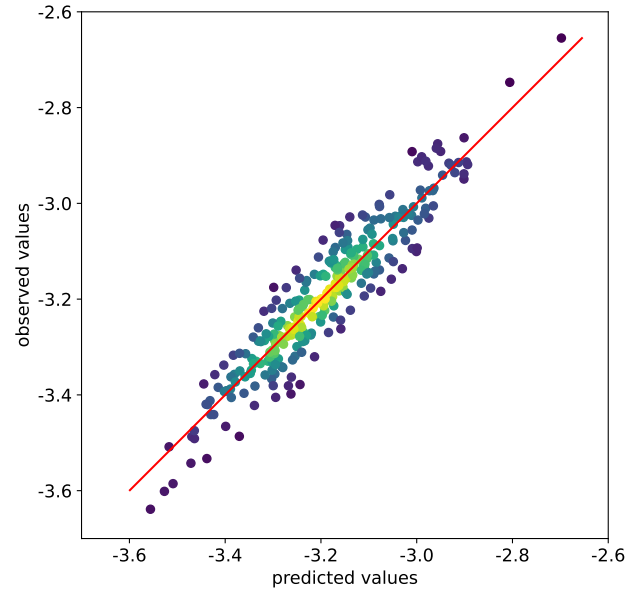

	Train	Test
R^2	0.914	0.883
MSE	0.0021	0.0026
RMSE	0.0462	0.0514
MAE	0.0301	0.0399

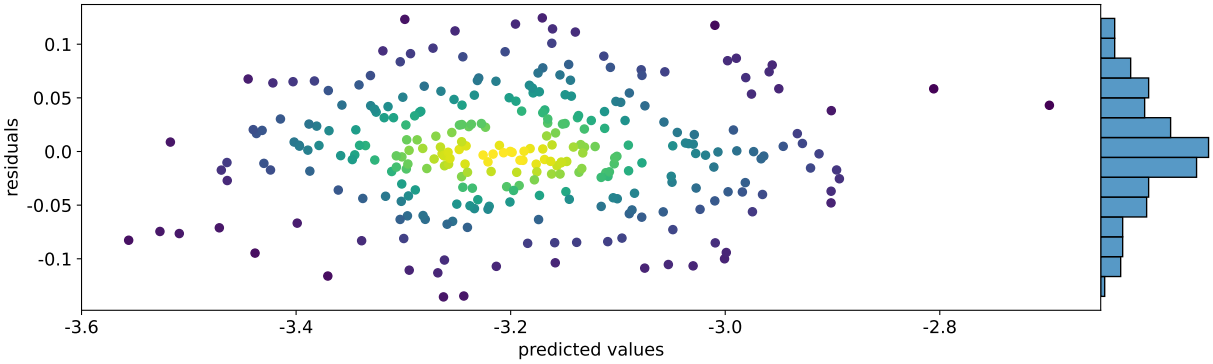

Figure 5.5. Plot of observed vs predicted values (top left), table of performance metrics (top right), and plot of residuals vs predicted values with a histogram of residuals (bottom)

the histogram in Figure 5.5 can be described with 0 mean (μ) and 0.051 standard deviation (σ)

in the transformed space, which means that, if needed, they should to be applied to the prediction before transforming the target displacement back to the original space. This distribution is used to calculate the confidence intervals of the predictions. By using this model, prediction curves can be made for any cross-section of interest, with regard to any parameters of interest. Figure 5.6 shows the predicted horizontal crown-displacements for an arbitrary levee section which satisfies the parameter bounds defined by this model. The predictions are constructed with increasing water level on the horizontal axis, and predicted displacements on the vertical axis, and multiple curves are created based on the initial water level on the land side prior to the high-water event (water on the surface, and at a depth of 3 m below the surface). 95% confidence intervals are also plotted for the two curves. In a similar fashion, plots can be generated to view the relationship between the displacements with regards to any other input parameter, such as flood duration, rate of increasing water-level, etc.

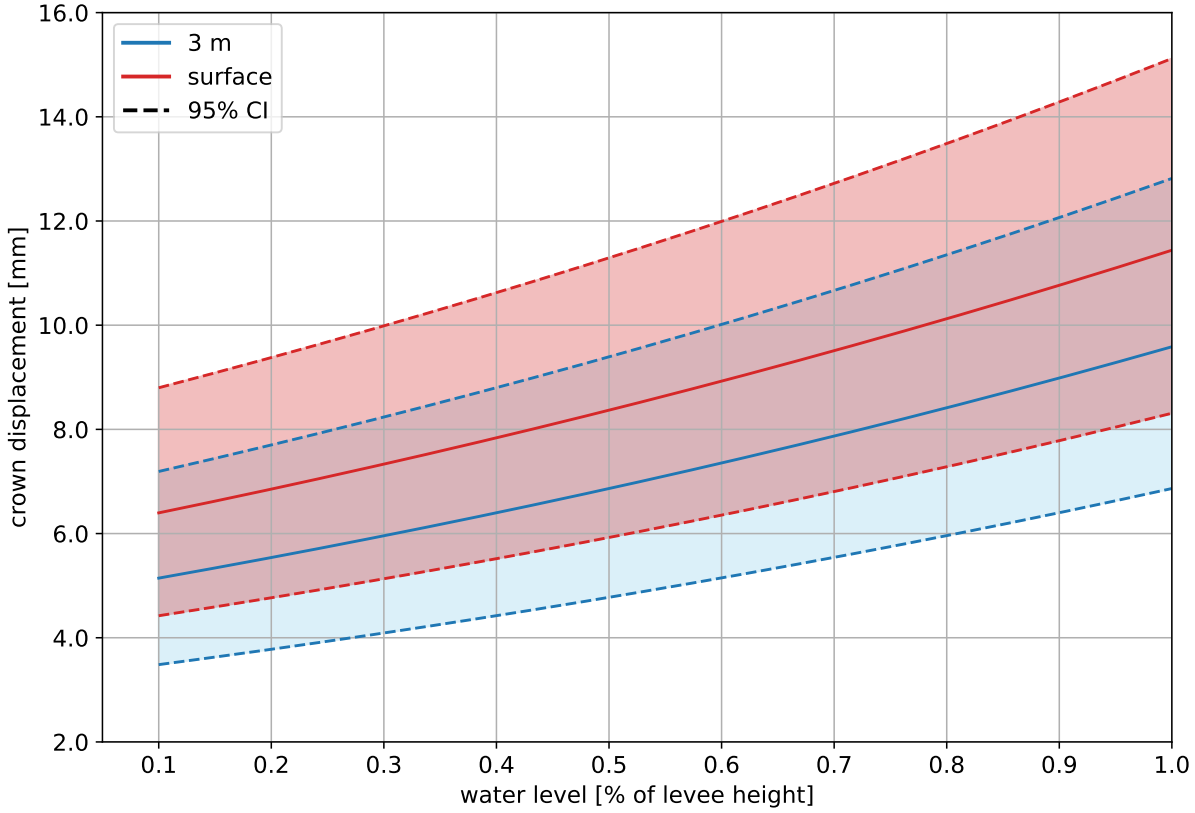

Figure 5.6. Predicted crown displacement versus water height for an arbitrary levee, for two initial water-levels in the landside area.

5.5.2 SVM for Factor of Safety Prediction

Due to the fact that stability problems follow deformations, a second predictive model is created by using the crown displacements as a new feature. This model thus has 41 features, with the

target being the factor of safety, and is trained on the previously described subset containing 376 observations. This reduced dataset is put thorough the same preprocessing steps as described previously for the original dataset. Due to lack of data and higher variability, the model does not perform as well as the first model, as shown in Figure 5.7, most likely due to a lack of parameters (features) which control this mechanism. The reason why such parameters, like for example the strength properties of other materials, may not have been identified by the methodology described in [202] is tied with the SRM analyses limitations mentioned in their paper, and this one as well. In the coupled flow–deformation analyses using the Hardening–Soil model, plastic failure often occurs within the river and channel slopes. The safety analyses that come afterwards identify these positions as critical for failure and a small failure surface develops on these positions. Those failure surfaces are not affected by the levee and core materials. Anyhow,

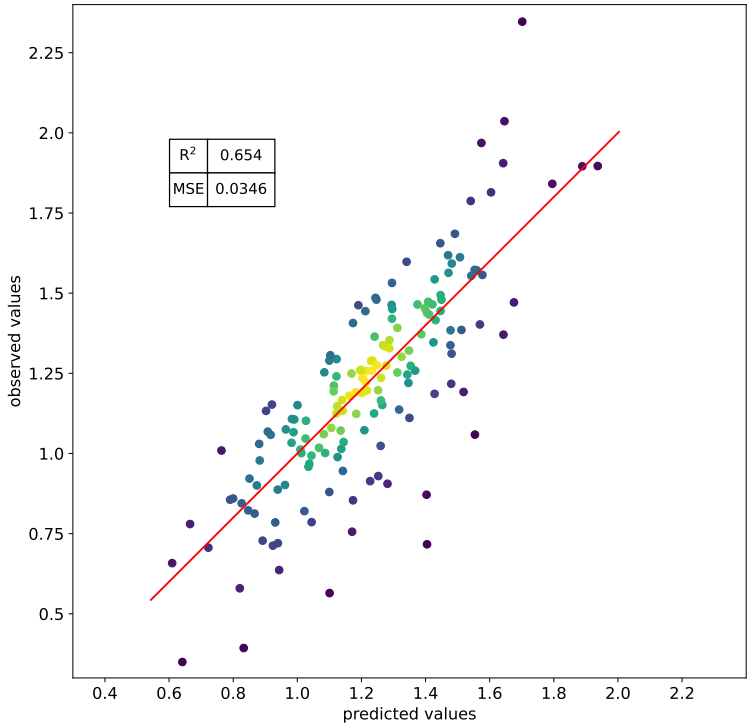

Figure 5.7. Plot of observed vs predicted values for the factor of safety prediction, with performance metrics

the error's distribution is again calculated using the residual errors from the test set, and is again a normal distribution with 0 mean (μ) and 0.186 standard deviation (σ) in the FS's transformed space. In this case, knowing this distribution allows for the calculations of a reliability index, β, according to Eq. (5.1).

$$\beta = \frac{\mu - FS_{crit}}{\sigma} \tag{5.1}$$

where μ is the mean (predicted) FS, σ the standard deviation of the FS residual errors, and FS_{crit} is the critical value of the factor of safety which defines an unwanted behaviour—1 for failure (the critical value should be considered in the transformed space). Assuming a normal distribution, the probability of failure (p_f) can be calculated from the standard normal cumula-

tive distribution function (Φ), by Eq. (5.2).

$$p_f = 1 - \Phi(\beta) \tag{5.2}$$

It should be noted that the variability used here to calculate the probability of failure is not connected to the inherent soil variability, or other types of uncertainties connected to the soil or construction methods, but only from the model's uncertainty.
By first predicting the crown displacement of the levee in Figure 5.6, and afterward predicting the mean FS, thus calculating the mean p_f for each water level, a fragility curve can be created which shows the conditional probability of failure (or unwanted behaviour) with increasing water level. Moreover, if we add the error term to the predicted displacement, and the prediction is then repeated many times, say 1000, then a statistical distribution of the mean probability of failure can be constructed and used to assess the probability that the p_f is found within a specific range, i.e. calculate the confidence intervals of the p_f. A fragility curve for the same arbitrary levee as before, together with the p_f distribution for an arbitrary water level, is shown in Figure 5.8. The probabilities shown in Figure 5.8 are conditional probabilities, i.e. $P(FS < 1 \mid H_p)$ which tell the probability of the factor of safety being less than 1 given that a specific water-level occurs. If the probabilities of water-level occurrences are also known, then actual yearly probabilities of failure can be calculated by $P(FS < 1 \mid H_p) \times P(H_p)$.

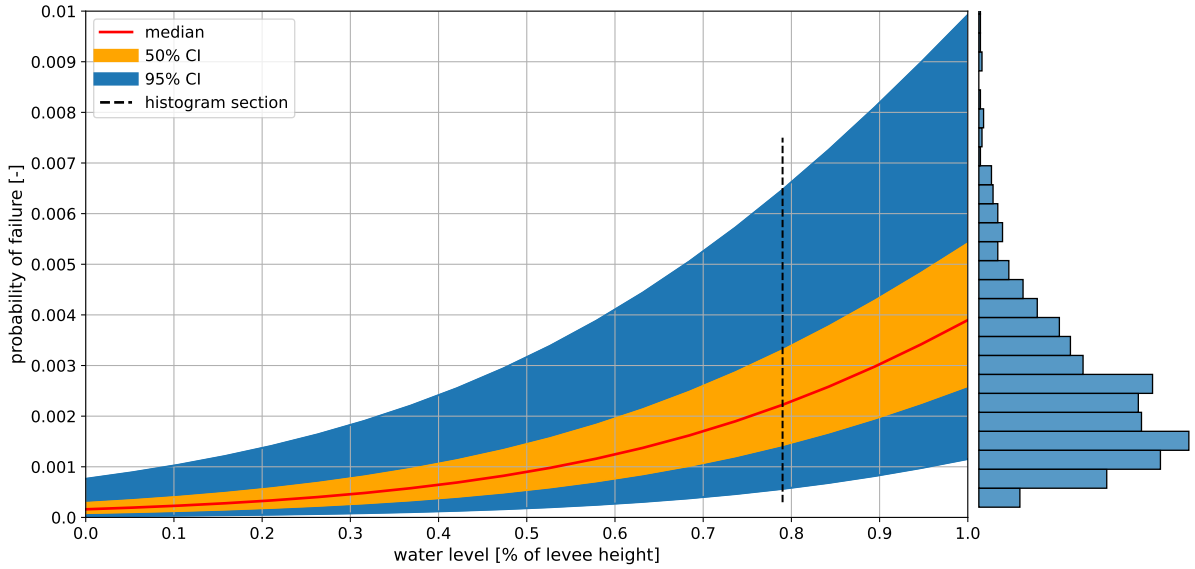

Figure 5.8. Fragility curves showing probability of failure for the sliding mechanism versus water height for an arbitrary levee.

5.5.3 SVM for Hydraulic Gradient Prediction

As with the prediction of displacements and factors of safety, a model is created to predict the exit hydraulic gradients. As mentioned previously, this model is divided into two models, the

first one for classifying the section of interest into one of the two groups—one having gradients < 0.1 and the other > 0.1. The metrics are calculated for each class, and are shown in Table 5.1, and Figure 5.9 shows the Precision–Recall curve and the confusion matrix. From the results it can be seen that the prediction of the no-gradient case is better than the other, which means that we can be more certain when the model predicts the first case, than the second. Both scores are high enough to make good predictions about whether a specific cross-section has the potential of developing high exit gradients or not. However, the model created for the prediction of the actual gradients, once it is established that they can develop, did not manage to predict the outcome in any sensible manner. This may be due to the small number of observations which were available for training.

Table 5.1. Classification metrics.

	Precision	Recall	F1
Gradient < 0.1	0.86	0.87	0.87
Gradient > 0.1	0.80	0.78	0.79

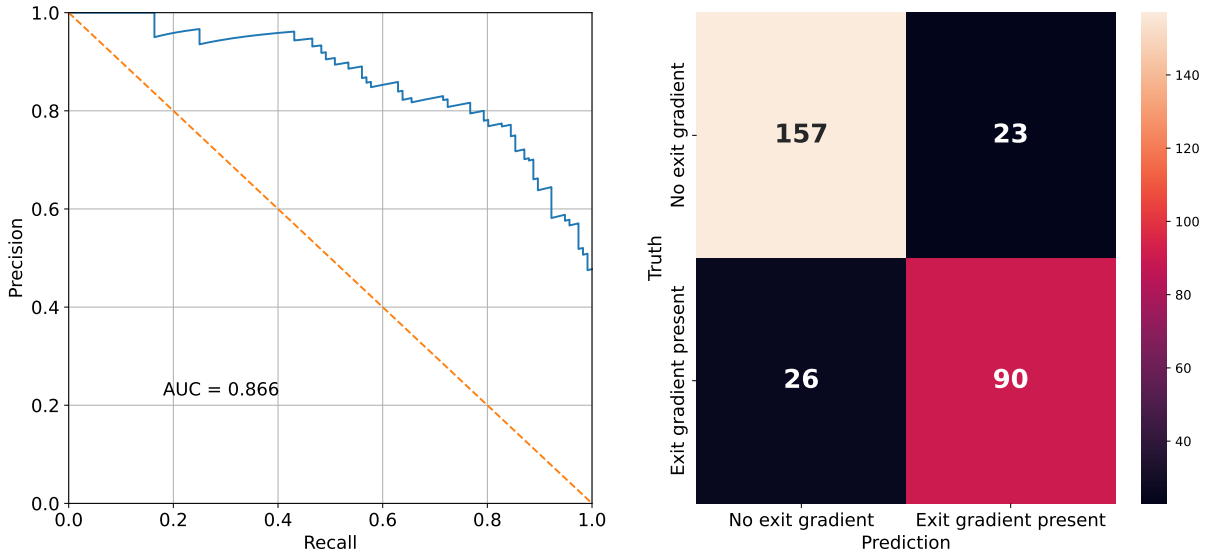

Figure 5.9. Precision–Recall curve on the left and the confusion matrix on the right.

5.5.4 Optimization of the Predictive Models

A test is made on the arbitrary levee used throughout this study. Let's say that for a high-water level corresponding to 40% of the levee height, the measured crown displacement amounts to 1.1 cm, while the model predicts a displacement of 0.7 cm. Say that out the 40 features, we are uncertain in the stiffness values of the levee body and the foundation soil. Now we choose the ranges for the possible values of those two parameters, while we fix the values of all the others. This makes PSO adjust only the parameters of interest. A result is found after 1000 iterations with an error of 6×10^{-9}, and the found parameters' values are $E_{body} = 31.7$ MPa

and $E_{found.soil} = 9.2$ MPa (from the initial values of 32.3 and 32.6 MPa respectively). It should be noted that: 1) the target displacement should be close to or within the range that the predictive model can handle, and 2) that the specified parameters' ranges are within the possible values used for the model training.

5.5.5 Models With Only Essential Parameters

In many occasions engineers are presented with only a very limited number of parameters to work with, usually only the most essential and common ones. In such cases the created models may still be used but with worse performance. The unknown parameters should be assigned a specific value throughout all the observations, which is usually the mean or median of the values observed in the training set. However, there is a group of parameters which should always be present and are the bare minimum results from the investigation works or can be easily assessed from technical drawings/scans of the cross section. The essential parameters, out of the 34 initially used, are most of the geometric parameters, and the bare minimum mechanical parameters generally required to perform the simplest analyses. If all the components of the levee and surroundings are present, then 27 such parameters are identified, while only 15 are always present, even for the simplest geometries. The performance of these models is then evaluated, and the observed versus predicted diagrams for the two predictive models (displacement and factor of safety) are shown in Figure 5.10 along with the performance metrics, while the performance metrics of the gradient classification model are shown in Table 5.2. It can be seen that the performance metrics are slightly worse, but actually very close to the original ones, which makes these models applicable even with the lack of some parameters. This also shows that the commonly available parameters for this case mostly correspond to the ones which control the behaviours.

Table 5.2. Classification metrics for only the essential parameters.

	Precision	Recall	F1
Gradient < 0.1	0.86	0.86	0.86
Gradient > 0.1	0.78	0.78	0.78

5.5.6 Statistics of Critical Zones

By observing all the results mentioned in Section 5.2, statistics are made regarding the positions of occurrence of each of the three results—maximum model deformations, maximum exit hydraulic gradient, and minimum factor of safety. A visual representation of the statistical distribution of each is shown in Figure 5.11, where red dots represent deformations, green curves represent slip surfaces, and purple lines represent hydraulic gradient locations. Each of these symbols' thickness is scaled according to the frequency of occurrence of the corresponding result in the specific position. It can be observed that most of the highest deformations occurred

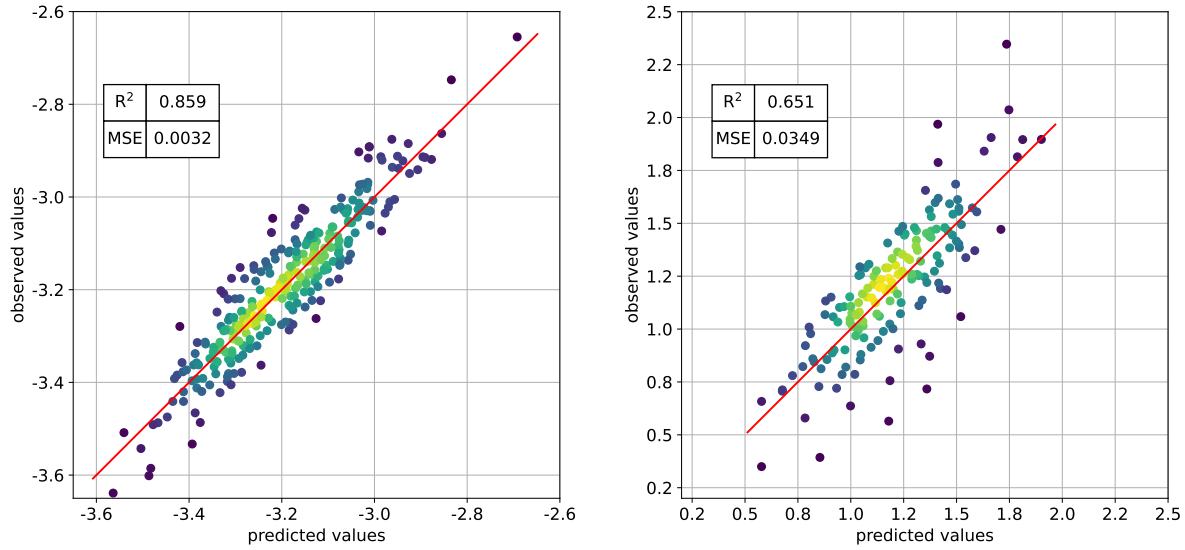

(a) (b)

Figure 5.10. Observed vs predicted values plots with performance metrics for only the essential parameters, for (a) horizontal crown displacement and (b) factor of safety

on the waterside part of the levee body, closer to the crown, which is somehow expected considering the shape of the levee and the water-load it endures. However, major deformations can also be found in other levee components, as seen in the figure. In this study the horizontal crown deformations are observed on the landside edge of the crown, but this statistic shows that the majority of times the largest deformations are found closer to the waterside edge. Perhaps a different monitoring point would result with better predictive models.

Regarding the hydraulic gradients, most of the critical ones occurred within the foundation soil, exiting within the channel.

The critical slip surfaces that directly affect the levee are mostly found starting in the body and exiting in the foundation soil, but very often the critical surfaces develop within only the river and channel banks, which are in fact usual cases in unprotected banks. In rare occasions the critical surfaces are found on the waterside slopes of the levee. One failure mechanism which isn't shown in the figure are the small and shallow slip surfaces which happen locally and are usually not immediately significant for the stability of the levee.

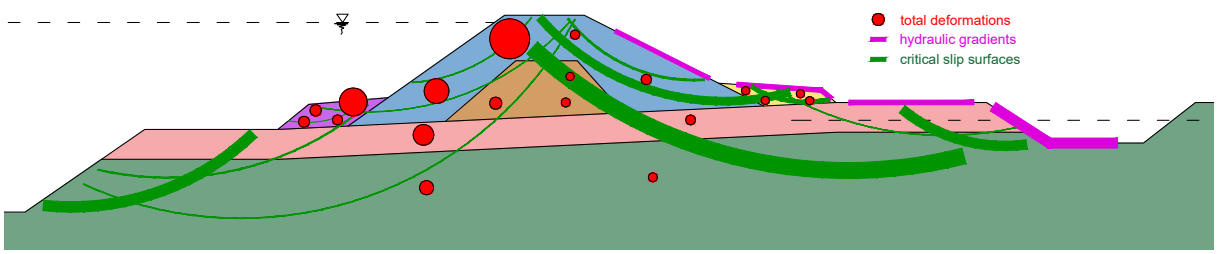

Figure 5.11. Statistics of levee responses to high-water events.

5.6 Conclusions

This paper presents a methodology for the assessment of the deformability and probability of unwanted behaviour of any section of interest which complies to the established ranges for each parameter which defines the section. The parameters to be used for the generalization of the levees within the specified area are presented in [202]. A functional relationship is established between these input parameters and the horizontal crown displacements in a range between 0 and approx. 1 cm. The model's uncertainties are taken into account to construct the confidence intervals of the predictions. It is shown that the largest deformations of a levee section can occur on various parts of the levee, which indicates that perhaps other monitoring locations may be more indicative for other specific behaviours. Simultaneous monitoring on multiple locations could also be employed to improve the models. The chosen locations also depend on the available monitoring equipment. For this model a back-analysis procedure with PSO is employed for the scenario where measured displacements differ from the predicted ones. The procedure showed the ability to optimize any number of parameters whose values are the most uncertain, to identify real values which lead the levee to experience the measured behaviour.

Due to the nature of stability failures, they follow the development of deformations, which is taken advantage of in the second model by using the observed crown displacements as a new feature for predicting the factors of safety. The purpose of the model is to be applied on existing slopes, and is thus trained to predict factors of safety larger than 1. This model's uncertainties are calculated in the same way as for the displacement model, and can be used to calculate the distribution of the predicted factors of safety. Probabilities of failure even in the most unacceptable cases are of the order of magnitude of 0.1 [90, 91], which means that the distribution statistics of the factor of safety can be reliably assessed by such model. The paper shows how these probabilities can be used to construct fragility curves, and if the uncertainty of the first model's prediction is also considered, then confidence intervals can be also generated for those fragility curves. Here, only the model's uncertainties are considered, while the variability of each parameter is not. They can, however, be considered too, which would only have the effect of increasing the confidence intervals depending on the importance and variability of the variable parameter. The critical factor of safety does not necessarily need to be 1, but any other value deemed as unwanted, as shown in [190].

There are a couple of reasons for constructing fragility curves, one for understanding the behaviour of levee, and another for the safety assessment of levees. In the second case, constructing single fragility curves is not efficient due to the number of different cross sections to consider. That is why generalization which is here achieved my machine learning models is of interest, as it enables a quick and efficient construction of fragility curves at any given moment and for any given levee that satisfies the constraints. With this it is also shown that the behaviour of levees found within a specific area where similar construction practices are present can be explained by a relatively modest number of parameters, and can be approximated by functions.

With such models forming relationships between the crown displacement and the factor of safety of the levee on the land side, the displacements which are in the domain of serviceability limit states (SLS) can be put in the context of ultimate limit states (ULS) with regards to slope stability. Khalilzad and Gabr [211] similarly defined limit-states based on deformations and hydraulic gradients, but with regard to the performance (functionality) of dams instead of actual failure. By evaluating the models using only the most commonly available parameters, it has been shown that these parameters mostly correspond to the ones which affect the levees' behaviour.

Results from the models created according to the methodology presented in this study and in [202], including the models themselves, are valid for any levees whose parameters' variations are similar to the ones used to train these models. In any other case the predictions are not guaranteed to be of the same quality, and is it advised against using the models on such data which lie outside the ranges. Instead, new models should be created following the same methodology on the new area of interest.

Potential further applications of such models on levees in practice involve categorisation of levees and deployment in early warning systems. The categorization would involve finding the critical sections or reaches, and based on the risks deciding which to observe with monitoring equipment. During high-water events the deformations are remotely monitored at the chosen locations, and can be compared at any moment with the deformations predicted by the model. If the total deformation, or rate of deformations, are higher than the predicted by a specified value, early reactions can be employed to ultimately prevent failure. Such applications would make the models part of risk-assessment and early-warning frameworks.

Chapter 6

Conclusions

6.1 Summary

This thesis is presented as a compilation of this thesis' author's scientific papers, each with their own conclusions. This chapter goes over the conclusions of each previous chapter, which individually contribute to the understanding of levee behaviour and improved management, and then puts them all together to form the final overall conclusions of this thesis.

Chapter 2 investigated the construction of fragility curves for two separate failure mechanisms—slope stability with inclusion of stresses due to water overflowing the crown, and internal erosion. This is done by means of numerical steady-state and transient seepage and load-deformation analyses coupled with probabilistic Limit Equilibrium Method (LEM) analyses performed with Monte Carlo sampling for the slope stability, and the analytical Sellmeijer 2-force rule with Monte Carlo sampling for the piping analyses. Even though the fragility curves are constructed only for a single cross section, the effect of different levels the parameters' variability, resulting from inherent variability, measurement error and transformation uncertainty, is investigated. The results gave insight into the effect that each investigated parameter has on the shape of the fragility curves, and which can be expected during the construction of other, similar curves. The curves which show the probability of failure for each level of the investigated parameter can also be deemed as boundary curves, meaning that any parameter realistically found between the investigated values would yield a fragility curve in between these boundary curves. If we consider failure in terms of the factor of safety, where anything less than 1 is failure, then as soon as the deterministic factor of safety from the analyses crosses the critical value (1), a lower variability becomes more unfavourable than a high variability where there can be more instances found with the factor of safety over 1. However, such situations in properly designed levees should not occur under normal circumstances, but rather only during extreme event combinations, but this conclusion can be extrapolated to such cases. Curves created in such a way can be applicable to whole reaches, defined by similarity in cross sections and material types, and not in materials' characteristics. This level of generalization first requires the division of

all the levees in an area of interest into reaches by the mentioned similarities, and constructing curves for each reach.

Chapter 3 investigates the behaviour of levee sections reinforced with multiple layers of geogrids, with some of the geogrids' and soils' parameters considered as random variables. The conditions assumed here regarding the reinforcement are that there is no face anchorage, and that there is no potential for local instability between the layers. The probabilities are calculated with the FORM, where the calculation of the reliability index assumes a linear performance function. This assumption is validated here by plotting the curvatures of the used performance functions, which are all very slight, such that no significant differences should occur by linearizing them instead. The said reliability index is found to approximately linearly increase with an increase of the interface friction angle between the soil and the grids, in proximity of the ULS. It is found that different slope stability mechanisms can occur, which result from small variations in the soil and reinforcement parameters' values. The failure mechanisms are identified as either shallow sliding or deep sliding, where the shallow sliding occurs by the soil sliding over the geogrid near the slope face, and the deep sliding mostly avoiding the geogrids (except the top which goes from slope to slope). To avoid shallow surfaces, the pull-out resistance of the soil over the grids need to increase, which is why an increase in the soil's internal friction angle and the interface friction angle tends to generate deep surfaces. Very few surfaces passed through the geogrids, which indicates complete activation of the geogrids' resistance. This split between shallow and deep surfaces with very similar factors of safety mostly occurred for loads which brought the levee close to the ULS. This was for situations where the stability was mostly dependent of the geogrids' resistance. On the other hand, when the friction angle had larger influence, the division between shallow and deep was not associated with the closeness to a limit state. This study uses a second order polynomial to approximate the levee's response, but lower and higher order trends are also identified, and should be considered in the appropriate situations, as described. When analysing the contribution of each of the considered variables' uncertainty—each grid's strength, soil internal friction angle—to the total uncertainty, it is found that most of the time (closer to the ULS) the internal friction angle is the dominant variable, having much larger variability then the grids' strength. However, in the case where soil friction angle is not dominant, the top grid's strength is, while in all cases the variability of the bottom and middle grids' strength has negligible effect. The conclusion drawn here are valid for systems similar to the analysed one, with the appropriate assumptions regarding the geogrids' installation. Otherwise, the understanding of the behaviour trends noted here can be applied on other, similar reinforced levee sections.

Chapter 4 has more focus on generalization than the previous. It introduces a methodology for the identification of the key levee parameters which govern the levees' behaviour with respect to multiple failure mechanisms, and quantifying their effects in a descending way, such that the procedure may be stopped early when a satisfactory number of parameters is found, or due to time constraints. On top of using complex numerical analyses, the methodology is based

on the Sequential Bifurcation method to efficiently identify the important parameters from the unimportant in a sequential procedure, with some prior preparation required to increase its efficiency. The application of this methodology required three quite strict assumptions, but this study shows how they can be handled in this geotechnical application. It is found that only about a third of over one hundred parameters required to uniquely define a levee section govern their behaviour. While this ratio should hold for different areas of interest, the actual parameters and their effects shall change from area to area, depending on the variability of each element and parameter of the levees encapsulated within the observed area. Unlike the previous studies, the variability does not come from the inherent soil variability, but from the ranges of the parameters' values observed in the selected area. The list of important parameters identified by this methodology does not indicate the parameters which generally have the most effect on the levee's behaviour, but rather the parameters which have the most effect on the behaviour of the observed levees in particular. Even if they do have some overlapping, these two should not be confused. This paper presents a methodology applicable to any set of levees of interest, but the results from the performed analyses are already of practical significance as they can be used for any levees whose sections have similar characteristics (mean values and ranges) to the ones used in the analyses.

Chapter 5 focuses on the prediction of the behaviour of levees under different failure mechanisms, with focus on generalization for the levees within the whole analysed area of interest. The models are first developed for the deformations prediction, then for factor of safety prediction, and finally for the hydraulic gradient classification and prediction. The first two models are then combined, such that a dependency of the factor of safety and the crown displacement is established, and fragility curves are constructed based on that. This way, new performance limit states can be defined with respect to stability, and depend on the developed displacements on the crown of the levee. A classification model is created to identify the sections under specific conditions which may potentially experience large gradients, and for which further investigations should be conducted. However, a model to predict the actual value of the hydraulic gradient which may be expected in those sections was not successfully created, which may indicate the lack of parameters on which the value depends. It is also demonstrated how an optimization algorithm can be used together with the developed model for deformation prediction after obtaining the deformation results of a levee under high-water load, to efficiently assess any number of uncertain parameters of the observed cross-section. Such assessment might indicate local problems or uncertainties occurring in the specific section. Even though this study uses the crown displacements, the methodology is adaptable to use any other location, and even measured quantities other than deformations (e.g. pore water pressures), which also depends on the available monitoring equipment. The models, once developed following this methodology, offer the possibility of quickly constructing fragility curves for any section of interest at any given time, and estimating the uncertainties connected with them, as shown in the study. Coupled with optimization algorithms for performing back-analyses, they can be used for assessment of

local problems/uncertainties in specific section.
Throughout this study new trends are observed and it has been shown that various machine learning models are applicable in finding functional relationships between the parameters of the natural and synthetic materials comprising a levee, and the various failure mechanisms which may occur during high-water (flood) events. The most important of those parameters are also identified. These relationship can be used to construct fragility curves for the safety assessment of the sections, reaches or levees of interest. The understanding of the materials' variability effect on the safety of levees is improved by analysing the trends seen in the fragility curves and predictive functions, in both reinforced and unreinforced levees. These are steps towards a successful implementation of the demonstrated methodologies to a more efficient flood protection management system.

6.2 Recommendations for Further Research

This thesis presents research in the domain of machine learning application for the probabilistic safety assessment of river levees. What follows are some comments on potential further research that would add to the conducted research. As seen in the study, some identified trends regarding levees' behaviour are only qualitatively defined, or defined for a single cross-section. Further research on this topic would have the purpose of generalizing the trends and/or defining them quantitatively. Throughout the study, various types of parameters' variability are considered, but mainly inherent variability which is often the main concern during design. In identifying the key parameters and developing the predictive models, however, this variability is not fully considered, but only guidelines are given on how can it be done, which can be expanded by further research. The various methodologies presented here are demonstrated on various case studies. Unfortunately, monitoring data for levees under high-water events was not available at the time of writing of this thesis, and thus validation of the models on real data has not yet been conducted. This shall be done upon collection of the required data. Next, their application for the classification of levees based on expected deformations, gradients and/or factors of safety should be investigated. Also, the application and incorporation of the developed methodologies and models into existing flood protection management systems should be investigated and demonstrated.

Bibliography

[1] Powledge George R. et al. “Mechanics of Overflow Erosion on Embankments. II: Hydraulic and Design Considerations”. In: *Journal of Hydraulic Engineering* 115.8 (Aug. 1, 1989). doi: 10.1061/(ASCE)0733-9429(1989)115:8(1056), pp. 1056–1075. DOI: 10.1061/(ASCE)0733-9429(1989)115:8(1056). URL: https://doi.org/10.1061/(ASCE)0733-9429(1989)115:8(1056) (visited on 06/23/2020).

[2] V. Elias, B. R. Christopher, and R. R. Berg. *Mechanically Stabilized Earth Walls and Reinforced Soil Slopes Design and Construction Guidelines*. FHWA-NHI-00-043. Washington, D.C.: National Highway Institute, Federal Highway Administration, U.S. Department of Transportation, 2001.

[3] R. Tourment et al. “European and US Levees and Flood Defences Characteristics, Risks and Governance”. report. irstea, 2018, p. 173. URL: https://hal.inrae.fr/hal-02609228 (visited on 02/03/2023).

[4] Francesco Serinaldi et al. “Flood Propagation and Duration in Large River Basins: A Data-Driven Analysis for Reinsurance Purposes”. In: *Natural Hazards* 94.1 (Oct. 1, 2018), pp. 71–92. ISSN: 1573-0840. DOI: 10.1007/s11069-018-3374-0. URL: https://doi.org/10.1007/s11069-018-3374-0 (visited on 01/30/2023).

[5] S. N. Jonkman. “Global Perspectives on Loss of Human Life Caused by Floods”. In: *Natural Hazards* 34.2 (Feb. 1, 2005), pp. 151–175. ISSN: 1573-0840. DOI: 10.1007/s11069-004-8891-3. URL: https://doi.org/10.1007/s11069-004-8891-3 (visited on 01/30/2023).

[6] Daniele Inaudi. “Optical Fiber Sensors for Dam and Levee Monitoring and Damage Detection”. In: *Levees and Dams: Advances in Geophysical Monitoring and Characterization*. Ed. by Juan Lorenzo and William Doll. Cham: Springer International Publishing, 2019, pp. 91–120. ISBN: 978-3-030-27367-5. DOI: 10.1007/978-3-030-27367-5_5. URL: https://doi.org/10.1007/978-3-030-27367-5_5 (visited on 02/03/2023).

[7] Hollie L. Ellis et al. *Risk Analysis Methodology*. Delta Levees Investment Strategy RV009910.0000. Roseville, California: Arcadis U.S., Inc., July 2016, p. 499.

[8] USACE CIRIA Ministry of Ecology. *The International Levee Handbook*. London: CIRIA, Nov. 2013. ISBN: 978-0-86017-734-0.

[9] Işil Ece Özer, Myron van Damme, and Sebastiaan N. Jonkman. "Towards an International Levee Performance Database (ILPD) and Its Use for Macro-Scale Analysis of Levee Breaches and Failures". In: *Water* 12.1 (1 Jan. 2020), p. 119. DOI: 10.3390/w12010119. URL: https://www.mdpi.com/2073-4441/12/1/119 (visited on 12/28/2020).

[10] Jaap H. Nienhuis et al. "A Global Open-Source Database of Flood-Protection Levees on River Deltas (openDELvE)". In: *Natural Hazards and Earth System Sciences* 22 (2022), pp. 4087–4101. DOI: 10.5194/nhess-22-4087-2022.

[11] *Levee | National Geographic Society*. URL: https://education.nationalgeographic.org/resource/levee (visited on 02/03/2023).

[12] Sayyed Mahdi Hejazi et al. "A Simple Review of Soil Reinforcement by Using Natural and Synthetic Fibers". In: *Construction and Building Materials* 30 (May 1, 2012), pp. 100–116. ISSN: 0950-0618. DOI: 10.1016/j.conbuildmat.2011.11.045. URL: https://www.sciencedirect.com/science/article/pii/S0950061811006763 (visited on 02/03/2023).

[13] Sharon L. Cundill et al. *Flood Control 2015: Five Years of Innovation in Flood Risk*. Ed. by Kees Vermeer et al. Foundation Flood Control 2015, Nov. 2012. ISBN: 978-90-90-27247-4.

[14] L. van Vliet, A.R. Koelewijn, and M. van der Vat. *Sensors*. Foundation for Applied Water Research (STOWA), Deltares, Aug. 2012.

[15] Zbigniew Bednareczyk. "Engineering Application of Smart Slope Stability In-Situ and Remote Monitoring Methods in Lignite Opencast Mine". In: 6th International Conference on Geotechnical and Geophysical Site Characterization (ISC2020). Budapest, Hugary, Sept. 26–29, 2021. DOI: 10.53243/ISC2020-33.

[16] Victor Hopman et al. "How to Create a Smart Levee". In: *8th International Symposium on Field Measurements in GeoMechanics*. Berlin, Germany, Sept. 12–16, 2011, pp. 12–16.

[17] A.R. Koelewijn and R. Bridle. "Internal Erosion in Dams and Dikes: A Comparison". In: *25th Meeting of the European Working Group on Internal Erosion*. Delft, The Netherlands, Sept. 4–7, 2017.

[18] Sharon L. Cundill. "Investigation of Remote Sensing for Dike Inspection". PhD thesis. The Netherlands: University of Twente, 2016.

[19] Ernst Niederleithinger, Andreas Weller, and Ronald Lewis. "Evaluation of Geophysical Techniques for Dike Inspection". In: *Journal of Environmental and Engineering Geophysics* 17.4 (Dec. 1, 2012), pp. 185–195. ISSN: 1083-1363. DOI: 10.2113/JEEG17.4.185. URL: https://library.seg.org/doi/abs/10.2113/JEEG17.4.185 (visited on 05/17/2021).

[20] Xianwei Wang, Lingzhi Wang, and Tianqiao Zhang. “Geometry-Based Assessment of Levee Stability and Overtopping Using Airborne LiDAR Altimetry: A Case Study in the Pearl River Delta, Southern China”. In: *Water* 12.2 (2 Feb. 2020), p. 403. DOI: 10.3390/w12020403. URL: https://www.mdpi.com/2073-4441/12/2/403 (visited on 09/14/2021).

[21] N. B. Melnikova, G. S. Shirshov, and V. V. Krzhizhanovskaya. “Virtual Dike: Multi-scale Simulation of Dike Stability”. In: *Procedia Computer Science*. Proceedings of the International Conference on Computational Science, ICCS 2011 4 (Jan. 1, 2011), pp. 791–800. ISSN: 1877-0509. DOI: 10.1016/j.procs.2011.04.084. URL: https://www.sciencedirect.com/science/article/pii/S1877050911001426 (visited on 02/04/2023).

[22] K. Ganjalipour. “Review of Inclinometer Errors and Provide Correction Methods for Bias Shift Error and Depth Position Error of the Probe”. In: *Geotechnical and Geological Engineering* 39.6 (Aug. 1, 2021), pp. 4017–4034. ISSN: 1573-1529. DOI: 10.1007/s10706-021-01743-w. URL: https://doi.org/10.1007/s10706-021-01743-w (visited on 12/09/2021).

[23] *Inclinometer Accuracy - DGSI*. URL: https://durhamgeo.com/resources/tech-notes/inclinometers/inclinometer-accuracy/ (visited on 12/09/2021).

[24] Thomas F. Wolff. “Reliability of Levee Systems”. In: *Reliability-Based Design in Geotechnical Engineering*. Ed. by Kok-Kwang Phoon. London, England: Taylor & Francis, 2008, pp. 448–496. ISBN: 978-0-429-15256-6.

[25] Robert V. Whitman. “Organizing and Evaluating Uncertainty in Geotechnical Engineering”. In: *Journal of Geotechnical and Geoenvironmental Engineering* 126.7 (July 1, 2000), pp. 583–593. ISSN: 1090-0241. DOI: 10.1061/(ASCE)1090-0241(2000)126:7(583). URL: https://ascelibrary.org/doi/10.1061/%28ASCE%291090-0241%282000%29126%3A7%28583%29 (visited on 02/04/2023).

[26] Yoshihisa Miyata and Richard J. Bathurst. “Reliability Analysis of Geogrid Installation Damage Test Data in Japan”. In: *Soils and Foundations* 55.2 (Apr. 1, 2015), pp. 393–403. ISSN: 0038-0806. DOI: 10.1016/j.sandf.2015.02.013. URL: http://www.sciencedirect.com/science/article/pii/S0038080615000335 (visited on 09/02/2020).

[27] Gordon A. Fenton et al. “Reliability-Based Geotechnical Design in the 2014 Canadian Highway Bridge Design Code”. In: *Canadian Geotechnical Journal* 53.2 (2016), pp. 236–251. DOI: 10.1139/cgj-2015-0158.

[28] *Eurocode 7 - Geotechnical Design - Part 1: General Rules*. European Standard. Brussels, Belgium: CEN, 2004.

[29] Gregory B. Baecher and John T. Christian. *Reliability and Statistics in Geotechnical Engineering*. England: Wiley, 2003. 605 pp.

[30] D. V. Griffiths and Gordon A. Fenton, eds. *Probabilistic Methods in Geotechnical Engineering*. CISM Courses and Lectures. Springer Wien New York, 2007.

[31] Kok-Kwang Phoon, ed. *Reliability-Based Design in Geotechnical Engineering*. Abingdon, Oxon, England: Taylor & Francis, 2008. 530 pp.

[32] R. P. Kennedy et al. "Probabilistic Seismic Safety Study of an Existing Nuclear Power Plant". In: *Nuclear Engineering and Design* 59.2 (Aug. 1, 1980), pp. 315–338. ISSN: 0029-5493. DOI: 10.1016/0029-5493(80)90203-4. URL: https://www.sciencedirect.com/science/article/pii/0029549380902034 (visited on 08/25/2021).

[33] W. DePoto and I. Gindi. *Hydrology Manual*. Policy Guidance Memorandum. Los Angeles county Department of Public Works, Jan. 1991.

[34] W. DePoto and I. Gindi. *Hydrology Manual*. Policy Guidance Memorandum. Los Angeles county Department of Public Works, Jan. 1993.

[35] Firas H. Jasim and Farshid Vahedifard. "Fragility Curves of Earthen Levees under Extreme Precipitation". In: *Geotechnical Frontiers 2017 GSP 278*. Orlando, Florida: American Society of Civil Engineers, Mar. 12–15, 2017, pp. 353–362. DOI: 10.1061/9780784480458.035. URL: https://ascelibrary.org/doi/abs/10.1061/9780784480458.035 (visited on 08/25/2021).

[36] Karlo Martinović, Cormac Reale, and Kenneth Gavin. "Fragility Curves for Rainfall-Induced Shallow Landslides on Transport Networks". In: *Canadian Geotechnical Journal* 55.6 (Oct. 26, 2017), pp. 852–861. ISSN: 0008-3674. DOI: 10.1139/cgj-2016-0565. URL: https://www.nrcresearchpress.com/doi/abs/10.1139/cgj-2016-0565 (visited on 09/04/2020).

[37] Hongqiang Hu, Yu Huang, and Zhiyi Chen. "Seismic Fragility Functions for Slope Stability Analysis with Multiple Vulnerability States". In: *Environmental Earth Sciences* 78.24 (Dec. 3, 2019), p. 690. ISSN: 1866-6299. DOI: 10.1007/s12665-019-8696-z. URL: https://doi.org/10.1007/s12665-019-8696-z (visited on 09/04/2020).

[38] Pierpaolo Oreste. "Back-Analysis Techniques for the Improvement of the Understanding of Rock in Underground Constructions". In: *Tunnelling and Underground Space Technology* 20.1 (Jan. 1, 2005), pp. 7–21. ISSN: 0886-7798. DOI: 10.1016/j.tust.2004.04.002. URL: https://www.sciencedirect.com/science/article/pii/S0886779804002883 (visited on 12/07/2021).

[39] Changxing Zhu, Hongbo Zhao, and Ming Zhao. “Back Analysis of Geomechanical Parameters in Underground Engineering Using Artificial Bee Colony”. In: *The Scientific World Journal* 2014 (July 17, 2014), e693812. ISSN: 2356-6140. DOI: 10.1155/2014/693812. URL: https://www.hindawi.com/journals/tswj/2014/693812/ (visited on 12/07/2021).

[40] Hongming Tian et al. “Application of the Orthogonal Design Method in Geotechnical Parameter Back Analysis for Underground Structures”. In: *Bulletin of Engineering Geology and the Environment* 75.1 (Feb. 1, 2016), pp. 239–249. ISSN: 1435-9537. DOI: 10.1007/s10064-015-0730-0. URL: https://doi.org/10.1007/s10064-015-0730-0 (visited on 07/20/2021).

[41] Yang Sun et al. “A Back-Analysis Method Using an Intelligent Multi-Objective Optimization for Predicting Slope Deformation Induced by Excavation”. In: *Engineering Geology* 239 (May 18, 2018), pp. 214–228. ISSN: 0013-7952. DOI: 10.1016/j.enggeo.2018.03.019. URL: https://www.sciencedirect.com/science/article/pii/S0013795217307792 (visited on 07/19/2021).

[42] Hong-bo Zhao and Shunde Yin. “Geomechanical Parameters Identification by Particle Swarm Optimization and Support Vector Machine”. In: *Applied Mathematical Modelling* 33.10 (Oct. 1, 2009), pp. 3997–4012. ISSN: 0307-904X. DOI: 10.1016/j.apm.2009.01.011. URL: https://www.sciencedirect.com/science/article/pii/S0307904X09000250 (visited on 12/07/2021).

[43] Zhan-ping Song, An-nan Jiang, and Zong-bin Jiang. “Back Analysis of Geomechanical Parameters Using Hybrid Algorithm Based on Difference Evolution and Extreme Learning Machine”. In: *Mathematical Problems in Engineering* 2015 (Oct. 19, 2015), e821534. ISSN: 1024-123X. DOI: 10.1155/2015/821534. URL: https://www.hindawi.com/journals/mpe/2015/821534/ (visited on 12/07/2021).

[44] Yuzhen Yu, Bingyin Zhang, and Huina Yuan. “An Intelligent Displacement Back-Analysis Method for Earth-Rockfill Dams”. In: *Computers and Geotechnics* 6.34 (2007), pp. 423–434. ISSN: 0266-352X. DOI: 10.1016/j.compgeo.2007.03.002. URL: https://www.infona.pl//resource/bwmeta1.element.elsevier-4a593cf2-f30e-3cdd-a6a8-68f7291d3408 (visited on 12/07/2021).

[45] Wendy D. Fisher, Tracy K. Camp, and Valeria V. Krzhizhanovskaya. “Crack Detection in Earth Dam and Levee Passive Seismic Data Using Support Vector Machines”. In: *Procedia Computer Science*. International Conference on Computational Science 2016, ICCS 2016, 6-8 June 2016, San Diego, California, USA 80 (Jan. 1, 2016), pp. 577–586. ISSN: 1877-0509. DOI: 10.1016/j.procs.2016.05.339. URL: https://www.sciencedirect.com/science/article/pii/S1877050916307542 (visited on 01/13/2023).

[46] Xia-Ting Feng, Hongbo Zhao, and Shaojun Li. "A New Displacement Back Analysis to Identify Mechanical Geo-Material Parameters Based on Hybrid Intelligent Methodology". In: *International Journal for Numerical and Analytical Methods in Geomechanics* 28.11 (2004), pp. 1141–1165. ISSN: 1096-9853. DOI: 10.1002/nag.381. URL: https://onlinelibrary.wiley.com/doi/abs/10.1002/nag.381 (visited on 12/07/2021).

[47] Zhihao Liao and Zhiwei Liao. "Slope Stability Evaluation Using Backpropagation Neural Networks and Multivariate Adaptive Regression Splines". In: *Open Geosciences* 12.1 (Jan. 1, 2020), pp. 1263–1273. ISSN: 2391-5447. DOI: 10.1515/geo-2020-0198. URL: https://www.degruyter.com/document/doi/10.1515/geo-2020-0198/html (visited on 12/10/2021).

[48] Lin Wang et al. "Probabilistic Stability Analysis of Earth Dam Slope under Transient Seepage Using Multivariate Adaptive Regression Splines". In: *Bulletin of Engineering Geology and the Environment* 79.6 (Aug. 1, 2020), pp. 2763–2775. ISSN: 1435-9537. DOI: 10.1007/s10064-020-01730-0. URL: https://doi.org/10.1007/s10064-020-01730-0 (visited on 09/04/2020).

[49] Aditi Kuchi et al. "Machine Learning Applications in Detecting Sand Boils from Images". In: *Array* 3–4 (Sept. 1, 2019), p. 100012. ISSN: 2590-0056. DOI: 10.1016/j.array.2019.100012. URL: https://www.sciencedirect.com/science/article/pii/S2590005619300128 (visited on 03/09/2022).

[50] Capucine Durand et al. "A New Simple Neural-Network Based Approach to Predict the Seismic Response of Levees and Small Height Earth Dams". In: *7th International Conference on Earthquake Geotechnical Engineering (ICEGE 2019)*. Ed. by Francesco Silvestri and Nicola Moraci. Earthquake Geotechnical Engineering for Protection and Development of Environment and Constructions. Rome, Italy: CRC Press, June 2019. URL: https://hal.archives-ouvertes.fr/hal-02175756.

[51] Hans Sellmeijer et al. "Fine-Tuning of the Backward Erosion Piping Model through Small-Scale, Medium-Scale and IJkdijk Experiments". In: *European Journal of Environmental and Civil Engineering* 15.8 (Jan. 1, 2011). doi: 10.1080/19648189.2011.9714845, pp. 1139–1154. ISSN: 1964-8189. DOI: 10.1080/19648189.2011.9714845. URL: https://doi.org/10.1080/19648189.2011.9714845.

[52] Dorota Mirosław-Świątek et al. "Analysis of Factors Influencing Levee Safety Using the DEMATEL Method". In: *PLOS ONE* 16.9 (Sept. 10, 2021), e0255755. ISSN: 1932-6203. DOI: 10.1371/journal.pone.0255755. URL: https://journals.plos.org/plosone/article?id=10.1371/journal.pone.0255755 (visited on 12/09/2021).

[53] Jack P.C. Kleijnen. *Design and Analysis of Simulation Experiments*. Second. Vol. 230. International Series in Operations Research & Management Science. Cham, Switzerland: Springer International Publishing, 2015. ISBN: 978-3-319-18086-1 978-3-319-18087-8.

[54] B Bettonvil. "Detection of Important Factors by Sequential Bifurcation". PhD thesis. Tilburg, The Netherlands: Tilburg University, 1990.

[55] Stoyan Andreev and Aleksandar Zhivkov Zhelyazkov. "Probability of Failure of an Embankment Dam Due to Slope Instability and Overtopping: First Order Second Moment Method for Assessment of Uncertainty". In: *13th ICOLD International Benchmark Workshop on Numerical Analysis of Dams*. Lausanne, Switzerland, Sept. 9–11, 2015, pp. 207–215.

[56] Dongwoo Ko and Joongu Kang. "Experimental Studies on the Stability Assessment of a Levee Using Reinforced Soil Based on a Biopolymer". In: *Water* 10.8 (8 Aug. 2018), p. 1059. DOI: 10.3390/w10081059. URL: https://www.mdpi.com/2073-4441/10/8/1059 (visited on 09/03/2021).

[57] Dongwoo Ko and Joongu Kang. "Biopolymer-Reinforced Levee for Breach Development Retardation and Enhanced Erosion Control". In: *Water* 12.4 (4 Apr. 2020), p. 1070. DOI: 10.3390/w12041070. URL: https://www.mdpi.com/2073-4441/12/4/1070 (visited on 09/03/2021).

[58] J.W. van der Meer, W.L.A. ter Horst, and E.H. van Valzen. "Calculation of Fragility Curves for Flood Defence Assets". In: *Flood Risk Management: Research and Practice*. London: Taylor & Francis Group, 2009, pp. 567–573. ISBN: 978-0-415-48507-4. DOI: 10.1201/9780203883020.ch65.

[59] J. B. Sellmeijer and M. A. Koenders. "A Mathematical Model for Piping". In: *Applied Mathematical Modelling* 15.11 (Nov. 1, 1991), pp. 646–651. ISSN: 0307-904X. DOI: 10.1016/S0307-904X(09)81011-1. URL: http://www.sciencedirect.com/science/article/pii/S0307904X09810111 (visited on 06/19/2020).

[60] V.m. Van Beek et al. "Initiation of Backward Erosion Piping in Uniform Sands". In: *Géotechnique* 64.12 (Dec. 1, 2014), pp. 927–941. ISSN: 0016-8505. DOI: 10.1680/geot.13.P.210. URL: https://www.icevirtuallibrary.com/doi/10.1680/geot.13.P.210 (visited on 09/21/2020).

[61] T. Planès et al. "Time-Lapse Monitoring of Internal Erosion in Earthen Dams and Levees Using Ambient Seismic Noise". In: *Géotechnique* 66.4 (2016), pp. 301–312. DOI: http://dx.doi.org/10.1680/jgeot.14.P.268.

[62] Alessandro Fascetti and Calgar Oskay. "Dual Random Lattice Modeling of Backward Erosion Piping". In: *Computers and Geotechnics* 105 (2019), pp. 265–276. DOI: 10.1016/j.compgeo.2018.08.018.

[63] B. Akbas and N. Huvaj. “Probabilistic Slope Stability Analyses Using Limit Equilibrium and Finite Element Methods”. In: Geotechnical Safety and Risk V: Fifth International Symposium on Geotechnical Safety and Risk (ISGSR). Rotterdam, Netherlands: IOS Press, 2015. ISBN: 978-1-61499-580-7. DOI: 10.3233/978-1-61499-580-7-716. URL: https://repository.tudelft.nl/islandora/object/uuid%3A2ae20baf-9e5a-456e-adc8-76b14d9ab3a4 (visited on 09/04/2020).

[64] Michelle Deng. “Reliability-Based Optimization Design of Geosynthetic Reinforced Embankment Slopes”. PhD thesis. Missouri: Missouri S&T, Jan. 1, 2015. URL: https://scholarsmine.mst.edu/doctoral_dissertations/2407.

[65] Yajun Li et al. “On Two Approaches to Slope Stability Reliability Assessments Using the Random Finite Element Method”. In: *Applied Sciences* 9.20 (20 Jan. 2019), p. 4421. DOI: 10.3390/app9204421. URL: https://www.mdpi.com/2076-3417/9/20/4421 (visited on 09/03/2021).

[66] Amanuel Petros Wolebo. “Advanced Probabilistic Slope Stability Analysis on Rissa Slope”. In: 2016. URL: https://www.semanticscholar.org/paper/Advanced-Probabilistic-Slope-Stability-Analysis-on-Wolebo/7251072756ff76fe15c48c6969447a46f17ec860 (visited on 02/04/2023).

[67] Ronny Vergouwe. *The National Flood Risk Analysis for the Netherlands*. Ed. by Heleen Sarink. Rijkswaterstaat VNK Project Office, Nov. 2014.

[68] Xi Xiong et al. “Unsaturated Slope Stability around the Three Gorges Reservoir under Various Combinations of Rainfall and Water Level Fluctuation”. In: *Engineering Geology* 261 (Nov. 1, 2019), p. 105231. ISSN: 0013-7952. DOI: 10.1016/j.enggeo.2019.105231. URL: http://www.sciencedirect.com/science/article/pii/S0013795218321616 (visited on 09/04/2020).

[69] Lancine Doumbouya, Chang Sheng Guan, and Victor Mwango Bowa. “Influence of Rainfall Patterns on the Slope Stability of the Lumwana (the Malundwe) Open Pit”. In: *Geotechnical and Geological Engineering* 38.2 (Apr. 1, 2020), pp. 1337–1346. ISSN: 1573-1529. DOI: 10.1007/s10706-019-01094-7. URL: https://doi.org/10.1007/s10706-019-01094-7 (visited on 09/04/2020).

[70] Qiu-jing Pan, Xing-ru Qu, and Xiang Wang. “Probabilistic Seismic Stability of Three-Dimensional Slopes by Pseudo-Dynamic Approach”. In: *Journal of Central South University* 26.7 (July 1, 2019), pp. 1687–1695. ISSN: 2227-5223. DOI: 10.1007/s11771-019-4125-4. URL: https://doi.org/10.1007/s11771-019-4125-4 (visited on 09/04/2020).

[71] M.E. Hynes-Griffin. *The Joint Occurrence of Earthquakes and Floods*. Final Report GL-80-10. Vicksburg, Mississippi: U.S. Army Engineer Waterways Experiment Station, Sept. 1980.

[72] Steven A. Hughes. *Combined Wave and Surge Overtopping of Levees: Flow Hydrodynamics and Articulated Concrete Mat Stability*. ERDC/CHL TR-08-10. Vicksburg, Mississippi: USACE, Engineer Research and Developement Center, Coastal and Hydraulics Laboratory, 2008.

[73] S. A. Hughes and N. C. Nadal. "Laboratory Study of Combined Wave Overtopping and Storm Surge Overflow of a Levee". In: *Coastal Engineering* 56.3 (Mar. 1, 2009), pp. 244–259. ISSN: 0378-3839. DOI: 10.1016/j.coastaleng.2008.09.005. URL: http://www.sciencedirect.com/science/article/pii/S0378383908001531 (visited on 05/14/2020).

[74] Steven A. Hughes, Justin M. Shaw, and Isaac L. Howard. "Earthen Levee Shear Stress Estimates for Combined Wave Overtopping and Surge Overflow". In: *Journal of Waterway, Port, Coastal, and Ocean Engineering* 138.3 (May 1, 2012), pp. 267–273. DOI: 10.1061/(ASCE)WW.1943-5460.0000135. URL: https://doi.org/10.1061/(ASCE)WW.1943-5460.0000135 (visited on 05/14/2020).

[75] USACE. *Investigation of Underseepage and Its Control, Lower Mississippi River Levees*. Vicksburg, Mississippi, 1956.

[76] Mahdi Shadab Far and Hongwei Huang. "A Hybrid Monte Carlo-Simulated Annealing Approach for Reliability Analysis of Slope Stability Considering the Uncertainty in Water Table Level". In: *Procedia Structural Integrity*. First International Symposium on Risk Analysis and Safety of Complex Structures and Components (IRAS 2019) 22 (Jan. 1, 2019), pp. 345–352. ISSN: 2452-3216. DOI: 10.1016/j.prostr.2020.01.043. URL: http://www.sciencedirect.com/science/article/pii/S2452321620300986 (visited on 09/04/2020).

[77] Rennie B. Kaunda. "A Neural Network Assessment Tool for Estimating the Potential for Backward Erosion in Internal Erosion Studies". In: *Computers and Geotechnics* 69 (2015), pp. 1–6. DOI: 10.1016/j.compgeo.2015.04.010.

[78] Bryant Andrew Robbins. "Numerical Modeling of Backward Erosion Piping". In: 4th Itasca Symposium on Applied Numerical Modeling. Lima, Peru, 2016.

[79] R. Aboul Hosn et al. "A Discrete Numerical Model Involving Partial Fluid-Solid Coupling to Describe Suffusion Effects in Soils". In: *Computers and Geotechnics* 95 (2018), pp. 30–39. DOI: 10.1016/j.compgeo.2017.11.006.

[80] Jie Yang et al. "Analysis of Suffusion in Cohesionless Soils with Randomly Distributed Porosity and Fines Content". In: *Computers and Geotechnics* 111 (2019), pp. 157–171. DOI: 10.1016/j.compgeo.2019.03.011.

[81] K. Du Thinh. “Probabilistic Approach to the Design of Spread Footings: Application of Eurocode 7”. In: *16th International Conference on Soil Mechanics and Geotechnical Engineering*. Osaka, Japan: IOS Press, Amsterdam, Netherlands, Sept. 12–16, 2005, pp. 2797–2800. DOI: doi:10.3233/978-1-61499-656-9-2797.

[82] *Eurocode - Basis of Structural Design*. European Standard. Brussels, Belgium: CEN, 2005.

[83] *Canadian Highway Bridge Design Code*. CAN/CSA-S6-14. Canadian Standards Association, 2014.

[84] Kok-Kwang Phoon and Fred H. Kulhawy. “Characterization of Geotechnical Variability”. In: *Canadian Geotechnical Journal* 36.4 (1999), pp. 612–624. DOI: 10.1139/t99-038.

[85] B. K. Low and Kok-Kwang Phoon. “Reliability-Based Design and Its Complementary Role to Eurocode 7 Design Approach”. In: *Computers and Geotechnics* 65 (2015), pp. 30–44. DOI: 10.1016/j.compgeo.2014.11.011.

[86] Hamed Hamedifar et al. “Role of Probabilistic Methods in Sustainable Geotechnical Slope Stability Analysis”. In: *Procedia Earth and Planetary Science*. The Third Italian Workshop on Landslides: Hydrological Response of Slopes through Physical Experiments, Field Monitoring and Mathematical Modeling 9 (Jan. 1, 2014), pp. 132–142. ISSN: 1878-5220. DOI: 10.1016/j.proeps.2014.06.009. URL: http://www.sciencedirect.com/science/article/pii/S1878522014000381 (visited on 06/25/2020).

[87] M. Mazzoleni et al. “Flooding Hazard Mapping in Floodplain Areas Affected by Piping Breaches in the Po River, Italy”. In: *Journal of Hydrologic Engineering* 19.4 (Apr. 1, 2014), pp. 717–731. ISSN: 1943-5584. DOI: 10.1061/(ASCE)HE.1943-5584.0000840. URL: https://ascelibrary.org/doi/abs/10.1061/%28ASCE%29HE.1943-5584.0000840 (visited on 12/28/2020).

[88] T. Schweckendiek, A. C. W. M. Vrouwenvelder, and E. O. F. Calle. “Updating Piping Reliability with Field Performance Observations”. In: *Structural Safety* 47 (Mar. 1, 2014), pp. 13–23. ISSN: 0167-4730. DOI: 10.1016/j.strusafe.2013.10.002. URL: http://www.sciencedirect.com/science/article/pii/S0167473013000799 (visited on 12/28/2020).

[89] Farrokh Nadim. “Tools and Strategies for Dealing with Uncertainty in Geotechnics”. In: *Probabilistic Methods in Geotechnical Engineering*. Ed. by D. V. Griffiths and Gordon. A. Fenton. CISM Courses and Lectures. Vienna: Springer, 2007, pp. 71–95. ISBN: 978-3-211-73366-0. DOI: 10.1007/978-3-211-73366-0_2. URL: https://doi.org/10.1007/978-3-211-73366-0_2 (visited on 01/25/2021).

[90] USACE. *Introduction to Probability and Reliability Methods for Use in Geotechnical Engineering*. Technical Letter 1110-2-547. Washington, D.C., 1997.

[91] J. C. Santamarina, A. G. Altschaeffl, and J. L. Chameau. "Reliability of Slopes: Incorporating Qualitative Information". In: *Rockfall Prediction and Control and Landslide Case Histories*. Transportation Research Record 1343. Transportation Research Board, 1992, pp. 1–5. ISBN: 0-309-05206-8.

[92] Jonathan Simm and Owen Tarrant. "Development of Fragility Curves to Describe the Performance of UK Levee Systems". In: *Twenty-Sixth International Congress on Large Dams*. ICOLD 2018. Vienna, Austria, July 1–7, 2018.

[93] TAW/ENW. *Technical report on sand boils (piping)*. TPN100400. Rijkswaterstaat, DWW, 1999. URL: http://resolver.tudelft.nl/uuid:f6d03006-7744-452e-8ff2-a4914f118184.

[94] Yingzi Xu, Lin Li, and Farshad Amini. "Slope Stability of Earthen Levee Strengthened by Roller-Compacted Concrete under Hurricane Overtopping Flow Conditions". In: *Geomechanics and Geoengineering* 8.2 (June 1, 2013). doi: 10.1080/17486025.2012.695400, pp. 76–85. ISSN: 1748-6025. DOI: 10.1080/17486025.2012.695400. URL: https://doi.org/10.1080/17486025.2012.695400.

[95] A. Kaur and Dr R. K. Sharma. "SLOPE STABILITY ANALYSIS TECHNIQUES : A REVIEW". In: 2016.

[96] Knut E. Petterson. "The Early History of Circular Sliding Surfaces". In: *Géotechnique* 5.4 (Dec. 1, 1955), pp. 275–296. ISSN: 0016-8505. DOI: 10.1680/geot.1955.5.4.275. URL: https://www.icevirtuallibrary.com/doi/10.1680/geot.1955.5.4.275 (visited on 09/07/2020).

[97] N. R. Morgenstern and V. E. Price. "The Analysis of the Stability of General Slip Surfaces". In: *Géotechnique* 15.1 (Mar. 1, 1965), pp. 79–93. ISSN: 0016-8505. DOI: 10.1680/geot.1965.15.1.79. URL: https://www.icevirtuallibrary.com/doi/abs/10.1680/geot.1965.15.1.79 (visited on 09/07/2020).

[98] E Spencer. "A Method of Analysis of the Stability of Embankments Assuming Parallel Inter-Slice Forces". In: *Géotechnique* 17.1 (Mar. 1, 1967), pp. 11–26. ISSN: 0016-8505. DOI: 10.1680/geot.1967.17.1.11. URL: https://www.icevirtuallibrary.com/doi/abs/10.1680/geot.1967.17.1.11 (visited on 09/07/2020).

[99] R. P. Hunter and E. T. Bowman. "Visualisation of Seepage-Induced Suffusion and Suffosion within Internally Erodible Granular Media". In: *Géotechnique* 68.10 (2018), pp. 918–930. DOI: 10.1680/jgeot.17.P.161.

[100] El Shamy Usama and Aydin Firat. “Multiscale Modeling of Flood-Induced Piping in River Levees”. In: *Journal of Geotechnical and Geoenvironmental Engineering* 134.9 (Sept. 1, 2008). doi: 10.1061/(ASCE)1090-0241(2008)134:9(1385), pp. 1385–1398. DOI: 10.1061/(ASCE)1090-0241(2008)134:9(1385). URL: https://doi.org/10.1061/(ASCE)1090-0241(2008)134:9(1385) (visited on 06/25/2020).

[101] Yue Liang et al. “Numerical Simulation of Backward Erosion Piping in Heterogeneous Fields”. In: *Water Resources Research* 53.4 (2017), pp. 3246–3261. DOI: 10.1002/2017WR020425.

[102] Alba Yerro, Alexander Rohe, and Kenichi Soga. “Modelling Internal Erosion with the Material Point Method”. In: 1st International Conference on the Material Point Method, MPM. Delft, The Netherlands, Jan. 10–13, 2017. DOI: 10.1016/j.proeng.2017.01.048.

[103] J. B. Sellmeijer. “Numerical Computation of Seepage Erosion below Dams (Piping)”. In: Delft, The Netherlands, 2006.

[104] Renier Kramer. “Piping Under Transient Conditions”. MA thesis. Enschede: University of Twente, Oct. 9, 2014.

[105] VNK2 project office. *Flood Risk in the Netherlands, VNK2: The Method in Brief*. HB 1679805. 2012.

[106] Ž. Krušelj. “Katastrofalne Poplave u Koprivničkoj i Đurđevačkoj Podravini 1965., 1966. i 1972. Godine”. In: *Podravina: časopis za multidisciplinarna istraživanja* 16.31 (2017).

[107] H. R. Schneider. “Definition and Determination of Characteristic Soil Properties”. In: XII International Conference on Soil Mechanics and Geotechnical Engineering. Hamburg: Balkema, 1997.

[108] Ashraf Ahmed and Abdul-Hamid Soubra. “Extension of Subset Simulation Approach for Uncertainty Propagation and Global Sensitivity Analysis”. In: *Georisk: Assessment and Management of Risk for Engineered Systems and Geohazards* 6.3 (Sept. 1, 2012). doi: 10.1080/17499518.2012.656296, pp. 162–176. ISSN: 1749-9518. DOI: 10.1080/17499518.2012.656296. URL: https://doi.org/10.1080/17499518.2012.656296.

[109] Peter Lumb. “Safety Factors and the Probability Distribution of Soil Strength”. In: *Canadian Geotechnical Journal* 7.3 (1970). DOI: 10.1139/t70-032.

[110] Thomas Francis Wolff. “Analysis and Design of Embankment Dam Slopes: A Probabilistic Approach”. PhD thesis. Purdue University, 1985.

[111] *SWedge Documentation | Correlation Coefficient*. URL: https://www.rocscience.com/help/swedge/documentation/probabilistic-analysis/joint-properties/correlation-coefficient (visited on 01/16/2023).

[112] Kok-Kwang Phoon and Fred H. Kulhawy. “Evaluation of Geotechnical Property Variability”. In: *Canadian Geotechnical Journal* 36.4 (1999), pp. 625–639. DOI: 10.1139/t99-039.

[113] Fenton Gordon A. and Griffiths D. V. “Statistics of Free Surface Flow through Stochastic Earth Dam”. In: *Journal of Geotechnical Engineering* 122.6 (June 1, 1996). doi: 10.1061/(ASCE)0733-9410(1996)122:6(427), pp. 427–436. DOI: 10.1061/(ASCE)0733-9410(1996)122:6(427). URL: https://doi.org/10.1061/(ASCE)0733-9410(1996)122:6(427) (visited on 06/23/2020).

[114] D. V. Griffiths and Gordon A. Fenton. “The Random Finite Element Method (RFEM) in Stead Seepage Analysis”. In: *Probabilistic Methods in Geotechnical Engineering*. CISM Courses and Lectures. Springer Wien New York, 2007, pp. 225–241.

[115] Robert P. Chapuis and Deins E. Gill. “Hydraulic Anisotropy of Homogeneous Soils and Rocks: Influence of the Densification Process”. In: *Bulletin Of the International Association of Engineering Geology* 39 (1989). DOI: 10.1007/BF02592538.

[116] Muni Budhu. *Soil Mechanics and Foundations*. 3rd. USA: John Wiley & Sons, Inc., 2011.

[117] Harianto Rahardjo, Alfrendo Satyanaga, and Leong Eng Choon. “Hydraulic Anisotropy Behavior of Compacted Soil”. In: *Proceedings of the 19th International Conference on Soil Mechanics and Geotechnical Engineering*. 19th International Conference on Soil Mechanics and Geotechnical Engineering. Seoul, Sept. 17–21, 2017.

[118] D.G. Fredlund and R.E.G. Scoular. “Using Limit Equilibrium Concepts in Finite Element Slope Stability Analysis”. In: *Proceedings of the International Symposium on Slope Stability Engineering, IS-Shikoku ’99*. Slope Stability Engineering. Matsuyama, Shikoku, Japan, 1999, pp. 31–47.

[119] H.W.M. Hewlett, L.A. Boorman, and M.E. Bramley. *Design of Reinforced Grass Waterways*. CIRIA Report vol. 116. London: Construction and Industry Research and Information Association, 1987, p. 116.

[120] GEO-SLOPE. *Stability Modeling with GeoStudio*. Calgary, AB, Canada: GEO-SLOPE International, Ltd., 2017.

[121] *Eurocode 8 - Design of Structures for Earthquake Resistance - Part 1: General Rules, Seismic Actions and Rules for Buildings*. European Standard. Brussels, Belgium: CEN, 2004.

[122] *Eurocode 8 - Design of Structures for Earthquake Resistance - Part 5: Foundations, Retaining Structures and Geotechnical Aspects*. European Standard. Brussels, Belgium: CEN, 2004.

[123] A. Pickles and R. Sandham. *Application of Eurocode 7 to the Design of Flood Embankments (C749)*. London: CIRIA, 2014. 63 pp. ISBN: 978-0-86017-754-8.

[124] J.o. Avesani Neto, B.s. Bueno, and M.m. Futai. "A Bearing Capacity Calculation Method for Soil Reinforced with a Geocell". In: *Geosynthetics International* 20.3 (June 1, 2013), pp. 129–142. ISSN: 1072-6349. DOI: 10.1680/gein.13.00007. URL: https://www.icevirtuallibrary.com/doi/abs/10.1680/gein.13.00007 (visited on 11/04/2020).

[125] P. K. Kolay, S. Kumar, and D. Tiwari. *Improvement of Bearing Capacity of Shallow Foundation on Geogrid Reinforced Silty Clay and Sand*. Journal of Construction Engineering. June 19, 2013. DOI: 10.1155/2013/293809. URL: https://www.hindawi.com/journals/jcen/2013/293809/ (visited on 11/16/2020).

[126] Jia-Quan Wang et al. "Load-Settlement Response of Shallow Square Footings on Geogrid-Reinforced Sand under Cyclic Loading". In: *Geotextiles and Geomembranes* 46.5 (Oct. 1, 2018), pp. 586–596. ISSN: 0266-1144. DOI: 10.1016/j.geotexmem.2018.04.009. URL: http://www.sciencedirect.com/science/article/pii/S0266114418300311 (visited on 11/16/2020).

[127] Omid Reza Barani, Majid Bahrami, and Seyed Amirodin Sadrnejad. "A New Finite Element for Back Analysis of a Geogrid Reinforced Soil Retaining Wall Failure". In: *International Journal of Civil Engineering* 16.4 (Apr. 1, 2018), pp. 435–441. ISSN: 2383-3874. DOI: 10.1007/s40999-017-0150-6. URL: https://doi.org/10.1007/s40999-017-0150-6 (visited on 11/16/2020).

[128] Jia-Quan Wang et al. "Laboratory Study on Geogrid Reinforced Soil Wall with Modular Facing under Cyclic Strip Loading". In: *Arabian Journal of Geosciences* 13.11 (May 23, 2020), p. 398. ISSN: 1866-7538. DOI: 10.1007/s12517-020-05426-3. URL: https://doi.org/10.1007/s12517-020-05426-3 (visited on 11/16/2020).

[129] He Wang et al. "Static Structural Behavior of Geogrid Reinforced Soil Retaining Walls with a Deformation Buffer Zone". In: *Geotextiles and Geomembranes* 48.3 (June 1, 2020), pp. 374–379. ISSN: 0266-1144. DOI: 10.1016/j.geotexmem.2019.12.008. URL: http://www.sciencedirect.com/science/article/pii/S0266114419301785 (visited on 11/16/2020).

[130] Murad Y. Abu-Farsakh, Imran Akond, and Qiming Chen. "Evaluating the Performance of Geosynthetic-Reinforced Unpaved Roads Using Plate Load Tests". In: *International Journal of Pavement Engineering* 17.10 (Nov. 25, 2016), pp. 901–912. ISSN: 1029-8436. DOI: 10.1080/10298436.2015.1031131. URL: https://doi.org/10.1080/10298436.2015.1031131 (visited on 11/16/2020).

[131] E. V. Cuelho and S. W. Perkins. “Geosynthetic Subgrade Stabilization – Field Testing and Design Method Calibration”. In: *Transportation Geotechnics* 10 (Mar. 1, 2017), pp. 22–34. ISSN: 2214-3912. DOI: 10.1016/j.trgeo.2016.10.002. URL: http://www.sciencedirect.com/science/article/pii/S2214391216300988 (visited on 11/16/2020).

[132] Richard J. Varuso, John B. Grieshaber, and Mysore S. Nataraj. “Geosynthetic Reinforced Levee Test Section on Soft Normally Consolidated Clays”. In: *Geotextiles and Geomembranes* 23.4 (Aug. 1, 2005), pp. 362–383. ISSN: 0266-1144. DOI: 10.1016/j.geotexmem.2004.11.001. URL: http://www.sciencedirect.com/science/article/pii/S0266114404000755 (visited on 11/16/2020).

[133] F. B. Ferreira et al. “Reliability Analysis of Geosynthetic-Reinforced Steep Slopes”. In: *Geosynthetics International* 23.4 (Feb. 3, 2016), pp. 301–315. ISSN: 1072-6349. DOI: 10.1680/jgein.15.00057. URL: https://www.icevirtuallibrary.com/doi/abs/10.1680/jgein.15.00057 (visited on 11/16/2020).

[134] C. C. Hird and C. M. Kwok. “Finite Element Studies of Interface Behaviour in Reinforced Embankments of Soft Ground”. In: *Computers and Geotechnics* 8.2 (Jan. 1, 1989), pp. 111–131. ISSN: 0266-352X. DOI: 10.1016/0266-352X(89)90060-8. URL: http://www.sciencedirect.com/science/article/pii/0266352X89900608 (visited on 11/16/2020).

[135] R. K. Rowe and A. L. Li. “Reinforced Embankments over Soft Foundations under Undrained and Partially Drained Conditions”. In: *Geotextiles and Geomembranes* 17.3 (June 1, 1999), pp. 129–146. ISSN: 0266-1144. DOI: 10.1016/S0266-1144(98)00035-1. URL: http://www.sciencedirect.com/science/article/pii/S0266114498000351 (visited on 11/03/2020).

[136] R. Kerry Rowe et al. “Calculated and Observed Behaviour of a Reinforced Embankment over Soft Compressible Soil”. In: *Canadian Geotechnical Journal* (May 8, 1996). DOI: 10.1139/t96-010. URL: https://cdnsciencepub.com/doi/abs/10.1139/t96-010 (visited on 11/16/2020).

[137] S. Balakrishnan and B. V. S. Viswanadham. “Evaluation of Tensile Load-Strain Characteristics of Geogrids through in-Soil Tensile Tests”. In: *Geotextiles and Geomembranes* 45.1 (Feb. 1, 2017), pp. 35–44. ISSN: 0266-1144. DOI: 10.1016/j.geotexmem.2016.07.002. URL: http://www.sciencedirect.com/science/article/pii/S0266114416300838 (visited on 11/16/2020).

[138] Gang Zheng et al. “Stability Analysis of Stone Column-Supported and Geosynthetic-Reinforced Embankments on Soft Ground”. In: *Geotextiles and Geomembranes* 48.3 (June 1, 2020), pp. 349–356. ISSN: 0266-1144. DOI: 10.1016/j.geotexmem.2019.

12.006. URL: http://www.sciencedirect.com/science/article/pii/S0266114419301761 (visited on 11/03/2020).

[139] R. K. Rowe and K. L. Soderman. "An Approximate Method for Estimating the Stability of Geotextile-Reinforced Embankments". In: *Canadian Geotechnical Journal* (1985). DOI: 10.1139/t85-050. URL: https://cdnsciencepub.com/doi/abs/10.1139/t85-050 (visited on 11/03/2020).

[140] Priyanka Sharma et al. "Economical Design of Reinforced Slope Using Geosynthetics". In: *Geotechnical and Geological Engineering* 38.2 (Apr. 1, 2020), pp. 1631–1637. ISSN: 1573-1529. DOI: 10.1007/s10706-019-01118-2. URL: https://doi.org/10.1007/s10706-019-01118-2 (visited on 11/02/2020).

[141] R. K. Rowe and A. L. Li. "Geosynthetic-Reinforced Embankments over Soft Foundations". In: *Geosynthetics International* 12.1 (Jan. 1, 2005), pp. 50–85. ISSN: 1072-6349. DOI: 10.1680/gein.2005.12.1.50. URL: https://www.icevirtuallibrary.com/doi/full/10.1680/gein.2005.12.1.50 (visited on 11/03/2020).

[142] Rabah Derghoum and Mohamed Meksaouine. "Coupled Finite Element Modelling of Geosynthetic Reinforced Embankment Slope on Soft Soils Considering Small and Large Displacement Analyses". In: *Arabian Journal for Science and Engineering* 44.5 (May 1, 2019), pp. 4555–4573. ISSN: 2191-4281. DOI: 10.1007/s13369-018-3461-2. URL: https://doi.org/10.1007/s13369-018-3461-2 (visited on 11/02/2020).

[143] J. O. Avesani Neto, B. S. Bueno, and M. M. Futai. "Evaluation of a Calculation Method for Embankments Reinforced with Geocells over Soft Soils Using Finite-Element Analysis". In: *Geosynthetics International* 22.6 (Sept. 28, 2015), pp. 439–451. ISSN: 1072-6349. DOI: 10.1680/jgein.15.00024. URL: https://www.icevirtuallibrary.com/doi/10.1680/jgein.15.00024 (visited on 11/04/2020).

[144] Gh. Tavakoli Mehrjardi, A. Ghanbari, and H. Mehdizadeh. "Experimental Study on the Behaviour of Geogrid-Reinforced Slopes with Respect to Aggregate Size". In: *Geotextiles and Geomembranes* 44.6 (Dec. 1, 2016), pp. 862–871. ISSN: 0266-1144. DOI: 10.1016/j.geotexmem.2016.06.006. URL: http://www.sciencedirect.com/science/article/pii/S0266114416300735 (visited on 11/16/2020).

[145] V. Tandjiria, B. K. Low, and C. I. Teh. "Effect of Reinforcement Force Distribution on Stability of Embankments". In: *Geotextiles and Geomembranes* 20.6 (Dec. 1, 2002), pp. 423–443. ISSN: 0266-1144. DOI: 10.1016/S0266-1144(02)00015-8. URL: http://www.sciencedirect.com/science/article/pii/S0266114402000158 (visited on 11/03/2020).

[146] Mensur Mulabdić et al. *Priručnik za primjenu geosintetika u nasipima za obranu od poplava (Manual for application of geosynthetics in flood protection embankments)*. Osijek: Faculty of Civil Engineering Osijek, 2016. URL: https://www.bib.irb.hr/857951?rad=857951 (visited on 02/21/2021).

[147] Nicola Moraci et al. "Soil Geosynthetic Interaction: Design Parameters from Experimental and Theoretical Analysis". In: *Transportation Infrastructure Geotechnology* 1.2 (June 1, 2014), pp. 165–227. ISSN: 2196-7210. DOI: 10.1007/s40515-014-0007-2. URL: https://doi.org/10.1007/s40515-014-0007-2 (visited on 02/21/2021).

[148] Adis Skejic, Senad Medic, and Tomislav Ivšić. "Numerical Investigations of Interaction between Geogrid/Wire Fabric Reinforcement and Cohesionless Fill in Pull-out Test". In: *Gradevinar* 72/2020 (Apr. 10, 2020), pp. 237–252. DOI: 10.14256/JCE.2668.2019.

[149] Inc. Strata Systems. *Reinforced Soil Slopes and Embankments*. 100119. Cumming, Georgia, USA: Strata Systems, Inc., 2010.

[150] T. Yamanouchi and N. Fukuda. "Design and Observation of Steep Reinforced Embankments". In: *Third International Conference on Case Histories in Geotechnical Engineering*. Third International Conference on Case Histories in Geotechnical Engineering. St. Louis, Missouri, June 1–6, 1993. URL: https://scholarsmine.mst.edu/icchge/3icchge/3icchge-session15/3.

[151] GEO. *Guide to Reinforced Fill Structure and Slope Design*. Geoguide 6. Hong Kong: Geotechnical Engineering Office, Civil Engineering and Development Department, HKSAR Government, Continuously Updated E-Version released on 29 August 2017, p. 218.

[152] V. S. Ozgur Kirca and R. Evren Kilci. "Mechanism of Steady and Unsteady Piping in Coastal and Hydraulic Structures with a Sloped Face". In: *Water* 10.12 (12 Dec. 2018), p. 1757. DOI: 10.3390/w10121757. URL: https://www.mdpi.com/2073-4441/10/12/1757 (visited on 09/03/2021).

[153] Filip Bujakowski and Tomasz Falkowski. "Hydrogeological Analysis Supported by Remote Sensing Methods as A Tool for Assessing the Safety of Embankments (Case Study from Vistula River Valley, Poland)". In: *Water* 11.2 (2 Feb. 2019), p. 266. DOI: 10.3390/w11020266. URL: https://www.mdpi.com/2073-4441/11/2/266 (visited on 09/14/2021).

[154] Kevin MacKillop et al. "Assessing Submarine Slope Stability through Deterministic and Probabilistic Approaches: A Case Study on the West-Central Scotia Slope". In: *Geosciences* 9.1 (1 Jan. 2019), p. 18. DOI: 10.3390/geosciences9010018. URL: https://www.mdpi.com/2076-3263/9/1/18 (visited on 09/03/2021).

[155] Shaohe Zhang et al. “Reliability Analysis of Layered Soil Slopes Considering Different Spatial Autocorrelation Structures”. In: *Applied Sciences* 10.11 (11 Jan. 2020), p. 4029. DOI: 10.3390/app10114029. URL: https://www.mdpi.com/2076-3417/10/11/4029 (visited on 09/14/2021).

[156] Nicola Rossi et al. “Development of Fragility Curves for Piping and Slope Stability of River Levees”. In: *Water* 13.5 (2021), p. 19. DOI: 10.3390/w13050738.

[157] A. M. Hasofer and M. C. Lind. “An Exact and Invariant First Order Reliability Format”. In: *Journal of Engineering Mechanics* 100.1 (1974), pp. 111–121.

[158] Jasbir Singh Arora. “Additional Topics on Optimum Design”. In: *Introduction to Optimum Design*. Fourth. Academic Press, 2017, pp. 795–849. ISBN: 978-0-12-800806-5. DOI: 10.1016/C2013-0-15344-5. URL: https://linkinghub.elsevier.com/retrieve/pii/C20130153445 (visited on 02/22/2021).

[159] Kok-Kwang Phoon. “Numerical Recipes for Reliability Analysis - a Primer”. In: *Reliability-Based Design in Geotechnical Engineering*. Ed. by Kok-Kwang Phoon. Abingdon, Oxon, England: Taylor & Francis, 2008, pp. 1–75.

[160] Rüdiger Rackwitz. “Reliability Analysis—a Review and Some Perspectives”. In: *Structural Safety* 23.4 (Oct. 1, 2001), pp. 365–395. ISSN: 0167-4730. DOI: 10.1016/S0167-4730(02)00009-7. URL: http://www.sciencedirect.com/science/article/pii/S0167473002000097 (visited on 08/28/2020).

[161] Gregory B. Baecher and John T. Christian. “The Hasofer-Lind Approach (FORM)”. In: *Reliability and Statistics in Geotechnical Engineering*. England: Wiley, 2003, pp. 377–397.

[162] A. H. I. Sia and N. Dixon. “Distribution and Variability of Interface Shear Strength and Derived Parameters”. In: *Geotextiles and Geomembranes* 25.3 (June 1, 2007), pp. 139–154. ISSN: 0266-1144. DOI: 10.1016/j.geotexmem.2006.12.003. URL: http://www.sciencedirect.com/science/article/pii/S026611440600094X (visited on 11/16/2020).

[163] Yan Yu and Richard J. Bathurst. “Influence of Selection of Soil and Interface Properties on Numerical Results of Two Soil–Geosynthetic Interaction Problems”. In: *International Journal of Geomechanics* 17.6 (June 1, 2017), p. 04016136. DOI: 10.1061/(ASCE)GM.1943-5622.0000847. URL: https://ascelibrary.org/doi/abs/10.1061/%28ASCE%29GM.1943-5622.0000847 (visited on 11/16/2020).

[164] R. A. Jewell. “Application of Revised Design Charts for Steep Reinforced Slopes”. In: *Geotextiles and Geomembranes* 10.3 (Jan. 1, 1991), pp. 203–233. ISSN: 0266-1144. DOI: 10.1016/0266-1144(91)90056-3. URL: http://www.sciencedirect.com/science/article/pii/0266114491900563 (visited on 11/17/2020).

[165] M Pendola et al. “Combination of Finite Element and Reliability Methods in Nonlinear Fracture Mechanics”. In: *Reliability Engineering & System Safety* 70.1 (Oct. 1, 2000), pp. 15–27. ISSN: 0951-8320. DOI: 10.1016/S0951-8320(00)00043-0. URL: http://www.sciencedirect.com/science/article/pii/S0951832000000430 (visited on 07/21/2020).

[166] L. Librić, M. S. Kovačević, and G. Ivoš. “Determining of Risk Ranking for Otok Virje – Brezje Levee Reconstruction”. In: *ICONHIC2019*. Chania, Greece, June 23–26, 2019. URL: https://www.bib.irb.hr/1016185 (visited on 02/22/2021).

[167] Aleck Wu. *Locating General Failure Surfaces in Slope Analysis via Cuckoo Search*. Rocscience Inc., 2012.

[168] *Radni Obilazak Gradilišta Vodoopskrbnog Sustava Općine Cestica i Nasipa Otok Virje - Brezje | Hrvatske Vode*. URL: https://www.voda.hr/hr/radni-obilazak-gradilista-vodoopskrbnog-sustava-opcine-cestica-nasipa-otok-virje-brezje (visited on 02/22/2021).

[169] Motoyuki Suzuki et al. “Interface Shear Strength between Geosynthetic Clay Liner and Covering Soil on the Embankment of an Irrigation Pond and Stability Evaluation of Its Widened Sections”. In: *Soils and Foundations* 57.2 (Apr. 1, 2017), pp. 301–314. ISSN: 0038-0806. DOI: 10.1016/j.sandf.2017.03.007. URL: https://www.sciencedirect.com/science/article/pii/S0038080617300392 (visited on 08/24/2021).

[170] Ivan Vaníček, Danijel Jirásko, and Martin Vaníček. *Modern Earth Structures for Transport Engineering*. Taylor & Francis, 2020. ISBN: 978-0-367-20834-9.

[171] Rudolf Hufenus et al. “Strength Reduction Factors Due to Installation Damage of Reinforcing Geosynthetics”. In: *Geotextiles and Geomembranes* 23.5 (Oct. 1, 2005), pp. 401–424. ISSN: 0266-1144. DOI: 10.1016/j.geotexmem.2005.02.003. URL: http://www.sciencedirect.com/science/article/pii/S0266114405000385 (visited on 09/02/2020).

[172] Richard J. Bathurst, Bingquan Huang, and Tony M. Allen. “Analysis of Installation Damage Tests for LRFD Calibration of Reinforced Soil Structures”. In: *Geotextiles and Geomembranes* 29.3 (3 2011), pp. 323–334. ISSN: 02661144. DOI: 10.1016/j.geotexmem.2010.10.003. URL: https://www.mendeley.com/catalogue/0853bf3d-131a-3cbf-8ede-3efe303eb6ea/ (visited on 07/10/2020).

[173] R.J. Bathurst, B.-Q. Huang, and T.m. Allen. “Interpretation of Laboratory Creep Testing for Reliability-Based Analysis and Load and Resistance Factor Design (LRFD) Calibration”. In: *Geosynthetics International* 19.1 (Feb. 1, 2012), pp. 39–53. ISSN: 1072-6349. DOI: 10.1680/gein.2012.19.1.39. URL: https://www.icevirtuallibrary.com/doi/10.1680/gein.2012.19.1.39 (visited on 09/02/2020).

[174] Alfredo Hua-Sing Ang and Wilson H. Tang. *Probability Concepts in Engineering Planning and Design, Volume 1: Basic Principles*. Vol. 1. 2 vols. New York: Wiley, 1975.

[175] Trevor L. L. Orr and Denys Breysse. "Eurocode 7 and Reliability-Based Design". In: *Reliability-Based Design in Geotechnical Engineering*. Abingdon, Oxon, England: Taylor & Francis, 2008.

[176] Kok-Kwang Phoon and Farrokh Nadim. "Modeling Non-Gaussian Random Vectors for FORM: State-of-the-Art Review". In: *International Workshop on Risk Assessment in Site Characterization and Geotechnical Design*. Bangalore, India: Indian Institute of Science, Nov. 26–27, 2004, pp. 55–85.

[177] R P. *Sigm_fit (https://www.mathworks.com/matlabcentral/fileexchange/42641-sigm_fit)*. MATLAB Central File Exchange. 2016.

[178] Douglas C. Montgomery. *Design and Analysis of Experiments*. 9th ed. Hoboken, NJ, USA: Wiley, 2017.

[179] R.C.H. Cheng. "Searching For Important Factors: Sequential Bifurcation Under Uncertainty". In: *Winter Simulation Conference Proceedings,* Winter Simulation Conference Proceedings, Dec. 1997, pp. 275–280. DOI: 10.1145/268437.268491.

[180] Hong Wan, Bruce E. Ankenman, and Barry L. Nelson. "Controlled Sequential Bifurcation: A New Factor-Screening Method for Discrete-Event Simulation". In: *Operations Research* 54.4 (Aug. 1, 2006), pp. 743–755. ISSN: 0030-364X. DOI: 10.1287/opre.1060.0311. URL: https://pubsonline.informs.org/doi/10.1287/opre.1060.0311 (visited on 11/15/2021).

[181] Hong Wan, Bruce E. Ankenman, and Barry L. Nelson. "Improving the Efficiency and Efficacy of Controlled Sequential Bifurcation for Simulation Factor Screening". In: *INFORMS Journal on Computing* 22.3 (Aug. 2010), pp. 482–492. ISSN: 1091-9856. DOI: 10.1287/ijoc.1090.0366. URL: https://pubsonline.informs.org/doi/abs/10.1287/ijoc.1090.0366 (visited on 07/18/2022).

[182] Regine Pei Tze Oh et al. "Efficient Experimental Design Tools for Exploring Large Simulation Models". In: *Computational and Mathematical Organization Theory* 15.3 (Nov. 6, 2009), p. 237. ISSN: 1572-9346. DOI: 10.1007/s10588-009-9059-1. URL: https://doi.org/10.1007/s10588-009-9059-1 (visited on 07/18/2022).

[183] Susan M. Sanchez, Hong Wan, and Thomas W. Lucas. "Two-Phase Screening Procedure for Simulation Experiments". In: *ACM Transactions on Modeling and Computer Simulation* 19.2 (Mar. 23, 2009), 7:1–7:24. ISSN: 1049-3301. DOI: 10.1145/1502787.1502790. URL: https://doi.org/10.1145/1502787.1502790 (visited on 07/18/2022).

[184] W. Shi, Jack P.C. Kleijnen, and Zhixue Liu. “Factor Screening for Simulation with Multiple Responses: Sequential Bifurcation”. In: *Factor Screening for Simulation with Multiple Responses*. CentER Discussion Paper 2012–032 (2012). Pagination: 37.

[185] Wen Shi et al. “Optimal Design of the Auto Parts Supply Chain for JIT Operations: Sequential Bifurcation Factor Screening and Multi-Response Surface Methodology”. In: *European Journal of Operational Research* 236.2 (July 16, 2014), pp. 664–676. ISSN: 0377-2217. DOI: 10.1016/j.ejor.2013.11.015. URL: https://www.sciencedirect.com/science/article/pii/S0377221713009144 (visited on 11/29/2022).

[186] Lidija Tadić, Ognjen Bonacci, and Tamara Dadić. “Analysis of the Drava and Danube Rivers Floods in Osijek (Croatia) and Possibility of Their Coincidence”. In: *Environmental Earth Sciences* 75.18 (Sept. 12, 2016), p. 1238. ISSN: 1866-6299. DOI: 10.1007/s12665-016-6052-0. URL: https://doi.org/10.1007/s12665-016-6052-0 (visited on 12/21/2022).

[187] Mario Bačić, Librić Lovorka, and Meho Saša Kovačević. “Application of Geosynthetics as Hydraulic Barriers in Flood Protection Embankments”. In: *Proceedings of the 1st International Conference CoMS_2017*. 1st International Conference on Constructio Materials for Sustainable Future. Zadar, Croatia, Apr. 19–21, 2017, p. 677. URL: https://www.bib.irb.hr/871949 (visited on 12/21/2022).

[188] A. M. Dean and S. M. Lewis. “Comparison of Group Screening Strategies for Factorial Experiments”. In: *Computational Statistics & Data Analysis* 39.3 (May 28, 2002), pp. 287–297. ISSN: 0167-9473. DOI: 10.1016/S0167-9473(01)00082-2. URL: https://doi.org/10.1016/S0167-9473(01)00082-2 (visited on 11/04/2022).

[189] Jack P. C. Kleijnen, Bert Bettonvil, and Fredrik Persson. “Screening for the Important Factors in Large Discrete-Event Simulation Models: Sequential Bifurcation and Its Applications”. In: *Screening: Methods for Experimentation in Industry, Drug Discovery, and Genetics*. Ed. by Angela Dean and Susan Lewis. New York, NY: Springer, 2006, pp. 287–307. ISBN: 978-0-387-28014-1. DOI: 10.1007/0-387-28014-6_13. URL: https://doi.org/10.1007/0-387-28014-6_13 (visited on 11/15/2021).

[190] Nicola Rossi et al. “Fragility Curves for Slope Stability of Geogrid Reinforced River Levees”. In: *Water* 13.19 (19 Jan. 2021), p. 2615. DOI: 10.3390/w13192615. URL: https://www.mdpi.com/2073-4441/13/19/2615 (visited on 12/10/2021).

[191] Amanuel Petros Wolebo. “Advanced Probabilistic Slope Stability Analysis on Rissa Slope”. MA thesis. Trondheim, Norway: Norwegian University of Science and Technology, 2016. URL: https://ntnuopen.ntnu.no/ntnu-xmlui/handle/11250/2416465 (visited on 12/05/2022).

[192] Cormac Reale et al. “Cone Penetration Testing 2022”. In: *Assessment of the Spatial Variability of a Croatian Flood Embankment Using the Cone Penetration Test*. CRC Press, June 23, 2022, pp. 1053–1057. ISBN: 978-1-00-330882-9. DOI: 10.1201/9781003308829-159. URL: https://www.taylorfrancis.com/chapters/oa-edit/10.1201/9781003308829-159/assessment-spatial-variability-croatian-flood-embankment-using-cone-penetration-test-reale-kova%C4%8Devi%C4%87-bacic-gavin (visited on 12/05/2022).

[193] Ben Chie Yen. “Hydraulics and Effectiveness of Levees for Flood Control”. In: *Paper Presented: US–Italy Research Workshop on the Hydrometeorology, Impacts, and Management of Extreme Floods*. Citeseer, 1995.

[194] Reuben A. Heine and Nicholas Pinter. “Levee Effects upon Flood Levels: An Empirical Assessment”. In: *Hydrological Processes* 26.21 (2012), pp. 3225–3240. ISSN: 1099-1085. DOI: 10.1002/hyp.8261. URL: https://onlinelibrary.wiley.com/doi/abs/10.1002/hyp.8261 (visited on 01/31/2023).

[195] OAR US EPA. *Climate Change Indicators: River Flooding*. July 1, 2016. URL: https://www.epa.gov/climate-indicators/climate-change-indicators-river-flooding (visited on 01/31/2023).

[196] W. Gibson. “PROBABILISTIC METHODS FOR SLOPE ANALYSIS AND DESIGN”. In: [TLDR] Methods like Monte Carlo simulation (MC), First Order Second Moment (FOSM) or Point Estimate Method (PEM) and may require tens to hundreds of analyses. 2011. URL: https://www.semanticscholar.org/paper/PROBABILISTIC-METHODS-FOR-SLOPE-ANALYSIS-AND-DESIGN-Gibson/bf6b8e795f0f63673572e2d3a244de9f42f2013d (visited on 02/10/2023).

[197] G. Kaggwa and Y. Kuo. “Probabilistic Techniques in Geotechnical Modelling - Which One Should You Use?” In: (2011). ISSN: 0818-9110. URL: https://digital.library.adelaide.edu.au/dspace/handle/2440/71912 (visited on 02/10/2023).

[198] Anna Szostak-Chrzanowski, Michel Massiéra, and Yousef Hammamji. “Numerical Analysis of Large Earth Dams Deformations as a Tool for Designing Geodetic Monitoring Schemes”. In: Canadian Dam Association Annual Conference. Quebec City, Canada, 30 Sept - 6 Oct. 2006.

[199] J. W. Salamon et al. “Seismic Analysis of Pine Flat Concrete Dam: Formulation and Synthesis of Results”. In: *Numerical Analysis of Dams*. Ed. by Gabriella Bolzon et al. Lecture Notes in Civil Engineering. Cham: Springer International Publishing, 2021, pp. 3–97. ISBN: 978-3-030-51085-5. DOI: 10.1007/978-3-030-51085-5_1.

[200] Axel Moellmann, Pieter A. Vermeer, and Maximilian Huber. “A Probabilistic Finite Element Analysis of Embankment Stability under Transient Seepage Conditions”. In: *Proceedings of the 6th Internation Probabilistic Workshop*. 6th International Probabilistic Workshop. Varijabilinost "k". Darmstadt, Germany, 26–Nov. 27, 2008.

[201] S. Javankhoshdel and R. J. Bathurst. “Deterministic and Probabilistic Failure Analysis of Simple Geosynthetic Reinforced Soil Slopes”. In: *Geosynthetics International* 24.1 (Feb. 2017), pp. 14–29. ISSN: 1072-6349. DOI: 10.1680/jgein.16.00012. URL: https://www.icevirtuallibrary.com/doi/abs/10.1680/jgein.16.00012 (visited on 02/10/2023).

[202] Nicola Rossi et al. “Methodology for Identification of the Key Levee Parameters for Limit-State Analyses Based on Sequential Bifurcation”. In: *Sustainability* 15.6 (6 Jan. 2023), p. 4754. ISSN: 2071-1050. DOI: 10.3390/su15064754. URL: https://www.mdpi.com/2071-1050/15/6/4754 (visited on 04/25/2023).

[203] J. Deng and C. Lee. “Displacement Back Analysis for a Steep Slope at the Three Gorges Project Site”. In: (2001). DOI: 10.1016/S1365-1609(00)00077-0.

[204] Bernhard E. Boser, Isabelle M. Guyon, and Vladimir N. Vapnik. “A Training Algorithm for Optimal Margin Classifiers”. In: *Proceedings of the Fifth Annual Workshop on Computational Learning Theory*. COLT ’92. New York, NY, USA: Association for Computing Machinery, July 1, 1992, pp. 144–152. ISBN: 978-0-89791-497-0. DOI: 10.1145/130385.130401. URL: https://doi.org/10.1145/130385.130401 (visited on 01/27/2023).

[205] Vladimir N. Vapnik. *The Nature of Statistical Learning Theory*. New York, NY: Springer, 2000. ISBN: 978-1-4419-3160-3 978-1-4757-3264-1. DOI: 10.1007/978-1-4757-3264-1. URL: http://link.springer.com/10.1007/978-1-4757-3264-1 (visited on 01/14/2023).

[206] J. Kennedy and R. Eberhart. “Particle Swarm Optimization”. In: *Proceedings of ICNN’95 - International Conference on Neural Networks*. Proceedings of ICNN’95 - International Conference on Neural Networks. Vol. 4. Nov. 1995, 1942–1948 vol.4. DOI: 10.1109/ICNN.1995.488968.

[207] Meho Saša Kovačević et al. “Assessment of Long-Term Deformation of a Tunnel in Soft Rock by Utilizing Particle Swarm Optimized Neural Network”. In: *Tunnelling and Underground Space Technology* 110 (Apr. 1, 2021), p. 103838. ISSN: 0886-7798. DOI: 10.1016/j.tust.2021.103838. URL: https://www.sciencedirect.com/science/article/pii/S0886779821000298 (visited on 02/13/2023).

[208] *PLAXIS 2D Reference Manual*. 2019.

[209] Ralph B. D'Agostino. "An Omnibus Test of Normality for Moderate and Large Size Samples". In: *Biometrika* 58.2 (1971), pp. 341–348. ISSN: 0006-3444. DOI: 10.2307/2334522. JSTOR: 2334522. URL: https://www.jstor.org/stable/2334522 (visited on 01/15/2023).

[210] Ralph D'Agostino and E. S. Pearson. "Tests for Departure from Normality. Empirical Results for the Distributions of b^2 and sqrt b^1". In: *Biometrika* 60.3 (1973), pp. 613–622. ISSN: 0006-3444, 1464-3510. DOI: 10.1093/biomet/60.3.613. URL: https://academic.oup.com/biomet/article-lookup/doi/10.1093/biomet/60.3.613 (visited on 02/14/2023).

[211] M. Khalilzad and M. A. Gabr. "Deformation-Based Limit States for Earth Embankments". In: (Apr. 26, 2012), pp. 3639–3648. DOI: 10.1061/41165(397)372. URL: https://ascelibrary.org/doi/abs/10.1061/41165%28397%29372 (visited on 03/11/2021).

Biography

Nicola Rossi was born in 1994 in Zagreb, Croatia. In 2012 he starts his studies at the Faculty of Civil Engineering of the University of Zagreb, and in 2015 obtains the Bachelor's degree. From 2015 to 2017 he continues his studies on the Department of Geotechnics at the same faculty, and obtains the Master's degree in Civil Engineering. In 2017 he begins his position as a Research and Teaching Assistant at the Department of Geotechnics, Faculty of Civil Engineering, University of Zagreb, and engages in the the doctoral programme to obtain his PhD, which is now presented here. During the time as an assistant, Nicola Rossi participated in the making of various geotechnical projects, and published the following papers:

1. Rossi N, Bačić M, Librić L., Kovačević MS., Methodology for Identification of the Key Levee Parameters for Limit-State Analyses Based on Sequential Bifurcation. Sustainability 2023;15,4754. https://doi.org/10.3390/su15064754
2. Kurečić T, Hajek-Tadesse V, Wacha L, Horvat M, Trinajstić N, Mišur I, et al. Clastic sediments and sub-recent microfauna at the bottom of the Njemica cave (Biokovo, Croatia) 2022:44–5.
3. Rossi N, Bačić M, Kovačević MS, Librić L. Fragility Curves for Slope Stability of Geogrid Reinforced River Levees. Water 2021;13:2615. https://doi.org/10.3390/w13192615.
4. Rossi N, Bačić M, Kovačević MS. Evaluation of seismic resilience of levees through the development of fragility curves 2021:373–83. https://doi.org/10.5592/CO/1CroCEE.2021.273.
5. Rossi N, Bačić M, Kovačević MS, Librić L. Development of Fragility Curves for Piping and Slope Stability of River Levees. Water 2021;13:19. https://doi.org/10.3390/w13050738.
6. Kovačević MS, Gavin K, Stipanović Oslaković I, Librić L, Rossi N. Monitoring of long term deformations in Bobova tunnel 2018:1507–13. https://doi.org/10.5592/CO/cetra.2018.844.

7. Rossi N, Mance M, Kovačević M-S. The development of block theory in rock engineering 2018:208–14. https://doi.org/10.31534/CO/ZT.2018.29.

8. Jurić Kaćunić D, Bačić M, Rossi N. Application of geosynthetics for reinforcement of flood protection embankments 2017:234–43.